



**HAL**  
open science

# Magnetization dynamics induced by photons, phonons and electrons in (Ga,Mn)As

L. Thevenard

► **To cite this version:**

L. Thevenard. Magnetization dynamics induced by photons, phonons and electrons in (Ga,Mn)As. Materials Science [cond-mat.mtrl-sci]. Sorbonne Université, 2021. tel-03182763

**HAL Id: tel-03182763**

**<https://hal.science/tel-03182763>**

Submitted on 26 Mar 2021

**HAL** is a multi-disciplinary open access archive for the deposit and dissemination of scientific research documents, whether they are published or not. The documents may come from teaching and research institutions in France or abroad, or from public or private research centers.

L'archive ouverte pluridisciplinaire **HAL**, est destinée au dépôt et à la diffusion de documents scientifiques de niveau recherche, publiés ou non, émanant des établissements d'enseignement et de recherche français ou étrangers, des laboratoires publics ou privés.

# Sorbonne Université

École doctorale 397: Physique et Chimie des Matériaux

Candidature à l'habilitation à diriger des recherches

Spécialité Physique

présentée par

Laura Thevenard

## Magnetization dynamics induced by photons, phonons and electrons in (Ga,Mn)As

soutenue le 24 mars 2021

Devant le jury composé de:

Rapporteur	Sebastian Goennenwein (University of Konstanz, Allemagne)
Examinatrice	Stefania Pizzini (Institut Néel, Grenoble)
Rapporteuse	Silvia Tacchi (Istituto Officina dei Materiali, Université de Pérouse, Italie)
Rapporteur	Stéphane Mangin (Institut Jean Lamour, Université de Lorraine, Nancy)
Président	Andrea Gauzzi (IMPMC, Sorbonne Université, Paris)

# Contents

<b>Acknowledgements</b>	<b>3</b>
<b>Introduction, organization of the manuscript, remarks</b>	<b>3</b>
<b>I (Ga,Mn)As, a model weak ferromagnet</b>	<b>8</b>
1 Overview of the material . . . . .	8
1.1 Structure, electrical properties . . . . .	8
1.2 Origin and description of the ferromagnetic phase . . . . .	9
1.3 The Curie temperature quest . . . . .	9
2 Magnetic anisotropy . . . . .	10
2.1 From in-plane to out-of-plane magnetized . . . . .	10
2.2 Uniaxial anisotropy . . . . .	12
3 Successes . . . . .	12
<b>II Domain wall dynamics</b>	<b>13</b>
1 Context . . . . .	13
2 Master equations . . . . .	15
2.1 Domain-wall width . . . . .	15
2.2 “ $q - \varphi - \Delta$ ” model equations . . . . .	16
2.3 Domain-wall propagation regimes: stationary and precessional . . . . .	17
3 Experimental tools for the study of domain-wall dynamics . . . . .	18
4 Field-driven dynamics . . . . .	19
4.1 High domain-wall velocities in planar layers . . . . .	19
4.2 Role of flexural modes in domain-wall dynamics . . . . .	21
5 Current-driven dynamics . . . . .	23
5.1 Current-induced spin-transfer and spin-orbit torques . . . . .	23
5.2 Intriguing observations, a possible evidence of momentum transfer ? . . . . .	25
<b>III Light-induced magnetization dynamics</b>	<b>28</b>
1 Context . . . . .	28
2 Influence of the phosphorus content on the exchange constant . . . . .	29
3 The magneto-optical illusion . . . . .	30
4 Pump-driven transient and stationary heating . . . . .	31
4.1 Role of transient heating in precession . . . . .	31
4.2 Magnetism reversal driven by optical pulses . . . . .	32
4.3 Steady-state thermal gradient induced by the pump beam . . . . .	32
<b>IV Magneto-acoustics</b>	<b>34</b>
1 Context . . . . .	35
2 Acoustic waves . . . . .	36
2.1 Wave equations . . . . .	36
2.2 Different transduction mechanisms . . . . .	37
3 Experimental developments . . . . .	40
4 Magneto-acoustic ferromagnetic resonance (SAW-FMR) in (Ga,Mn)As . . . . .	42

4.1	Magneto-elasticity and magnetostriction . . . . .	42
4.2	Coupled magnetic and elastic equations . . . . .	43
4.3	Magnetoacoustics with optically excited BAWs . . . . .	44
4.4	Magnetoacoustics with electrically excited SAWs . . . . .	45
4.5	Magnon-polarons . . . . .	51
4.5.1	Motivations . . . . .	51
4.5.2	Looking for $f(k)$ avoided crossing in FeGa, Nickel and Co . . . . .	53
4.5.3	Successful endeavors of other groups since then . . . . .	56
5	SAW-driven or -assisted magnetization switching . . . . .	57
5.1	Resonant SAW-driven precessional switching . . . . .	57
5.2	Non-resonant SAW-assisted switching . . . . .	61
6	Comments & Perspectives . . . . .	62
<b>V</b>	<b>Future work: acoustics for antiferromagnets</b>	<b>65</b>
1	Context, scientific objectives and research hypothesis . . . . .	65
2	Innovative and ambitious nature of the project, state of the art . . . . .	66
3	Methodology . . . . .	67
<b>VI</b>	<b>Carrier overview</b>	<b>68</b>
1	CV . . . . .	68
1.1	Academic training . . . . .	68
1.2	Professional experience . . . . .	68
2	Research credentials . . . . .	68
2.1	Research topics and main experimental techniques . . . . .	68
2.2	Contracts . . . . .	69
2.3	Main collaborations . . . . .	69
2.4	Full list of publications and talks . . . . .	70
3	Activities not directly related to research . . . . .	72
3.1	Expertise . . . . .	73
3.2	Lab responsibilities . . . . .	73
3.3	Other responsibilities . . . . .	73
3.4	Teaching . . . . .	73
3.5	Outreach . . . . .	74
4	Supervising responsibilities . . . . .	74

*A mes parents, Alain et Eveline*

# Acknowledgements

I am truly grateful to have crossed paths and worked with many great minds since I first stepped into a laboratory, some of whom were much older or younger than me, some full professors, others technicians, some here in Paris, others from across the world.

I would like to start by thanking the members of the jury. Although the COVID crisis has left little hope for a rewarding gathering in Paris this year, they have generously accepted to consider my manuscript. I am delighted that it will be examined by world-renowned experts of ferromagnetic resonance, magnonics, magnetic semiconductors, magnetoacoustics, domain-wall propagation, current-driven torques, spin-currents, antiferromagnets and light-driven dynamics - to cite just a few of the topics they master. In the years leading up to the writing of this manuscript, I have spent a great deal of time on some of their papers, and I hope that our interactions will carry on beyond this present academic 'exercise'.

On a more personal level, I wish to acknowledge two people in particular, who have trusted me and provided me with a constant source of support and inspiration. As mentors, and with great generosity, they managed the delicate task of transmitting their mastery of physics, reasoning, techniques, concepts and methods, whilst also giving me the space to develop my own ideas and acknowledging my efforts. I thank them for this and for all that they have done to help further my career. Aristide Lemaître (LPN, now C2N) was the first researcher with whom I worked. He is one of the best examples one could find of someone passionate about physics, overflowing with ideas coming from many different domains, and with a profound physical intuition. Catherine Gourdon welcomed me at INSP to work with her as a CNRS researcher, and I have been learning at her side ever since. I never cease to be amazed by her incredible experimental skills on an optical table, her acute memory and detailed knowledge of vast areas of solid state physics, and also her capacity to model just about anything elegantly. I would also like to express my profound thanks to Jean-Yves Duquesne. He has always welcomed my ideas, questions and doubts with benevolence. We will miss him as he leaves INSP in a few months to retire.

I would like to thank those who offered me the possibility to teach: N. Witkowski, M. Marangolo and D. Roditchev. It has been a particularly rewarding experience which I hope to continue. Likewise, I thank the students I have worked with, and who have produced a good part of the work presented here.

Finally, I am grateful to have several different scientific circles from which to draw ideas, strength, motivation and sympathy. Here, at INSP, I am especially indebted to the PMTeQ group (among which V. Voliotis, M. Combescot, F. Dubin, B. Eble, R. Hostein, S. Hameau), our incredible technical support team (M. Bernard, M. Vabre and F. Margaillan, S. Majrab and F. Breton), and our intergroup magnetism collective. At a national level, I acknowledge the friendly and dynamic French magnetism community.

Let me conclude with the following: the benevolence, mutual aid and shared energy I have sometimes witnessed are made possible in a system where researchers do not see their colleagues as competitors for funds, where post-docs do not consider PhD students as threats to their publication list, and in which you can be successful researcher and have a family at a reasonable age. It is with great bitterness that I see this system being constantly endangered by successive governments. But let us hope that if any good comes out of this crisis, surely it will be to underline, once more, the relevance of long-term, correctly funded research, and properly trained students and citizens.

# Introduction, organization of the manuscript, remarks

The rise of (Ga,Mn)As accompanied that of spintronics but rested on the shoulders of decades of theoretical and experimental work on magnetic semiconductors. These were initially bulk stoichiometric crystals such as EuO ( $T_c=69$  K), EuS ( $T_c=17$  K), or CdCr<sub>2</sub>S<sub>4</sub> ( $T_c=87$  K) chalcogenide spinels. They were valued for their magneto-optical properties [239], but also for being an ideal playground on which to test the Heisenberg model of ferromagnetism. The difficulty to synthesize them as integrable thin films using the new growth techniques of the 1960's and 70's drove the progressive shift to a new class of systems: thin films in which a semiconductor matrix (IV-VI PbSe, II-VI CdTe, ZnTe, HgTe) was doped with magnetic atoms. Among them, Cd<sub>1-x</sub>Mn<sub>x</sub>Te rapidly emerged as a model dilute magnetic semiconductor (DMS). The exchange interaction between the  $d$  electrons of the localized magnetic ions and the delocalized  $sp$  band electrons led to a phenomenal Zeeman splitting under field resulting in giant magneto-optical effects, a strongly spin-polarized high-mobility electron gas, and the formation of bound magnetic polarons [50]. Importantly, all these properties could be finely tuned by varying the manganese composition. In the absence of field, the dominant antiferromagnetic Mn-Mn interaction however left those compounds paramagnetic, antiferromagnetic or spin-glass-like, or at best weakly ferromagnetic upon  $p$ -doping ( $T_c \ll 4$  K) [50].

Although III-V semiconductors are usually more easily doped than II-VIs, it took almost an extra decade for III-Mn-V thin films to emerge: In<sub>1-x</sub>Mn<sub>x</sub>As in 1989 [142], and Ga<sub>1-x</sub>Mn<sub>x</sub>As in 1996 [149]. This was due to the poor solubility of manganese atoms in the host matrices, an issue solved by doing the growth at low temperature (250°C). Being intrinsically sufficiently  $p$ -doped, both materials were ferromagnetic, but the higher  $T_c$  (60K versus 7.5K) and wider band-gap of (Ga,Mn)As made it the horse on which to bet, with a foreseeable incorporation to GaAs-based (opto)electronic devices.

In parallel, the discovery of giant magnetoresistance in 1988 by Albert Fert and Peter Grünberg opened up new avenues in terms of magnetic data storage and logic devices. The strong dependence of the resistance of particular stacks on its magnetic state allowed the gradual replacement of anisotropic magnetoresistance (AMR) hard disk read-heads by GMR (and eventually TMR) devices. Their much higher sensitivity made disk drive densities rocket. Conversely the possibility to control a magnetic state by a spin-polarized current (spin transfer torque) meant one could imagine magnetic random access memories (MRAMs) bridging the material gap between the semiconductor-based processing unit and an all-magnetic storage unit. As highlighted in a recent very comprehensive review by Dietl *et al.* [42], the search for materials combining magnetic and semiconducting properties triggered three avenues of “materials” research: (i) metallic ferromagnetic/semiconductor heterostructures : taking advantage of the high spin polarization of the metal, the challenge was then to optimize the spin injection into the semiconductor, e.g. Fe/GaAs, (ii) turning ferrimagnetic oxides such as ZnNiFe<sub>2</sub>O<sub>4</sub> into good semiconductors, and finally, (iii) turning semiconductors into room-temperature ferromagnets. The 2001 prediction by this same author [43] that this could be obtained in (Ga,Mn)As - provided a 12.5% manganese concentration and  $3.5 \cdot 10^{20} \text{ cm}^{-3}$  hole doping were reached - triggered an intense activity for the next ten years. It was led by several groups across the world, in particular (but not limited to...): the groups of T. Dietl (Polish Academy of Sciences, Warsaw) and of H. Ohno (Tohoku University), the groups of B. Gallagher (University of Nottingham) and of T. Jungwirth (Institute of Physics of Prague), an intense activity around DMS in Germany (groups of L. Molenkamp and M. Brandt), or the group of J. Furdyna in University of Notre-Dame (USA).

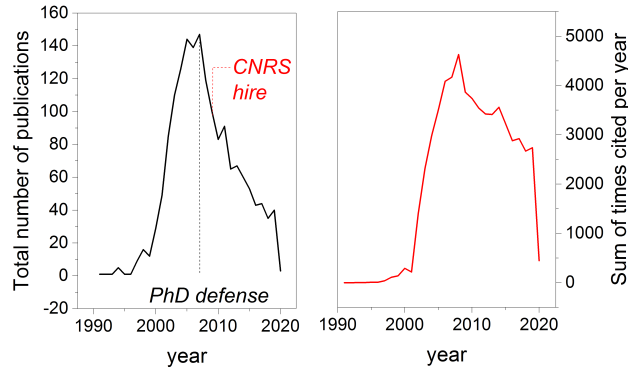


Figure 1: Web of knowledge: number of hits for the word “(Ga,Mn)As” in the topic [Jan. 2021]

My adventure with (Ga,Mn)As began in the Spring of 2004, during my Master internship at the Laboratoire des Nanostructures (Marcoussis). I was under the inspiring supervision of Aristide Lemaître who had begun growing (Ga,Mn)As in 2002, and who then accepted me as a PhD student for the following 3 years. After completing a 2 year post-doc at Imperial College working on nickel nanostructures, I was hired by the CNRS to join the Institut des Nanosciences de Paris in Catherine Gourdon’s team in 2009, at a moment when the material had reached maturity. My research project consisted in implementing different strategies to act on the dynamic magnetization of (Ga,Mn)As: magnetic fields, light waves, electrical currents, and picosecond acoustic waves. The samples made by A. Lemaître were to incorporate a varying quantity of Phosphorus dopants in order to finely adjust their magnetic properties (see next Chapter) and study these 4 different dynamics. For the last three stimuli - currents, light and strain - the overarching aim was to use (Ga,Mn)As as a model material on which to refine a field-free manipulation of the magnetization, or more modestly to rely on magnetic fields as a simple bias, but to let faster, and less power-greedy levers govern the dynamics. Particularly interesting was using the strongly non-uniform excitation by light and strain waves to generate  $\omega \neq 0, k \neq 0$  spin-waves, an approach that would appeal to the magnonics community.

This manuscript follows closely the initial workplan and is divided into three “results” chapters (**II**, **III**, **IV**), the first and last being by choice a lot more developed. They are preceded by a short introduction on (Ga,Mn)As and followed by a short research proposal for the coming years. An overview of my credentials and responsibilities concludes the document.

- I. (Ga,Mn)As, a model weak ferromagnet**
- II. Domain-wall dynamics**
- III. Light-induced magnetization dynamics**
- IV. Magneto-acoustics**
- V. Future work: acoustics for antiferromagnets**
- VI. Carrier overview**

- Although it bulks up a little bit the manuscript, I have made the choice of also showing experiments that did not work and/or are unpublished. In the best of cases, the reader will enlighten me with his/her interpretation of my data, else it will at least honor dedicated students who were often involved in these studies.
- Across the text and in the Bibliography section, my publications have been highlighted in **bold**. Video links temporarily point to [this DropBox folder](#).



# Chapter I

## (Ga,Mn)As, a model weak ferromagnet

The following sections are by no means a full review of the microscopic properties of (Ga,Mn)As, but rather a summary of the key points necessary to understand what follows. More details can be found for instance in Refs. [42, 92], and the introduction of the thesis manuscript of S. Shihab [179].

### 1 Overview of the material

#### 1.1 Structure, electrical properties

(Ga,Mn)As adopts the zinc blende crystal structure of GaAs. A small number of Ga atoms, typically a few percents, are randomly replaced by Mn atoms. Each of those, having one electron less than Ga on its outer shell, provides a weakly delocalized hole, as well as a spin  $S = 5/2$ . About 15% of the manganese atoms go in interstitial positions, where they behave as double donors partially cancelling out the hole density brought by the substitutional Mn. They also couple antiferromagnetically with nearby  $Mn_{Ga}$ , which reduces the total magnetization of the layer, so that one often sees mention of the effective (rather than the nominal) Mn concentration,  $x_{eff}$ . Other defects such as Arsenic atoms in Ga antisites favored by the low-temperature growth also act as compensating double donors. Their concentration can be greatly diminished by a careful adjustment of anion and cation fluxes during the growth. The presence of these defects prohibits the high mobility and fine spectral lines obtained in (Cd,Mn)Te.

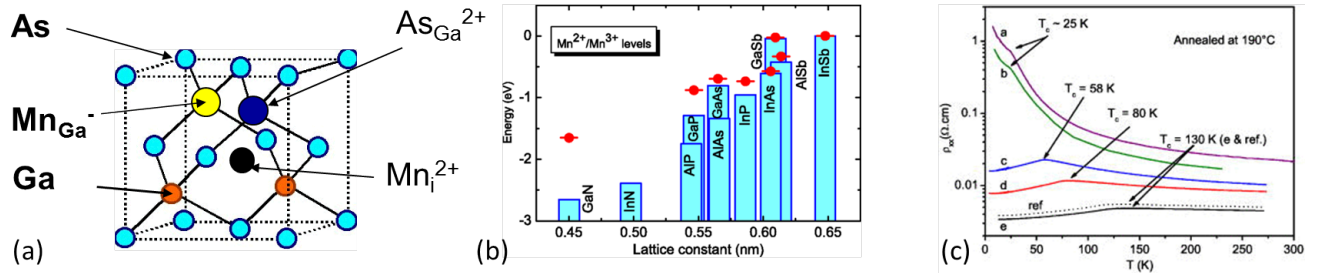


Figure I.1: (a) [190] (Ga,Mn)As lattice with substitutional Mn atoms, and the two main types of defects: interstitial Mn atoms and As atoms in Ga anti-sites. (b)[42] Compilation of experimental energies of Mn levels in the gap of III-V compounds with respect to the valence-band edges. (c) [199] Longitudinal resistivity for samples of different doping levels (sample a to e:  $p=10^{17}$ - $10^{20}$  cm<sup>-3</sup>, adjusted by hydrogenation) showing metallic or insulating behavior at low temperature. The Curie temperature ( $T_c$ , temperature at which  $\frac{\partial \rho}{\partial T} = 0$ ) increases with doping.

The Mn level lies 113 meV above the top of the valence band, so that typical carrier densities are in the  $10^{19}$ - $10^{21}$  cm<sup>-3</sup> range. (Ga,Mn)As is a decent electrical conductor ( $\rho \sim 1 - 10$  mΩ.cm), lying close to the metal-insulator transition at low temperature (Fig. I.1).

Most of our samples were made by Aristide Lemaitre (LPN, then C2N).

## 1.2 Origin and description of the ferromagnetic phase

The localized Mn atoms being prohibitively far from each other for any substantial direct interaction to take place, it was established early on that it is the delocalized holes that mediate an RKKY-like Mn-Mn exchange interaction<sup>1</sup>. It oscillates around zero with varying  $k_{F\tau}r_{MnMn}$ , product of the Fermi wave-vector and the Mn-Mn distance. In the common doping regime of (Ga,Mn)As, this product is small, and the Mn spin-spin interaction is in fact always positive, i.e. ferromagnetic. The RKKY model then becomes equivalent to the more tractable Zener model describing the role of delocalized carriers in the ferromagnetic coupling between localized magnetic spins. Physically, one can say that delocalized holes and localized  $3d$  electrons of manganese atoms mutually polarize each other via an antiferromagnetic  $pd$  interaction  $N_0\beta_{pd}$ . The total Ginzburg-Landau free energy functional  $\mathcal{F}[\mathbf{M}]$  is given by [43]:

$$\mathcal{F}[\mathbf{M}] = \mathcal{F}_S[\mathbf{M}] + \mathcal{F}_c[\mathbf{M}]$$

$\mathcal{F}_S[\mathbf{M}]$  is the free-energy of the localized spins, in absence of carriers, while  $\mathcal{F}_c[\mathbf{M}]$  is the delocalized carrier contribution. The corresponding partition function  $Z$  determines the thermodynamical properties of the system, in particular  $M_s(T)$  and the Curie temperature  $T_c$ . Most of the interesting physics of (Ga,Mn)As is encapsulated in  $\mathcal{F}_c[\mathbf{M}]$  [43].

The starting point for the calculation of this term is the Kohn-Luttinger six band  $k.p$  model: spin-split heavy and light hole bands, and spin-orbit coupling split-off bands<sup>2</sup>. For (Ga,Mn)As thin films in epitaxial strain on the GaAs substrate, one needs to add:

- a Bir-Pikus strain Hamiltonian, which splits these heavy-hole ( $J_z = \pm 3/2$ ) and light-hole ( $J_z = \pm 1/2$ ) subbands at the center of the Brillouin zone, with their respective position given by the sign of the epitaxial strain (compressive/tensile).
- the  $pd$  exchange contribution between average<sup>3</sup> Mn spins  $\langle S \rangle$  and hole spins  $s$ :  $\mathcal{H}_{pd} = -x_{eff}N_0\beta_{pd}s\langle S \rangle = 6B_G\mathbf{s}\cdot\mathbf{m}$ , with the unit magnetization vector  $\mathbf{m} = \frac{\mathbf{M}}{M_s}$  and  $B_G \propto M_s$  a convenient parameter to quantify the spin-splitting of the valence subbands with (Fig. I.2).

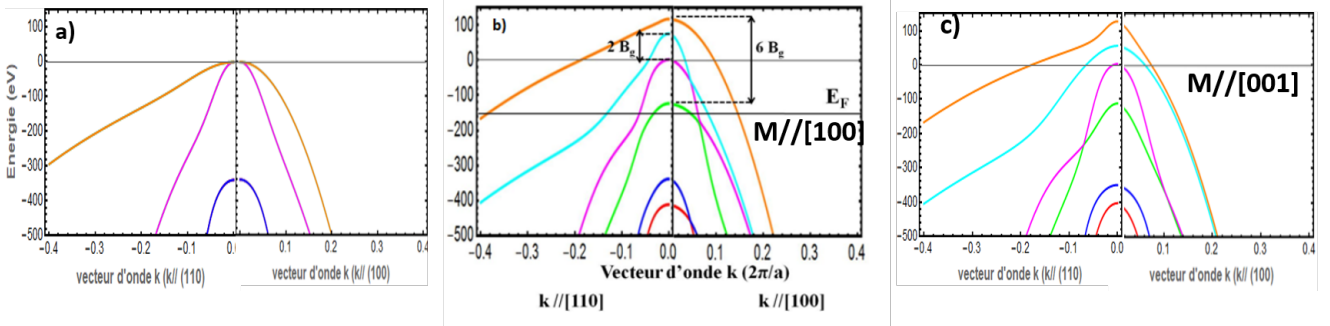


Figure I.2: [104] (a) Bulk GaAs valence band structure. (b-c) (Ga,Mn)As band structure ( $x_{Mn}=5\%$ , compressive strain), magnetization along [100] or [001].  $E_F$  is the Fermi energy. The Fermi surface is strongly anisotropic.

## 1.3 The Curie temperature quest

Minimizing  $\mathcal{F}[\mathbf{M}] = \mathcal{F}_S[\mathbf{M}] + \mathcal{F}_c[\mathbf{M}]$  gives the magnetization of (Ga,Mn)As implicitly, as a function of the effective field created by the spin-polarized holes  $B_c = -\frac{\partial \mathcal{F}_c[\mathbf{M}]}{\partial M}$ .

<sup>1</sup>For some period there was actually a heated debate as to whether the holes are truly delocalized, or reside in an impurity band at the top of the valence band. Some consensus has been reached on the former, see for instance Ref. [42] for more details.

<sup>2</sup>In the native GaAs matrix, valence states with  $L = 1$  orbital quantum number and  $S = 1/2$  spin are split by the spin-orbit interaction into  $J = 3/2$  and  $J = 1/2$  states.

<sup>3</sup>This is done in the virtual-crystal and molecular-field approximations. Note that one can also take into account the much smaller ferromagnetic  $sd$  Hamiltonian involving the electrons of the conduction band:  $\mathcal{H}_{sd} = -x_{Mn}N_0\alpha_{sd}s\langle S \rangle$ .

$$M_s = g\mu_B S N_0 x_{eff} B_s \left[ \frac{g\mu_B \left( -\frac{\partial \mathcal{F}_c[\mathbf{M}]}{\partial M} + \mu_0 H_{ext} \right)}{k_B (T + T_{AF})} \right]$$

$N_0$  is the density of Ga atoms. Residual anti-ferromagnetic interactions are taken into account by adding  $T_{AF}$ . The expansion of the Brillouin function  $B_s$  for small magnetization close to  $T_c$  gives a simple, mean-field expression of the Curie temperature:

$$T_c = \frac{N_0 \beta^2 x_{eff} S(S+1) \rho(E_F)}{12k_B} - T_{AF} \quad (\text{I.1})$$

As underlined by Dietl *et al.*, [42], because the  $pd$  interaction (for holes) is typically 4 times higher than the  $sd$  one for electrons, and the hole density at the Fermi level  $\rho(E_F)$  is higher for the (heavier) holes than for electrons, the Curie temperature has from the start been quite decent for the intrinsically  $p$ -doped (Ga,Mn)As. It is roughly proportional to  $x_{eff} p^{1/3}$  (Fig. I.1c). It is moreover inversely proportional to the unit cell (via  $N_0$ ), since smaller lattice constants should encourage a stronger overlap of wave-functions.

The first layers of (Ga,Mn)As were 150 nm thick, and had a Curie temperature of about 60 K [149]. It was soon realized that  $T_c$  could be substantially increased by playing on the density of defects, both during and after the growth, and by keeping layers thin enough (<50 nm). Low-temperature (200°C) anneals make the interstitial manganese dopants migrate to the surface/interface, restoring delocalized carriers to the matrix, and freeing the  $Mn_{Ga}$  to which they were AF coupled. Although many other strategies were explored, such as electric gating [32], applying hydrostatic pressure [63], or using a nearby layer to provide extra-carriers [143], no other substantial breakthrough was made to increase the Curie temperature, and the record  $T_c=190$  K was reached in 2013 [144, 216]. While early predictions announced a room temperature Curie temperature for an effective manganese concentration of 12.5% combined with a hole density of  $3.5 \cdot 10^{20} \text{ cm}^{-3}$  [43], several reasons - both experimental and intrinsic limitations of the  $pd$  Zener model - cap this value [92, 42]:

- (i) the carrier density in a semiconductor host cannot increase indefinitely, but is regulated by self-compensating mechanisms, for instance by the favored formation of donor defects such as  $Mn_i$ .
- (ii) as the density of manganese atoms increases, so does the contribution of their antiferromagnetic interaction (which affects  $T_{AF}$  in Eq. I.1)
- (iii) parameters entering the model such as  $N_0\beta$  or  $T_{AF}$  are poorly known
- (iv) Khazen *et al.* [95] have also suggested that as the hole density increases, their mean free path decreases, so does the distance over which the hole remains spin-polarized. The carriers then polarize less efficiently the manganese spins.

Despite this fall-through, (Ga,Mn)As has remained a model material. The main reason is the incredible tunability of its magnetic anisotropy.

## 2 Magnetic anisotropy

### 2.1 From in-plane to out-of-plane magnetized

Despite a lower density of magnetic atoms giving a very weak shape anisotropy, (Ga,Mn)As exhibits crystalline magnetic anisotropies comparable to some metals, due to the large spin-orbit splitting of the valence band. The crystalline anisotropy constants can be obtained in the  $k.p$  model described above by calculating how the carrier energy varies with magnetization orientation: the Fermi energy is integrated for a given hole density  $p$  and magnetization orientation,  $\mathcal{F}_c[\mathbf{M}] = \int_0^p E_F(\mathbf{M}, p') dp'$ . Because heavy and light holes wave-functions are fundamentally different (pure  $\uparrow$  or  $\downarrow$  spin states for HH, or mixed states for LH), the amplitude of their spin-splitting is quite anisotropic, with the total hole energy very dependent on the orientation of the magnetization with respect to the host crystalline axes (see Fig. I.2 or the thesis of M. Elsen [48]). By performing this lengthy calculation for different orientations of  $\mathbf{M}$ , the easy magnetic axis is obtained as the one yielding the lowest energy. The following overall phenomenology is calculated [233, 1, 43] and observed experimentally (Fig. I.3a):

- in the absence of strain, the crystalline anisotropy is cubic, and oscillates either side of zero with doping density. Under strain, it splits into  $K_{4\perp}, K_{4\parallel}$  components, and a uniaxial anisotropy  $K_{2\perp}$  appears:
- when the layer is in **compressive strain**, the easy axis is **in-plane** at standard doping levels ( $3 - 8.10^{20}$   $\text{cm}^{-3}$ ), out-of-plane for weak doping - growth on GaAs substrate for instance
- when the layer is in **tensile strain**, it is the opposite: the easy axis is **out-of-plane** at high doping and in-plane for weak doping - growth on ZnSe [232], on an (In,Ga)As buffer layer [200], or co-doping by Phosphorus [115]
- when the magnetization lies in-plane, the easy axis results from a competition between the cubic anisotropy  $K_{4\parallel}$ , and an additional uniaxial anisotropy  $K_{2\parallel}$  (see next section), the latter usually increasing with compressive lattice mismatch.

The final anisotropy arises from the competition between strain (tuning the HH/LH splitting, responsible for magnetoelasticity), electric doping (tuning  $E_F$ ), magnetic doping and temperature (tuning the spin-splitting parameter  $B_G \propto M_s(T)$ ). For that reason, it is not obvious to obtain a physical picture for this complex phenomenology. A pleasant, hand-waiving, argument had been proposed by Sawicki *et al.* [169] to explain the strain/doping dependency of  $K_{2\perp}$ , looking at the  $k = 0$  energy of HHs/LHs for two different orientations of the magnetization (Fig. I.3b): for a weakly-doped layer in compressive strain, only the first HH band is populated, with the moment  $J_z = 3/2$  of the carriers oriented along the growth axis [001]. In that case, their energy remains unaffected by an in-plane magnetization ( $\mathcal{H}_{pd} \propto \mathbf{s} \cdot \mathbf{m}_{\parallel} = 0$ ), but is lowered by  $\mathcal{H}_{pd}$  when  $\mathbf{m}$  lies along  $z$  (blue circle in Fig. I.3b). At higher density, the spin of the carriers flips in-plane due to the progressive filling of the light-hole bands. For tensile strain, the relative position of HH and LH is reversed, so are the easy axes. The strain-dependence of the anisotropy has for instance been observed in strained p:(Cd,Mn)Te quantum wells (Fig. I.3c). While this image is valid for weakly doped DMS presenting a moderate Zeeman splitting, it is somewhat too simplified in the case of (Ga,Mn)As, whose large Zeeman splitting of the holes (several tens of meV) competes with the heavy-hole/light-hole splitting: in that case, heavy-holes are always spin-split, regardless of the orientation of the magnetization (Fig. I.2b,c).

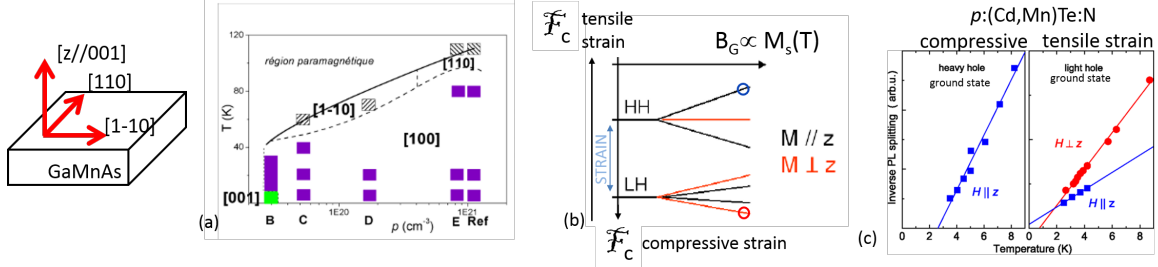


Figure I.3: (a) [198] Magnetic easy axes versus temperature, for a series of increasingly doped samples (compressive strain): at low doping (sample B), the magnetization points out of the plane at low temperature, then flips in-plane. For higher dopings (samples C-E), the temperature mainly drives an in-plane reorientation. (b) [169] Simplified scheme of valence band splitting for two orientations of magnetization with respect to the sample plane. In compressive strain (energy axis pointing down) and low doping, the ground state has a heavy-hole character with spins pointing out-of-plane (blue circle). For tensile strain (energy axis pointing up), the ground state is light-holes spin-split by an in-plane magnetization (red circle). (c) [42] adapted from [102] Photo-luminescence experiments in strained modulation doped p-(Cd,Mn)Te quantum wells illustrating (b). The line splitting is proportional to the magnetization.

The energy density can then be parametrized by 4 (sometimes 3) anisotropy constants and reads ( $\theta, \varphi$  angles given with respect to [001] and [100] axes):

$$f_{FMR} = -\mu_0 \vec{M} \cdot \vec{H} + \left( \frac{\mu_0 M_s^2}{2} - K_{2\perp} \right) \cos^2 \theta - \frac{K_{4\perp}}{2} \cos^4 \theta - \frac{K_{4\parallel}}{8} (3 + \cos 4\varphi) \sin^4 \theta - K_{2\parallel} \sin^2 \theta \sin^2 (\varphi - \frac{\pi}{4}) \quad (\text{I.2})$$

- We have had a long-standing collaboration with INSP ferromagnetic resonance (FMR) experts J. von Bardeleben and J. L. Cantin, who have continuously characterized our (Ga,Mn)As thin films. Knowing these parameters independently was instrumental in the development of phenomenological models to explain domain-wall dynamics, light-induced precession and magnetoacoustics (Chapters II, III, IV).

## 2.2 Uniaxial anisotropy

As explained above, the microscopic origin of the out-of-plane uniaxial anisotropy,  $K_{2\perp}$ , is well understood: it stems from the relative position of heavy and light-hole bands, and is thus directly proportional to the  $\varepsilon_{xx}, \varepsilon_{zz}$  epitaxial strains (here  $x, y$  are the in-plane  $\langle 100 \rangle$  axes of GaAs). Things are less obvious for the *in-plane* uniaxial anisotropy,  $K_{2\parallel}$ , distinguishing  $[110]$  and  $[1-10]$  axes, which should be equivalent in the  $D_{2d}$  symmetry group. Symmetry considerations however show that a static shear strain  $\varepsilon_{xy}$  - real or effective - would induce such an anisotropy. Surprisingly, it had never been observed experimentally though. There is at the moment no agreement concerning its microscopic origin.

Part of M. Kraimia's thesis consisted in exploring this issue. Using  $k.p$  modelling, she first estimated to about  $\varepsilon_{xy} \sim 10^{-4}$  the shear strain necessary to account for the strongest observed uniaxial anisotropies  $K_{2\parallel} \sim 1 \text{kJ/m}^3$ . If this strain were real, i.e. structural, it would subsist up to room temperature, and would imply a partial and anisotropic relaxation of the in-plane lattice, reminiscent of what was evidenced in thin uniaxial Fe layers by Thomas *et al.* [205]. Pairing up with L. Largeau (C2N) and B. Croset (INSP) to work at the SOLEIL synchrotron DiffAbs beamline with C. Mocuta, we strove to evidence this strain experimentally, but found no signature of it [106]. Although the definitive origin of the uniaxial anisotropy of (Ga,Mn)As remains elusive, one can now clearly rule out the presence of a physical shear strain, and instead invoke an effect that would lower the crystal symmetry to  $C_{2v}$ , such as the anisotropic concentration of Mn dimers along  $[110]$  and  $[1-10]$  directions proposed by Birowska *et al.* [17].

## 3 Successes

To summarize, although its Curie temperature did not live up to expectations, (Ga,Mn)As has been a model material for some of these qualities:

- (i) epitaxial properties
- (ii) large magneto-transport effects (anomalous Hall effect, AMR, planar Hall effect), due to strong SOI and low carrier densities [42, 90]
- (iii) fairly large magneto-optical effects (linear birefringence/dichroism effects, Kerr effect)
- (iv) large tunability of properties ( $T_c$ , magnetic anisotropy, spin polarization)
- (v) relatively straightforward theoretical predictions of the main properties using the  $k.p$  model
- (vi) low enough carrier density to be modified with electrical fields and light

Among the most striking successes, one can cite :

- (i) the control of magnetism using circularly polarized light [150]
- (ii) the electric-field control of magnetic anisotropy [32, 16, 33]
- (iii) spintronics functionalities, such as tunneling AMR, the electrical spin injection into a semiconductor (GaAs) [209] or all-electrical read/write cycles [129]
- (iv) the presence of Rashba and Dresselhaus spin-orbit effective fields [31, 49]
- (v) the confirmation of the role of the carrier polarization sign for spin-transfer torque [2, 229]

# Chapter II

## Domain wall dynamics

> **Students involved:** Sanaz Haghgoo (PhD 2010-2013), Asad Syed Hassen (M2, 2011), Sylvain Shihab (M2 and PhD, 2012-2015), Benoit Boutigny (M2, 2013), Nicholas Gsken (M2, 2014). Post-doc: Marina Tortarolo (punctual visits 2010&2011)

> **Related publications:**

- *High domain wall velocities in in-plane magnetized (Ga,Mn)(As,P) layers*, [L. Thevenard](#), S. Hussain, J. von Bardeleben, M. Bernard, A. Lematre, C. Gourdon, *Physical Review B* 85 064419 (2012)
- *Fast domain wall dynamics in MnAs/GaAs films*, M. Tortarolo, [L. Thevenard](#), H. J. von Bardeleben, M. Cubukcu, V. Etgens, M. Eddrief, C. Gourdon, *Applied Physics Letters* 101, 072408 (2012)
- *Domain wall propagation in ferromagnetic semiconductors: Beyond the one-dimensional model*, [L. Thevenard](#), C. Gourdon, S. Haghgoo, J.-P. Adam, J. von Berdeleben, A. Lematre, W. Schoch, A. Thiaville, *Physical Review B* 83, 245211 (2011)
- *Domain-wall flexing instability and propagation in thin ferromagnetic films*, C. Gourdon, [L. Thevenard](#), and S. Haghgoo, A. Cebers, *Phys. Rev. B* 88, 014428 (2013)
- *Spin transfer and spin-orbit torques in in-plane magnetized (Ga,Mn)As tracks*, [L. Thevenard](#), B. Boutigny, N. Gsken, L. Becerra, C. Ulysse, S. Shihab, A. Lematre, J.-V. Kim, V. Jeudy, C. Gourdon, *Physical Review B* 95 054422 (2017)

### 1 Context

The expansion of domains under an applied field or current is not the result of a torque onto the domains, but rather on the magnetization within the interface separating them, the domain walls (DW). Their role is critical in the coercivity of hard magnets [54], domain or magnetic-bubble-based memory devices, domain-wall logic components [234], but also spin-valves, nano-oscillators and memristors [116].

The magnetic domains of (Ga,Mn)As were studied as early as 2000 [181], in order to gain some insight on magnetization reversal mechanisms, gauge the quality of the layers, or anticipate their influence on micro-patterned structures. Domain-wall dynamics started being explored in 2006, with the seminal papers of Tang and Yamanouchi [186, 229] on magnetic field or current-driven DW dynamics, respectively in an in-plane biaxial layer and an out-of-plane magnetized layer (Fig. II.2).

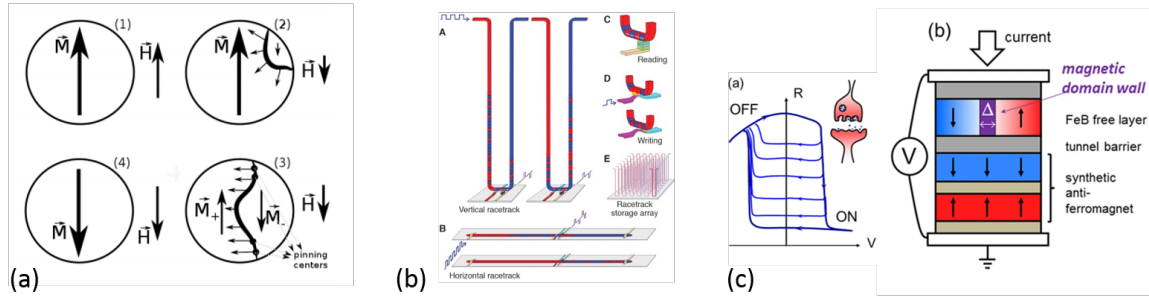


Figure II.1: (a) [54, 53] The coercivity of hard magnets such as NdFeB-based alloys was understood by D. Givord to be intrinsically due to their microstructure, which governs the nucleation, pinning and propagation of domain(-walls). (b)[153] The race-track memory proposed by S. S. Parkin relied on the sequential current-driven propagation of domain-walls, and a 3D geometry that would boost the density. (c) [116] Magnetic memristor mimicking the behavior of a biological synapse, by adopting different resistance levels depending on the stimulus: a domain-wall is shifted under current in the top layer.

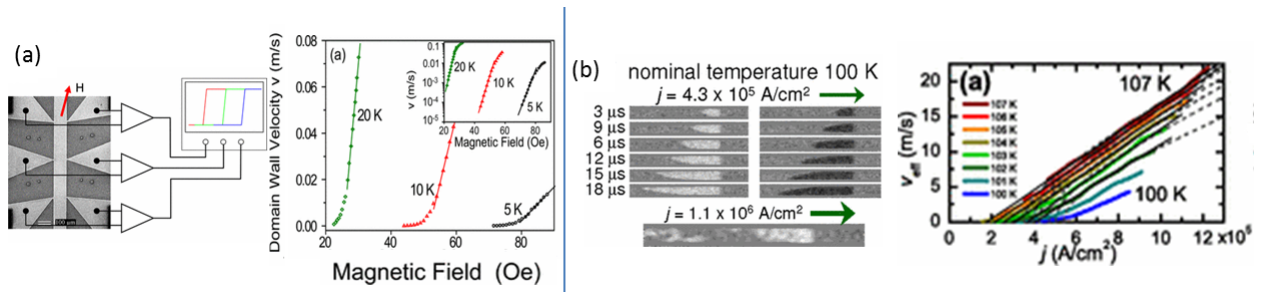


Figure II.2: (a) [186] Giant-planar Hall effect monitoring of the creep dynamics. Velocities follow an exponential law with in-plane drive field. (b)[229] Current-driven domain-wall dynamics. Threshold currents almost an order of magnitude lower than in metals were observed, due to the low saturation magnetization of (Ga,Mn)As. Working at constant cryostat temperature later turned out to be problematic to analyze the resulting  $v(J)$  curve since the Joule heating is substantial in this semiconductor.

Although the low Curie temperature ruled out using this material in any viable device, these studies provided valuable information on DW dynamics theory, and proved decisive in understanding spin-transfer torque driven domain-wall motion. Indeed, while being weakly magnetically doped, the material behaves very much like a “real” ferromagnet whose magnetic domain shape and domain-walls follow basic energy minimization principles between competing demagnetizing, Zeeman, and exchange energies. Because the anisotropy of (Ga,Mn)As can be adjusted continuously from in-plane biaxial or uniaxial, all the way to out-of-plane uniaxial, (Ga,Mn)As has been the perfect play-ground on which to test the dynamics of different domain-wall (DWs): uncharged Bloch, charged Néel or head-to-head/tail-to-tail (Fig. II.3).

The domain-wall dynamics studies we led at INSP since 2009 are a clear illustration of the versatility offered by this material. The following main results, detailed in the coming sections, were obtained:

- very high domain-wall propagation velocities (500 m/s) under field in in-plane magnetized (Ga,Mn)As [197]
- development of a semi-analytical model to explain velocity anomalies unaccounted for by the historical 1D model : these result from the excitation of domain-wall flexural modes [195, 61]
- competition between unusual spin-transfer, and spin-orbit torques in current-driven DW dynamics of in-plane magnetized (Ga,Mn)As layers [191]

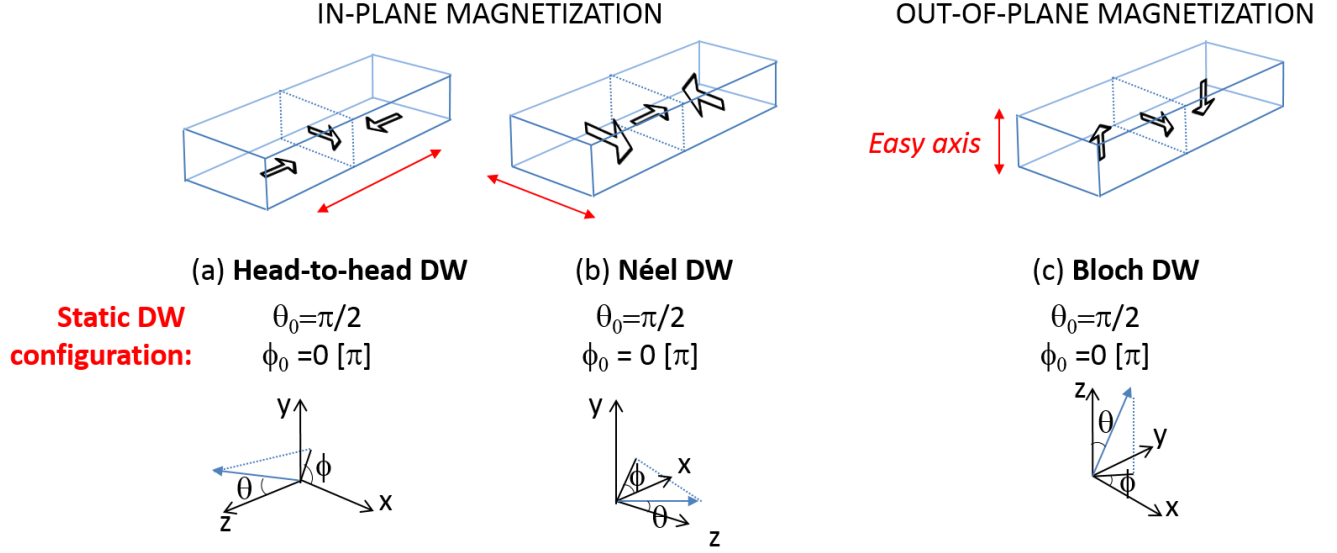


Figure II.3: The tunable anisotropy of (Ga,Mn)As makes it possible to study different types of domain-walls in a given material. An illustration here in the case of uniaxial anisotropy along [1-10] (a,b) or [001] (c). For each DW type, there are two possible orientations of the magnetization within the DW, i.e. two possible “winding” directions ( $\eta = \pm 1$  in Eq. II.1). By choosing the polar axis  $z$  along the magnetic easy axis, and  $(xz)$  the plane of the domain-wall, the angular-dependence of its width  $\Delta$  and velocity are identical for all 3 configurations (Eqs. II.1 and II.3).

## 2 Master equations

Before presenting our results, I am briefly summarizing below the different steps of the calculation of the domain-wall width, and velocity versus field in the flow regime.

### 2.1 Domain-wall width

The systems considered are thin films (thickness  $< 100\text{nm}$ ) that are either left bidimensional or patterned into narrow tracks of a few microns-width. Let us consider a stripe oriented along  $y$  of a material presenting two uniaxial anisotropies  $K_{2\parallel}$  and  $K_{2\perp}$ , respectively in-plane and out-of-plane. While (Ga,Mn)As also has second order cubic anisotropy terms  $K_{4\parallel}$ ,  $K_{4\perp}$ , dropping them for the description of the DW dynamics of *uniaxial* in-plane or out-of-plane (Ga,Mn)As layers has proved a decent hypothesis<sup>1</sup>. Within the domain-wall and in the absence of field, the energy of the system reads in the coordinates of Fig. II.3b for instance:

$$w = A_{ex} \left[ \left( \frac{\partial \theta}{\partial x} \right)^2 + \sin^2 \theta \left( \frac{\partial \varphi}{\partial x} \right)^2 \right] - K_{2\perp}^{eff} \sin^2 \theta \sin^2 \varphi - K_{2\parallel}^{eff} \cos^2 \theta$$

$A_{ex}$  is the exchange constant, and  $K_{2\parallel}$ ,  $K_{2\perp}$  have been replaced by  $K_{2\parallel}^{eff}$ ,  $K_{2\perp}^{eff}$  to take into account the effective anisotropy due to demagnetizing factors within the track cross-section (see for instance Aharoni *et al.* [3]). The ratio  $\kappa = \frac{K_{2\perp}^{eff}}{K_{2\parallel}^{eff}} < 0$  is defined. To obtain the static domain-wall width, the energy functional must be minimized, i.e.  $\frac{\delta w}{\delta \theta} = 0$  and  $\frac{\delta w}{\delta \varphi} = 0$ , which leads to the well-known domain-wall profile, static domain-wall width and energy  $\sigma_0$ :

$$\left\{ \begin{array}{l} \theta(x) = 2 \arctan[e^{\eta x / \Delta_0}] \\ \Delta_{0\parallel} = \sqrt{\frac{A_{ex}}{K_{2\parallel}^{eff}}}, \sigma_{0\parallel} = 4 \sqrt{A_{ex} K_{2\parallel}^{eff}} \quad \text{for in-plane magnetization} \\ \Delta_{0\perp} = \sqrt{\frac{A_{ex}}{K_{2\perp}^{eff}}}, \sigma_{0\perp} = 4 \sqrt{A_{ex} K_{2\perp}^{eff}} \quad \text{for out-of-plane magnetization} \end{array} \right. \quad (\text{II.1})$$

<sup>1</sup>But taking the biaxial anisotropy was necessary to explain the square domains found in certain conditions in (Ga,Mn)As [60]



The coefficient  $\eta$  corresponds to the two possible windings of the magnetization in the domain-wall. Typical values for (Ga,Mn)As are:  $\Delta_{0\perp} \sim 5\text{nm}$  and  $\Delta_{0\parallel} \sim 30\text{-}80\text{nm}$ .

## 2.2 “ $q - \varphi - \Delta$ ” model equations

There are two fundamentally different domain-wall dynamics regime:

- the **creep regime** where the DW behaves like an elastic interface exploring a pinning potential landscape (Fig. II.2a). Velocities are then generally low and follow an exponential law with drive (field or current). Creep studies in out-of-plane magnetized (Ga,Mn)As (and comparison to other materials) have proved very fertile for the search of “universality classes” of dynamics, i.e. evidencing a regime whose thermal activation physics is “universal”, e.g. equally relevant to wetting phenomena, the dynamics of ferroelectric domain walls or the propagation of fault lines [114, 86, 228].
- the so-called “**flow**” or “**steady-state**” regime where the propagation ignores pinning sites. The movement of this complex three dimensional vectorial object can, in the vast majority of cases, be described by that of a point-like magnetization in the center of the domain-wall, described by its position  $q$  and its angle  $\varphi$  with respect to the interface. This is the so-called “ $q - \varphi$ ” model, described in the much-cited seminal works of Thiele [204], Schryer & Walker [173], Slonczewski [182] and Malozemoff [123] (field-driven dynamics).

In the flow regime, the dynamics of the magnetization at the center of the domain-wall is described by the Landau-Lifshitz-Gilbert (LLG) equation:

$$\frac{\partial \vec{m}}{\partial t} = \gamma \mu_0 \vec{H}_{eff} \wedge \vec{m} + \alpha \vec{m} \wedge \frac{\partial \vec{m}}{\partial t} \quad (\text{II.2})$$

The effective field  $\mu_0 \vec{H}_{eff} = -\frac{\delta w}{\delta \vec{M}}$  contains magnetic anisotropy, exchange and Zeeman-like (applied field, non-adiabatic spin transfer, spin-orbit torques - see further in Sec. 5) terms. The outline of the calculation is detailed for a Néel DW under an in-plane field (Fig. II.4), and results for current dynamics given directly in the following sections.

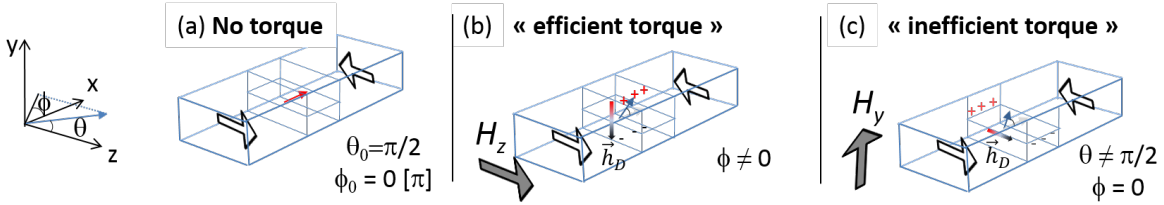


Figure II.4: General mechanism for Néel DW movement (here due to a field): (a) Static configuration. (b) An  $H_z$  field tilts the magnetization in the center of the domain-wall out of its plane. The torque of the resulting demagnetizing field onto the magnetization rotates the magnetization of the domain-wall, initiating movement. (c) An inefficient torque simply makes the magnetization rotate within the  $(xz)$  plane of the domain-wall.

Projecting Eq. II.2 in spherical coordinates gives:

$$\begin{cases} \dot{\varphi} \sin \theta = \frac{\gamma}{M_s} [-K_{2\perp}^{eff} \sin 2\theta \sin^2 \varphi + K_{2\parallel}^{eff} \sin 2\theta - 2A_{ex} \frac{\partial^2 \theta}{\partial x^2} + \mu_0 M_s H \sin \theta] + \alpha \dot{\theta} \\ \dot{\theta} \sin \theta = \frac{\gamma}{M_s} K_{2\perp}^{eff} \sin^2 \theta \sin 2\varphi - \alpha \dot{\varphi} \sin^2 \theta \end{cases} \quad (\text{II.3})$$

The key point of the “ $q - \varphi$ ” (or even “ $q - \varphi - \Delta$ ”) model is to suppose at this point that the domain-wall has the same type of profile as in the static regime, and moves without deformation :  $\theta(x, t) = 2 \arctan[e^{(x-q(t))/\Delta(t)}]$ ,

where  $q(t)$  denotes the center of the domain-wall and  $\Delta(t)$  is the dynamic domain-wall width<sup>2</sup>. One can then show<sup>3</sup> that Eq. II.3 becomes :

$$\left\{ \begin{array}{l} \dot{\varphi}(t) = \frac{1}{1+\alpha^2} \frac{\gamma}{M_s} [\mu_0 M_s - \alpha K_{2\perp}^{eff} \sin 2\varphi] \\ \dot{q} = \frac{\gamma}{M_s} K_{2\perp}^{eff} \sin 2\varphi - \alpha \dot{\varphi} \\ \Delta[\varphi(t)] = \sqrt{\frac{A}{K_{2\parallel}^{eff} - K_{2\perp}^{eff} \sin^2 \varphi(t)}} = \frac{\Delta_0}{\sqrt{1 - \kappa \sin^2 \varphi(t)}} \quad ; \quad \kappa < 0 \end{array} \right. \quad (\text{II.4})$$

### 2.3 Domain-wall propagation regimes: stationary and precessional

Based on these equations, which can be modified to account for current-induced torques (see Sec. 5), a domain-wall can propagate in two different regimes, stationary and precessional, separated by the so-called Walker break-down.

- **stationary regime:** under a  $H_z$  field, the magnetization progressively tilts out of the plane of the DW (Fig. II.4b). The resulting demagnetizing field that is created and the torque it induces corresponds to the  $\sin 2\varphi$  term of Eq. II.4. The field-induced tilt is exactly compensated by the damping, so that the magnetization remains at a constant angle within the domain-wall. Setting  $\dot{\varphi}(t) = 0$  in Eq. II.4 yields the stationary regime velocity  $\dot{q} = v_{steady}$  (Tab. II.1). When the tilt angle reaches  $\varphi = \pi/4$ , the magnetization cannot come further out of the DW plane since  $|\sin 2\varphi| = 1$ . This is the Walker breakdown field  $\mu_0 H_W = \frac{\alpha |K_{2\perp}^{eff}|}{M_s}$  (from Eq. II.4). It clearly appears that some torques will be more efficient than others: a field applied along  $y$  will have no effect, because colinear to the static magnetization in the domain-wall. An out-of-plane field (along  $y$  here) will rotate the magnetization in the plane of the domain wall. Because the track is usually much wider than it is thin, the torque of the resulting demagnetizing field will be weak (Fig. II.4c). Such a torque will thus be too inefficient to initiate domain-wall propagation, but will potentially play a role once the magnetization has started precessing within the wall.
- **Precessional regime:** beyond Walker breakdown, solving Eq. II.4 gives the explicit time-dependence of the precessing angle (Eqs. II.5), which inserted into the calculation of  $\langle \dot{q} \rangle$  yields the precessional velocity  $v_{prec}$  (Tab. II.1). The domain-wall center then essentially moves in a fairly inefficient “drunken” way, constantly going back and forth (see online animations). Different strategies have been explored to remain out of this regime such as structuring the track smartly to modify the charge of the domain-wall [117], engineering the domain-wall profile with Dzyloshinskii Moriya exchange interaction [64], or more recently working with ferrimagnets at angular compensation temperature [97].

$$\left\{ \begin{array}{l} \varphi_{prec}(t) = \arctan \left( \frac{H_W}{H} + \sqrt{1 - \left[ \frac{H_W}{H} \right]^2} \tan \left[ \frac{2\pi t}{T_{prec}} \right] \right) \\ T_{prec} = \frac{1+\alpha^2}{\gamma \mu_0 H_W} \frac{2\pi}{\sqrt{\left[ \frac{H_W}{H} \right]^2 - 1}} = \frac{2\pi}{\langle \dot{\varphi}_{prec}(t) \rangle} \end{array} \right. \quad (\text{II.5})$$

The final velocities and domain-wall widths are summarized below, and typical experimental and theoretical velocity versus field curves are shown in Fig. II.5.

<sup>2</sup> $\Delta(t)$  is often taken to be equal to the static  $\Delta_0$ , a legitimate assumption for anisotropy ratio  $|\kappa| \sim 1$ , much less justified for larger numbers as we'll see in Sec. 4.1.

<sup>3</sup>Using  $\frac{\partial \theta}{\partial x} = \frac{1}{\Delta(t)} \sin \theta$  and  $\frac{\partial^2 \theta}{\partial x^2} = \frac{1}{\Delta(t)^2} \sin \theta \cos \theta$

$$v_{steady} = \frac{\gamma \Delta_{steady}(H) \mu_0 H}{\alpha} ; \Delta_{steady}(H) = \frac{\Delta_0}{\sqrt{1 - \kappa \sin^2 \varphi(H)}}$$

$$\mu_0 H_W = \frac{\alpha |K_{21}^{eff}|}{M_s} \text{ for in-plane magnetization}$$

$$v_{prec}(t) = \frac{\gamma \langle \Delta_{prec} \rangle H}{\alpha} - \frac{\langle \Delta_{prec} \rangle}{\alpha} \gamma \mu_0 H_W \sqrt{\left[ \frac{H}{H_W} \right]^2 - 1} ; \Delta_{prec}(t, H) = \frac{\Delta_0}{\sqrt{1 - \kappa \sin^2 \varphi_{prec}(t, H)}}$$

Table II.1: Field-driven propagation: summary of steady and precessional velocities and domain-wall widths, and Walker fields. For out-of-plane magnetization, the Walker field does not depend on the crystalline anisotropy:  $\mu_0 H_W = \frac{\alpha M_s}{2} |N_z - N_x|$ .

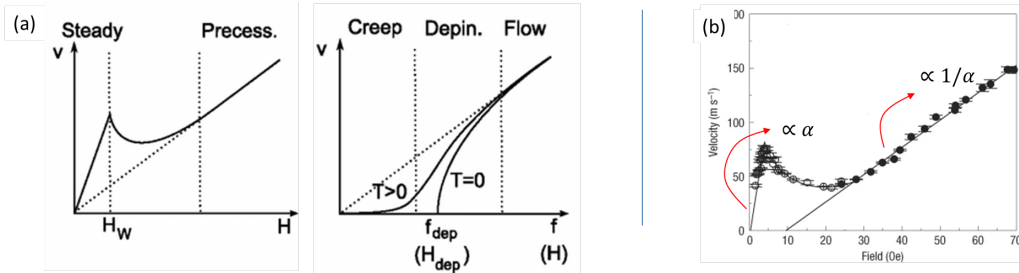


Figure II.5: (a) Adapted from [136] Theoretical variation of the velocity of a 1D interface in a 2D weakly disordered medium at zero and finite temperature,  $T$ . The creep, depinning, and flow regimes are labeled. (b) Adapted from [12] Domain-wall velocity versus field in Permalloy ( $\text{Ni}_{80}\text{Fe}_{20}$ ). stationary and precessional regimes clearly appear here.

### 3 Experimental tools for the study of domain-wall dynamics

The vast majority of papers rely on magneto-optical Kerr imaging to study DW dynamics : it is cost- and time-effective, and easily compatible with the cryogenics necessary for (Ga,Mn)As. But magnetotransport measurements [186], scanning Hall probe or scanning superconducting quantum interference device microscopy have also been used [181].

The studies presented below and in Chap. IV were performed on a **home-made Kerr microscope** first developed by C. Gourdon and V. Jeudy. It consists of an LED source ( $\lambda = 632 \text{ nm}$ ), a 0.4 numerical aperture objective, and high dynamic range “Clara” Andor camera ( $6.45 \mu\text{m}$  pixels,  $1046 \times 1396$  pixel sensor). An aperture diaphragm is conjugated with the *back* focal plane of the objective to provide defocused and homogeneous illumination of the sample (so-called Köhler illumination). The diaphragm is placed on a lateral piezo stage to swap between the polar Kerr configuration (normal incidence, sensitivity to the out-of-plane component of the magnetization) and the longitudinal Kerr one (oblique incidence at around  $20^\circ$  from the normal, sensitivity to the planar component of the magnetization in the incidence plane).

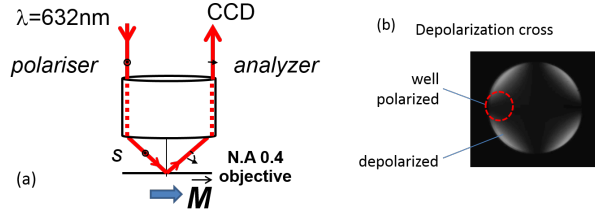


Figure II.6: (a) Oblique incidence obtained by deporting an aperture diaphragm focused in the back focal plane of the objective. (b) Image of the Fourier plane showing how an objective depolarizes a beam between crossed polarizer (see theory in [79]). Care must be taken to place the image of the aperture diaphragm on the arms of the cross (dotted red circle).

An important point to obtain decent longitudinal Kerr contrast has been: (i) to be very careful with stray light polluting the measurement, (ii) to make sure light arriving at large incidence hasn't been depolarized by the objective [79] (Fig. II.6b). Note that the necessity to have the sample in a cryostat rules out larger incidence angles, since very high NA objectives usually have very short working distances and depolarize a lot at non-zero incidence.

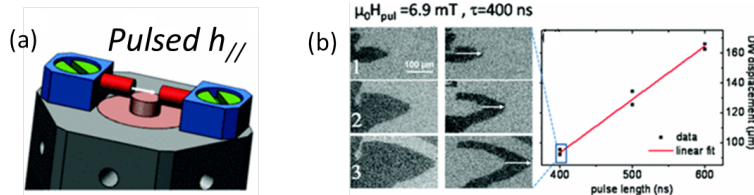


Figure II.7: (a) Micro-coils placed in the cryostat to create a pulsed in-plane field. (b) [197] Methodology for DW velocity measurement - The layer is saturated using a DC external field. A pulsed field of opposite sign then nucleates and propagates the domains. After each field or current propagation pulse, a snapshot is taken in zero field and the DW displacement measured on one or several domains. A linear regression of the displacement versus pulse length then gives the velocity. For a given field/current, between 3 and 5 different pulse lengths are used to eliminate the effect of the transients. Note that the fit has a negative  $y$ -intercept resulting from the finite rise time of the pulse and of the depinning field. Whereas out-of-plane domains are usually roughly circular in the plane, propagating isotropically, in-plane domains are pointy, in order to minimize the magnetostatic energy.

## 4 Field-driven dynamics

### 4.1 High domain-wall velocities in planar layers

When looking at the steady-state velocity,  $v_{steady} = \frac{\gamma \Delta_{steady}(H) \mu_0 H}{\alpha}$ , with  $\Delta_{steady}(H) = \frac{\Delta_0}{\sqrt{1 - \kappa \sin^2 \varphi(H)}}$ , one notices that:

- high mobilities will be obtained with large domain-walls and/or low damping. However there were, in 2010, surprisingly few studies on domain-wall propagation in planar materials other than Permalloy - which hosts wide DWs, velocities up to 400m/s [12, 73] - compared to perpendicularly magnetized materials - with narrow DWs and velocities in the 30-100m/s range [64, 44].
- this simple model does not take into account DW pinning, which leads to a threshold in the velocity, so that the intrinsic velocity then rejoins either the stationary or the precessional regime (Fig. II.5a).
- the DW velocity depends crucially on the ratio of the anisotropies,  $\kappa = \frac{K_2^{eff}}{K_2^{||}}$ , and on the values of the anisotropies themselves. This parameter intervenes in how the domain-wall width shrinks with field, which directly reflects on the maximum velocity and the shape of the stationary regime: from a linear field-dependency ( $|\kappa| \sim 1$ ) to a hump-back shape exhibiting a wide plateau (large  $|\kappa|$ , Fig. II.8a). In most magnetic metals,

this ratio cannot be tuned. For instance in Permalloy nanowires, the magnetic anisotropy mainly results from the shape of the wire, and typical  $|\kappa|$  values are close to 1.

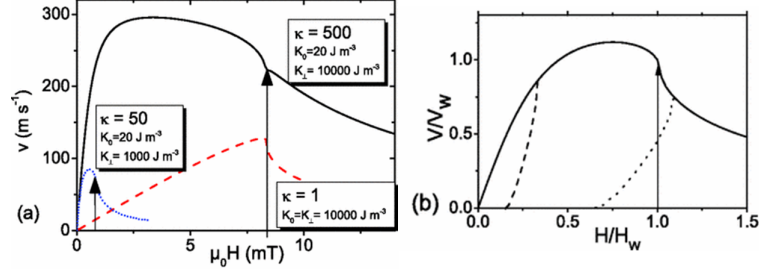


Figure II.8: [197] Computed 1D model  $v(H)$  curves. Vertical arrows indicate the Walker field. (a) Varying in-plane (here  $K_0$ ) and out-of-plane (here  $K_\perp$ ) anisotropies. No pinning. (b) When pinning is taken into account, the DW velocity may rejoin the intrinsic regime before Walker breakdown (dashed line) or afterwards (dotted line).

In (Ga,Mn)As on the contrary, a broad window can be explored, typically  $|\kappa| = 20\text{--}200$  for our samples, since  $K_{2\parallel}$  and  $K_{2\perp}$  can be adjusted during the growth by varying the lattice mismatch of the layer with its substrate - either by co-doping it with phosphorus, or by introducing more manganese (see Chap I, Sec. 2). It was thus the ideal material on which to test these ideas and predictions. There was at the time little in way of comparison, since the only published dynamics data on planar (Ga,Mn)As were in the creep regime [75, 186], with velocities below 0.1m/s (Fig. II.2a). We measured the DW velocity versus field in four (Ga,Mn)As samples with an in-plane easy axis along [1-10], and  $K_{2\parallel}$ ,  $K_{2\perp}$  anisotropies in different ratios.

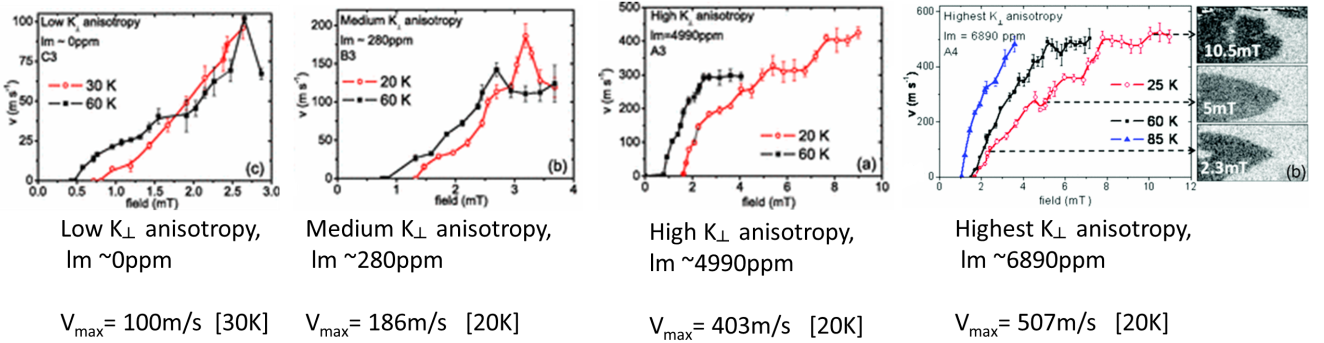


Figure II.9: [197] Domain wall velocity versus applied field in the  $[Mn]_{eff}=3.7\%$  series in order of increasing lattice mismatch ( $lm$ ) and uniaxial out-of-plane anisotropy.

This data very clearly confirmed that large domain-wall velocities (up to 500m/s) could be obtained, ten-fold higher than any recorded velocity in (Ga,Mn)As, provided the anisotropy is well chosen. This results from the increase of the domain-wall width with decreasing in-plane anisotropy, and the increase of the maximum accessible velocity with both DW width and  $K_{2\perp}^{eff}$  anisotropy:  $V_{max} = 2V_W \frac{\sqrt{1+\kappa}-1}{\kappa}$  where  $V_W = \frac{\gamma \Delta_{steady} K_{2\perp}^{eff}}{M_s}$ . Finally, the shape of the  $v(H)$  curve evolves in the series, and we could convince ourselves by overlaying this data with the 1D-model calculations of the  $v(H)$  curve (see Ref. [197] for details) that the two samples with the lowest anisotropy ( $lm$  0 and 280ppm) had a Walker field low enough for the measured peak velocity to arrive *after* breakdown (dotted line scenario in Fig. II.8b), while the last two ( $lm$  4990 and 6890ppm) depinned early enough to be able to rejoin the stationary steady state *before* Walker breakdown (dashed line scenario in Fig. II.8b). The high  $K_{2\perp}^{eff}$  anisotropy of these two samples is also responsible for the velocity plateaus observed (Fig. II.8a).

- During short visits of Marina Tortarolo (International French Argentinian Nanoscience Laboratory LIFAN between CNEA, CONICET, Argentina and CNRS, France), **a similar study was led on a 300nm thick MnAs/GaAs layer**. This material is another promising candidate for spintronics as it can be grown on GaAs. It exhibits a very strong in-plane uniaxial anisotropy ( $K_{2\parallel}, K_{2\perp} \sim 3.10^5 J/m^3$ ), responsible for saw-tooth type domains (Figs. II.10a-c), and a second order magnetostructural transition around room temperature, with the paramagnetic “beta” phase nucleating as early as 270K. The field-driven domain-wall dynamics study showed that very large velocities could be obtained far from the Curie temperature, up to 1km/s (Fig. II.10d). In this material, the high velocities do not stem from a wide domain-wall ( $\Delta_0 \sim 5\text{-}10$  nm) but rather from the large  $K_{2\perp}^{eff}$  term.

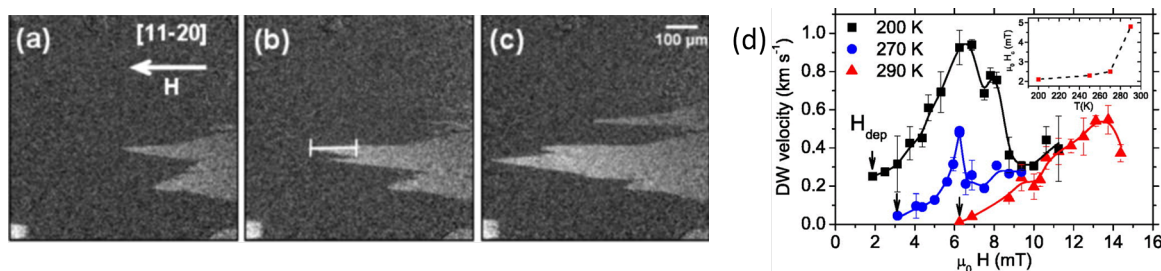


Figure II.10: [206] (a-c) Longitudinal Kerr microscopy images of MnAs magnetic domains taken at  $T=270$  K after 3 successive field propagation pulses. (d) DW velocity as a function of applied field. (inset) Dependence of the coercive field on temperature evidencing the onset of the paramagnetic beta stripes at around 270 K.

## 4.2 Role of flexural modes in domain-wall dynamics

We wished to address an intriguing observation: several articles reported “bumps” in the field-dependence of the domain-wall velocity curve, not anticipated by the 1D model described above. This seemed to occur in both in-plane and out-of-plane magnetized materials (Fig. II.11). An intuition formulated in 2008 by C. Gourdon and V. Jeudy was that these bumps resulted from an inherent limitation of the 1D model: the fact that it does not take into account a realistically 3D nature of the DW, both within the thickness of the film and along the length of the 2D interface (flexural modes calculated by Schlömann for instance [172]). We set out to explore this first hypothesis by studying the influence of the *thickness* of the (Ga,Mn)As layer on the domain walls’ 3D structure and velocity - experimentally, numerically and analytically. This work was done in collaboration with A. Thiaville and J.-P. Adam (LPS) who performed the initial simulations, A. Lemaître (LPN) and W. Schoch (Institut für Quantenmaterie, Ulm) who made the (Ga,Mn)As samples.

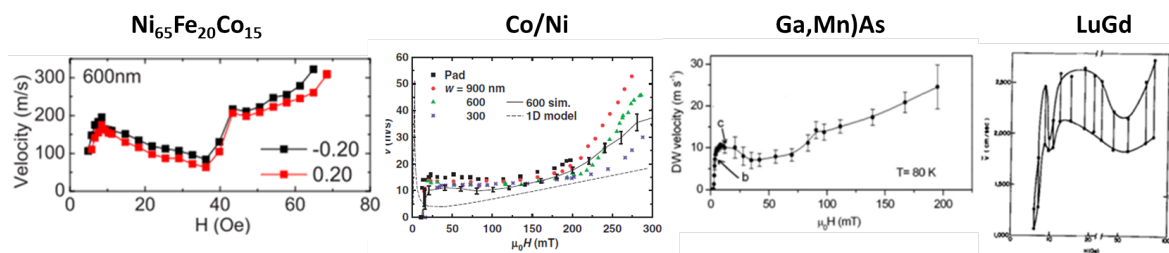


Figure II.11: Bumps in the precessional regime observed in different materials: (a) [140] In-plane magnetized tracks of  $Ni_{65}Fe_{20}Co_{15}$ . (b) [227] Out-of-plane magnetized Co/Ni multi-layers. (c) [44] Out-of-plane magnetized (Ga,Mn)As. (d) [210] Average wall velocity during bubble collapse in out-of-plane magnetized LuGd.

We measured velocity versus field in 20, 40 and 50 nm thick out-of-plane magnetized samples and evidenced that, although the  $v(H)$  curves roughly followed the 1D model prediction, they indeed also evidenced anomalies, namely kinks in the precessional regime, one at low field, one at high field (Fig. II.12).

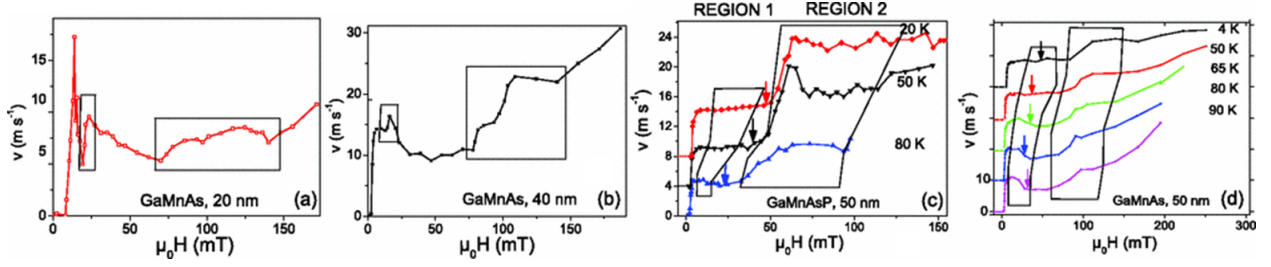


Figure II.12: [195] Velocity versus field for layers of different thickness  $h$ : (a)  $\text{Ga}_{0.93}\text{Mn}_{0.07}\text{As}$ ,  $h = 20$  nm. (b)  $h = 40$  nm. (c)  $\text{Ga}_{0.92}\text{Mn}_{0.08}\text{As}_{0.9}\text{P}_{0.1}$ ,  $h = 50$  nm. (d)  $\text{Ga}_{0.93}\text{Mn}_{0.07}\text{As}$ ,  $h = 50$  nm (from Ref. [44]). Polygons indicate the velocity anomaly regions, labeled 1 and 2. The arrows point to the  $H = 0$  resonance fields of the DW flexural modes, determined numerically.

We then performed the same “experiment” using micromagnetic (OOMMF) simulations on infinite layers of thickness 10 to 40 nm. Analyzing the time-dependence of the mean position of the domain-wall gives the velocity versus field (Fig. II.13), in which we clearly see a bump appearing as the thickness of the layer is increased to values greater than the exchange length ( $\Lambda_{ex} = \frac{2A_{ex}}{\mu_0 M_s^2} \sim 10$  nm). In the snapshot of Fig. II.13, one can clearly see that the DW twists and elongates during its motion, all the more so at the magnetic fields giving a velocity bump (Fig. II.13c). Moreover, we established by a separate set of simulations that the “kink” fields are exactly those at which the domain-wall precession frequency is equal to the eigen-frequency of the freely oscillating domain-wall. Very much like a pinched string of decreasing length resonates at increasing pitch, this resonance frequency becomes higher as the layer becomes thinner, pushing the resonance to higher fields.

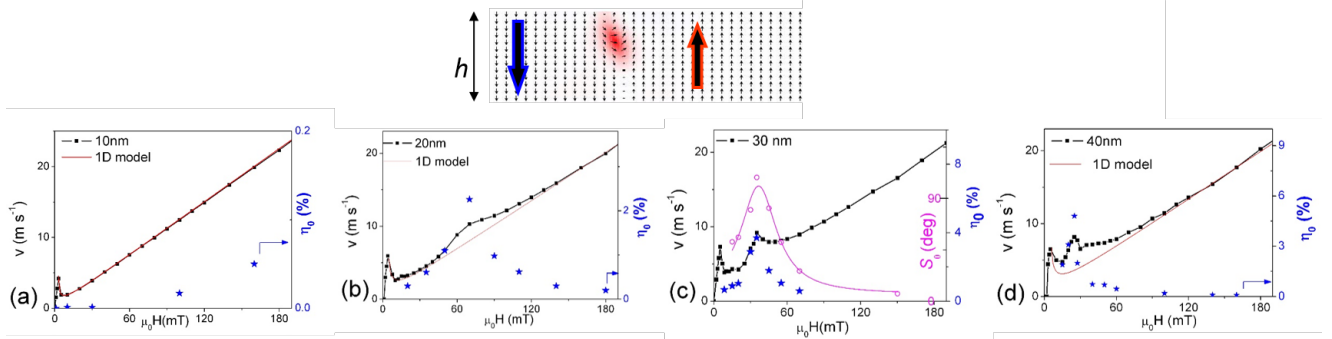


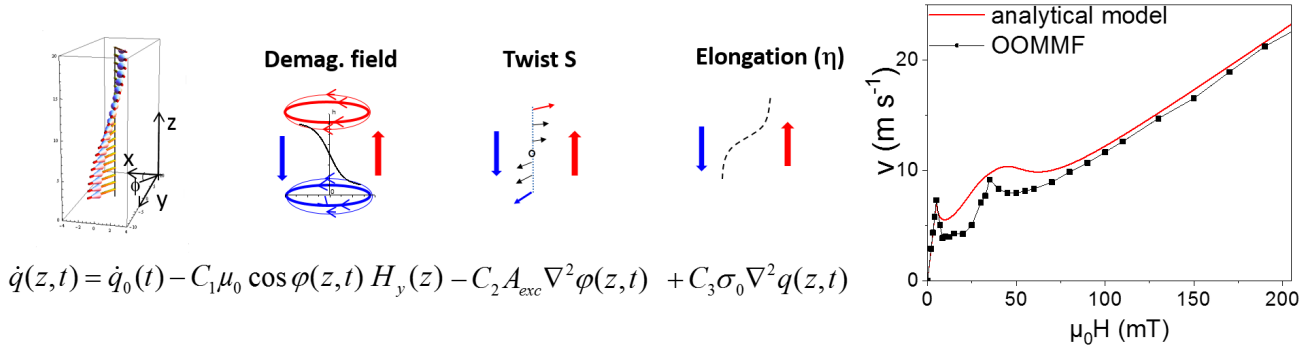
Figure II.13: [195] Snap shot of simulation (cross-section showing elongation and twist), clearer in full [movie on-line](#) made by A. Thiaville [*GMA-dyn30fx.avi*]. (a-d) Simulated velocity versus field (squares):  $h = 10, 20, 30$  and  $40$  nm. The stars are the maximum DW elongation  $\eta_0$ , and the open circles are the twist amplitude  $S_0$  (only shown for  $h=30$ nm for illustration purposes).

A reconstruction of the DW dynamics was done by analyzing the images of the simulations, in which each pixel at altitude  $z$  contains  $m_x(z, t), m_y(z, t), m_z(z, t)$  - see Fig. II.14 for a snapshot and [online animation](#) for the full movie [*DW\_flex\_phi\_stray.avi*]. Two effects - twist and elongation - are periodic and coupled, the domain-wall twist being maximum when the elongation is minimum, and vice-versa. To explain how they could affect the velocity, we developed a semi-analytical model (Fig. II.14) in which the *elastic* domain-wall energy was modified to account for the extra energy cost due to:

- a lengthening of the DW  $\propto \nabla^2 q(z, t)$
- a twist of the DW (exchange cost  $\propto A_{exc} \nabla^2 \varphi(z, t)$ )
- a time/space dependent demagnetizing field term stemming from the torque between the twisting DW magnetization and the static  $H_y(z)$ ,  $y$ -component of the stray field arising from up- and down-domains on either side of the DW (see [online animation](#) [*DW\_phi\_flex.avi*]).

By injecting the time/space dependence of twist and elongation found in the simulation into the analytical formula for  $\dot{q}(z, t)$  (Fig. II.14), the velocity was calculated as  $v = \langle \dot{q}(z, t) \rangle = \frac{1}{h} \frac{1}{T_{prec}} \int_{z=0}^h \int_{t=0}^{T_{prec}} \dot{q}(z, t) dz dt$ . The velocity kink was well reproduced, and shown to be due mainly to the “demag” term. It requires the DW to be twisted not to average out to zero ( $\cos\varphi(z, t)$  term in the equation of Fig. II.14).

While these conclusions on the numerics were quite satisfying, it was somewhat more disappointing in explaining our experimental data. The DW resonance fields estimated from OOMMF simulations for  $h=50$  nm were of the right order of magnitude to explain the low field anomalies, but slightly higher (arrows in Fig. II.12). The higher field velocities anomalies on the other hand were left unexplained; they are possibly due the parametric excitation put forward by Randoshkin [160] whereby the bulk spinwaves of the domains couple to the DW magnetization, thus providing an efficient energy dissipation channel, leading to a velocity increase.



$$\dot{q}(z, t) = \dot{q}_0(t) - C_1 \mu_0 \cos \varphi(z, t) H_y(z) - C_2 A_{exc} \nabla^2 \varphi(z, t) + C_3 \sigma_0 \nabla^2 q(z, t)$$

Figure II.14: **[195]** Snapshot of the DW twist and elongation reconstructed from OOMMF .ovf images (full movie [online](#)). Equation and schematics of the three components of the elastic DW model, and resulting calculation of the velocity versus field ( $h=30$ nm) - see corresponding article for the explicit expressions of the  $C_i$ .

## 5 Current-driven dynamics

As early as 1978, Berger imagined that : “electrons crossing a wall apply a torque to it, which tends to cant the wall spins” [14]. The early 2000s saw a huge effort dedicated to evidencing experimentally, optimizing and modelling these spin-transfer torques (STT), in parallel to the work being done on STT-driven magnetization reversal in spin-valves. Because (Ga,Mn)As is one of the rare hole-mediated ferromagnets, it proved decisive to demonstrate that the direction of propagation under STT - against or along the current direction - was indeed governed by the sign of the spin-polarization [2, 230, 37]. All these measurements were done on out-of-plane magnetized (Ga,Mn)As.

By the end of that decade, the limits of STT were appearing, among which the need for large current densities, and an efficiency capped by the - potentially mediocre - spin-polarization of the material and inconveniently inversely proportional to the layer thickness. The discovery that a pure spin-current generated in an adjacent layer via spin-orbit coupling could exert an efficient torque on the magnetization gave new impetus to the field [126], but also forced researchers to question their analysis of previous data [147, 137, 138]. Because of the sizable spin-orbit coupling in (Ga,Mn)As, this material again fed the discussion, with several articles reporting field-like (“efficient” in the sense of Fig. II.4) and anti-damping-like (“inefficient”) torques in *mono-domain* samples [49, 107, 31]. Contrary to the work being done on metals however, their role in domain-wall propagation was not explored. This is what we did at INSP between 2013 and 2015, in collaboration with V. Jeudy and A. Thiaville (LPS) and Joo-Von Kim (IEF, now C2N).

### 5.1 Current-induced spin-transfer and spin-orbit torques

In presence of current, several torques can be added to the LLG equation (Eq. II.2):



$$\frac{\partial \vec{m}}{\partial t} = \gamma \mu_0 \left( \vec{H}_{eff} + \vec{H}_{SO} \right) \wedge \vec{m} + \alpha \vec{m} \wedge \frac{\partial \vec{m}}{\partial t} - (\vec{u} \cdot \vec{\nabla}) \vec{m} + \beta \vec{m} \wedge [(\vec{u} \cdot \vec{\nabla}) \vec{m}] + \xi \vec{m} \wedge \vec{H}_{SO} \wedge \vec{m} \quad (\text{II.6})$$

The velocity under field and current in the steady and precessional states then becomes [203]:

$$\boxed{v_{steady} = \frac{\beta}{\alpha} u + \frac{\gamma \Delta_{steady}(H,u) \mu_0 H}{\alpha} \quad v_{prec} = \frac{\gamma \Delta_{prec} H}{\alpha} + \frac{\beta}{\alpha} u - \frac{\Delta_{prec}}{\alpha} \gamma \mu_0 H_{W0} \sqrt{\left[ \frac{H}{H_{W0}} + \frac{u}{u_{W0}} \right]^2 - 1}}$$

Breakdown is reached when  $\left| \frac{H}{H_{W0}} + \frac{u}{u_{W0}} \right| = 1$ . For in-plane magnetization:  $\mu_0 H_{W0} = \frac{\alpha |K_{2,1}^{eff}|}{M_s}$  and  $u_{W0} = \frac{\gamma |K_{2,1}^{eff}| \Delta_{\pi/4}}{M_s} \frac{\alpha}{(\beta - \alpha)}$  with  $\Delta_{\pi/4} = \frac{\Delta_0}{\sqrt{1 - \kappa/2}}$ .

> **Spin-transfer-torques** are proportional to the drift velocity  $u = \frac{JP_c g \mu_B}{2e M_s}$ , with  $P_c$  the carrier polarization and  $M_s$  the saturation magnetization. They require a magnetization gradient for the polarized current to transfer angular momentum to the domain-wall, either adiabatically ( $-(\vec{u} \cdot \vec{\nabla}) \vec{m}$  term) or non-adiabatically ( $\beta \vec{m} \wedge [(\vec{u} \cdot \vec{\nabla}) \vec{m}]$  term). The phenomenological constant  $\beta$  was introduced in 2005 [203, 236], and accounts for many different microscopic phenomena leading to spin relaxation such as spin-flip scattering or DW-induced relaxation. In metals it also covers the appearance of a DW resistance at abrupt interfaces [213], leading to a momentum transfer force never clearly identified experimentally [187, 66]. In (Ga,Mn)As,  $P_c < 0$  because of the antiferromagnetic coupling between holes and Mn spins, so that the DW is expected to move *against* the carrier flow (Fig. II.15).

There is a sizable spin-orbit coupling in GaAs - and therefore in (Ga,Mn)As - responsible for its strong anomalous Hall effect for instance. The heavy-light hole splitting modifies the usual spin transfer torques in the presence of a domain wall since valence states are not pure spin states. A significant hole reflection should occur at the domain-wall, leading to spin accumulation with predicted current mobilities  $\frac{\partial v}{\partial u} = \beta/\alpha \sim 8$  [52, 66], whereas experimental studies on OOP samples rather converged to a ratio of  $\beta/\alpha \sim 1$  [36, 2]. The super  $\beta$ -STT was shown to result microscopically from an “intradband” contribution to the spin-relaxation, i.e. how band populations are modified by an electric field via the Fermi-Dirac coefficient in the presence of strong spin-orbit interaction [52]. Interestingly, Garate *et al.* [52] predicted for this component a sign *opposite* to the traditional adiabatic STT - with no clear hand-waving argument as to why. It had up to then not been evidenced conclusively, but the high expected mobilities made it quite attractive, as it meant one could overcome the intrinsic limited efficiency of a total momentum-conserving torque transferring exactly  $\hbar$  between conduction carriers and local magnetic moments.

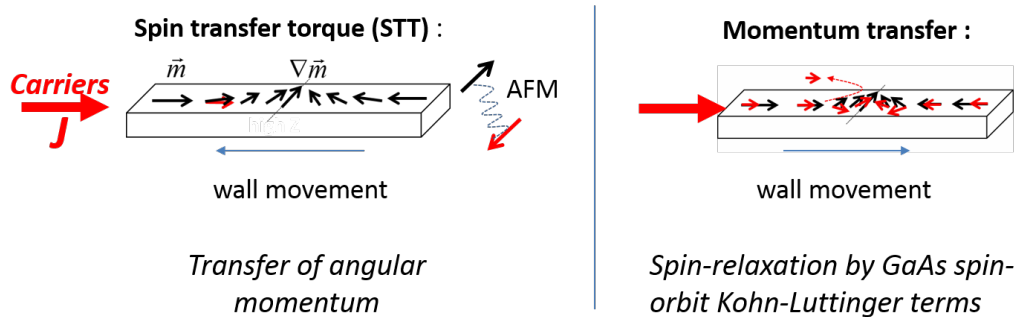


Figure II.15: Schematics of the different current-driven torques acting on (Ga,Mn)As domain-walls: spin-transfer, and momentum transfer, predicted by Garate *et al.* [52] to be of opposite sign in (Ga,Mn)As .

> **Spin-orbit torques**

In (Ga,Mn)As, spin-orbit coupling gives rise to two effects very different in magnitude. The main one is described by the Kohn-Luttinger (KL) Hamiltonian, which splits heavy holes ( $J = \pm 3/2$ ) and light holes ( $J = \pm 1/2$ ) states (see Chap. I). The second and much weaker effect is a lifting of this degeneracy analogous to a  $k$ -dependent magnetic field. This small spin-orbit effect arises from the lack of centrosymmetry of the zinc-blende lattice ( $k^3$  Dresselhaus term). A further lowering of the symmetry induced by epitaxial strain yields a Dresselhaus term linear in  $k$ . An even weaker Rashba term, also linear in  $k$ , exists due to the nonequivalence of  $[110]$  and  $[\bar{1}\bar{1}0]$  directions induced during the growth, formally equivalent to an in-plane shear strain or an electric field perpendicular to the interface (see Chap. I, Sec. 2.2). This is reminiscent of the one encountered in the  $z$ -asymmetric metallic stacks [138].

In (Ga,Mn)As, the Rashba and Dresselhaus spin-orbit interaction splitting of the valence bands results in the appearance of an out-of-equilibrium hole spin polarization under current. The antiferromagnetic exchange interaction between the carrier spins and the Mn spins then yields corresponding effective spin-orbit fields [31, 107, 49]. These fields are fairly small, typically a few tens of mT/TA/m<sup>-2</sup>. They are about 100 times weaker than the Rashba term in metals which were claimed to be responsible for fast DW dynamics against the electron direction [138]. There are two other important differences: (i) in (Ga,Mn)As, these spin-orbit fields come from the *bulk* of the sample, and do not require neighboring heavy-metal layers, (ii) because the layers do not need to be very thin for these fields to exist, the spin transfer torque is still sizable, and in direct competition with spin-orbit torques.

Dresselhaus and Rashba spin-orbit terms in strained (Ga,Mn)As induce a total effective field  $\vec{H}_{so}$  proportional to the current density, whose direction depends on the crystallographic direction considered. Similar to what has been calculated and observed in metals [218, 125], this field can act on the magnetization via two torques (Eq. II.6) [49, 107, 31]: a field-like torque (FL-SOT  $\vec{H}_{so} \times \vec{M}$ ) or a Slonczweski-like torque (SL-SOT,  $\xi \vec{M} \times (\vec{H}_{so} \times \vec{M})$ ). These will be “efficient” or “non-efficient” (in the sense of Fig. II.4) on domain-wall propagation depending on the DW type.

## 5.2 Intriguing observations, a possible evidence of momentum transfer ?

To study the effects of these spin-orbit coupling induced torques, two types of (Ga,Mn)As tracks were patterned from an in-plane uniaxial layer, using a hydrogen passivation technique developed at LPN during my thesis [201]. The idea was to have two configurations, where spin-orbit fields would be either parallel or perpendicular to the magnetization within the domain-wall.

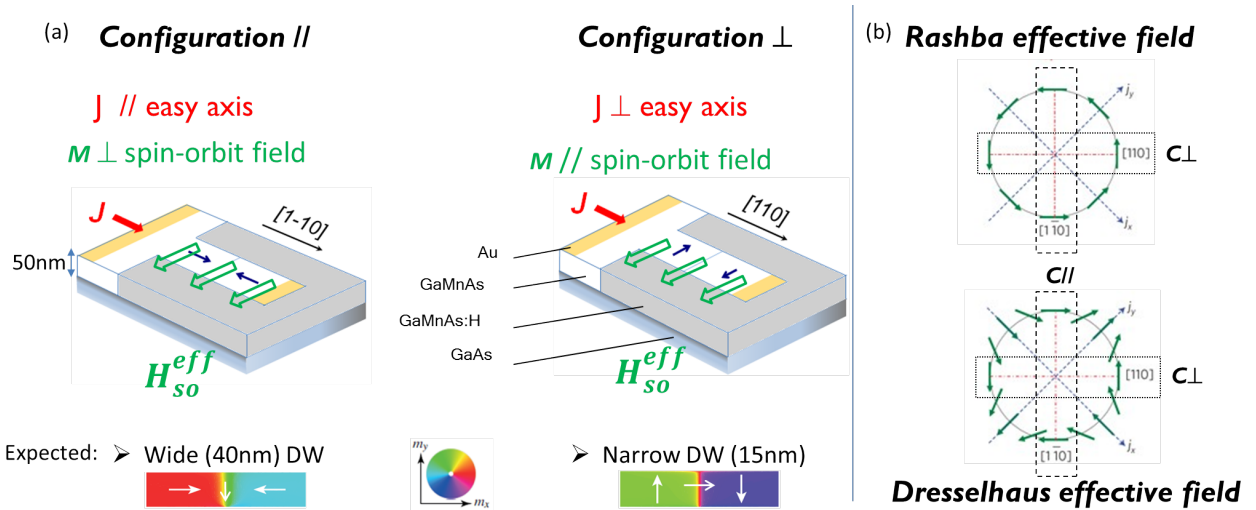


Figure II.16: [195] (a) Two types of tracks on which to study current-driven domain-wall propagation. The spin-orbit field can be either perpendicular ( $C_{\parallel}$ ) or collinear ( $C_{\perp}$ ) to the magnetization, a configuration usually difficult to obtain due to the lack of strongly uniaxial in-plane metals subject to spin-orbit fields. The width of the domain-wall is also expected to be in a ratio of almost 3 between the two configurations. (b) [31] Expected orientation of Dresselhaus and Rashba effective spin-orbit fields for different directions of the current.

We then performed current- and field-driven domain-wall propagation experiments (see methodology in Sec. 3). Two very surprising observations came out, confirmed by repeated and thorough measurements:

- In the  $C_{\parallel}$  tracks, DWs propagate *opposite* the direction expected from Spin Transfer Torque, in the direction of the hole current, and not opposite as observed in out-of-plane magnetized (Ga,Mn)As. In the  $C_{\perp}$  tracks, this effect seems to be in competition with another, “field-like” effect (that distinguishes  $\downarrow\uparrow$  and  $\uparrow\downarrow$  domain arrangement), that blocks every-other domain-wall (Fig. II.17).
- In both of these tracks, the DW mobility under current was very high, with an equivalent ratio of  $\beta/\alpha \sim 10$ , instead of the “usual” ratio of 1.

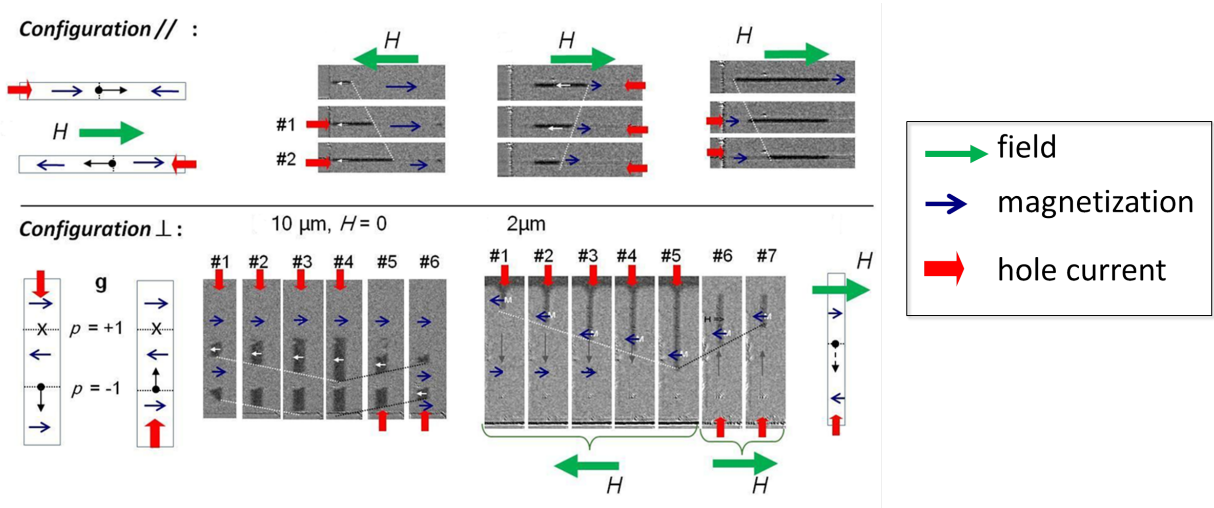


Figure II.17: [191] Summary of the phenomenology observed under current + field, for 2 and 10 micron-wide tracks - longitudinal Kerr microscopy. A field was necessary to depin domain-walls for the narrower tracks. Unexpected DW propagation direction: along the hole current for the  $C_{\parallel}$  tracks, and either along the hole current or blocked for  $C_{\perp}$  tracks, as if an opposite effect was in competition for some domain polarity  $p$ .

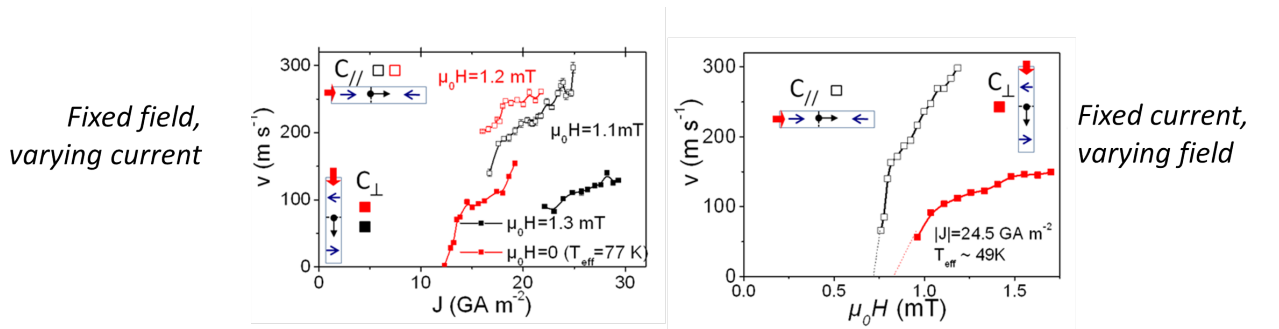


Figure II.18: [191] Under current assisted by field, the domain wall mobility  $\frac{\partial v}{\partial J}$  is ten times higher than in out-of-plane magnetized samples (equivalent ratio of  $\beta/\alpha \sim 10$ ). Under field assisted by current, the mobility  $\frac{\partial v}{\partial B}$  varies as expected with the domain-wall width, i.e. it is higher for the tracks with wider DWs.

By studying the DW depinning fields under current of positive and negative polarity, we were able to extract the respective efficiency of the two effects - the “STT-like” torque that pushes all the DWs in the same direction, and the “field-like” torque that behaves differently for  $\downarrow\uparrow$  and  $\uparrow\downarrow$  interfaces. The amplitude and sign of the latter

strongly pointed to an effective spin-orbit field, sum of Dresselhaus and Rashba fields. It was indeed completely inefficient for  $C_{||}$  tracks. Concerning the “STT-like” torque, we convinced ourselves that the very high  $\frac{\partial v}{\partial J} > 0$  DW mobility could not be explained by the arguments put forward in metallic structures, where similar effects were evidenced [138, 4, 131]. The existence of an efficient Kohn-Luttinger SOI momentum-transfer mechanism (predicted by Garate *et al.* [52]), overshadowing the usual spin-relaxation channel seems so far the most likely candidate. A very unsatisfying point of this conclusion is that this torque would somehow need to be much stronger for in-plane than for out-of-plane (Ga,Mn)As layers. We have not found any explanation for this, and hope someone will endeavor to repeat these experiments.

\* \* \*

The rich domain-wall physics unraveled in (Ga,Mn)As was made possible by the fact that, despite its quite weak concentration of magnetic atoms (less than 3% of the total number of atoms), it behaves in many ways like a “real” metallic ferromagnet, to which the Landau-Lifshitz-Gilbert equation, the Stoner Wohlfarth model, and the theory of domains can be applied. Again, most of the exciting features observed are related to the spin-orbit interaction governing the valence band structure.

# Chapter III

## Light-induced magnetization dynamics

> **Students involved:** Colin Delfaure (M1, 2011), Sylvain Shihab (PhD, 2012-2015), Hassen Riahi (short-term stays in 2013-2014 during his PhD in Tunisia), Hazem Bakr (M2, 2015), Piotr Kuszewski (PhD, 2015-2018), Meriam Kraimia (PhD 2016-2020)

> **Related publications:**

- “Counter-rotating standing spin waves: A magneto-optical illusion” S. Shihab, [L. Thevenard](#), A. Lemaître, and C. Gourdon, Physical Review B 95 144411 (2017)
- “Steady-state thermal gradient induced by pulsed laser excitation in a ferromagnetic layer”, S. Shihab, [L. Thevenard](#), A. Lemaître, J.-Y. Duquesne and C. Gourdon, J. Appl. Phys. 119, 153904 (2016)
- “Systematic study of the spin stiffness dependence on phosphorus alloying in the ferromagnetic semiconductor (Ga,Mn)As”, S. Shihab, H. Riahi, [L.Thevenard](#), H. J. von Bardeleben, A. Lemaître, Appl. Phys. Lett. 106 142408 (2015)

### 1 Context

The general idea of light-driven magnetization dynamics is to kick the system out of thermal equilibrium by a laser “pump” pulse, and then detect the dynamics using magneto-optical effects and a time-delayed “probe” pulse. Different mechanisms can be at work, e.g. a modification of the magnetic anisotropy via a transient variation of the temperature or the carrier density (photocreation of electron-hole pairs [72]), a decrease of the saturation magnetization by thermal or superdiffusive hot electron currents [13], or an effective field created by spin-polarized photo-electrons (“optical spin torque” [145], Fig. III.4). By mastering these physics, one could hope to control the magnetization all-optically, and on GHz timescales.

(Ga,Mn)As initially appeared as a model material with which to understand demagnetization processes [215]: light pulses falling on a ferromagnet excite carriers, whose temperature balances out with the lattice over a few picoseconds, before transferring to the magnetic system, leading to a decrease of the total magnetization. Because mobile carriers and localized spins are well separated in (Ga,Mn)As (as opposed to metals), one could hope to pinpoint more accurately the mechanisms of energy and angular momentum transfer between these different reservoirs. In fact, demagnetization studies were overall minority in (Ga,Mn)As, with instead a strong effort geared towards controlling coherent precession. Yet, these experiments were also a relevant probe of spin-orbit coupling, spin relaxation and coherence effects that are critical for spintronics.

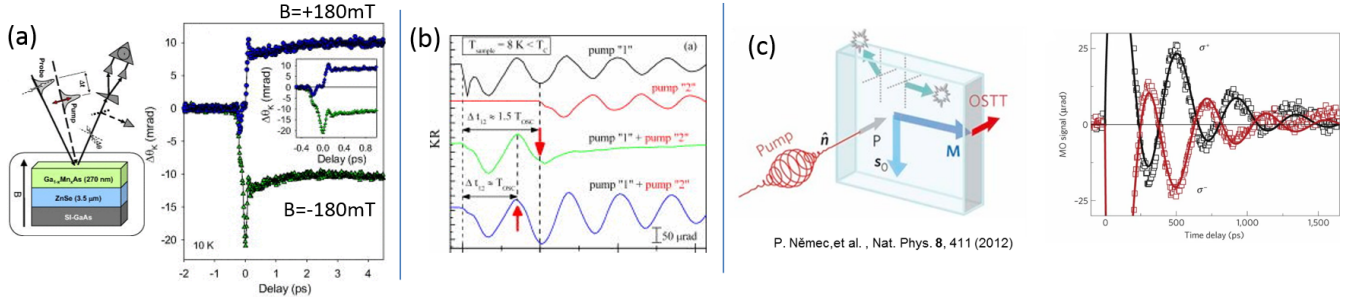


Figure III.1: (a) [232] Pump-driven demagnetization in out-of-plane magnetized (Ga,Mn)As. (b) [165] Double-pump Kerr rotation (KR). Each pump pulse alone triggers precession of magnetization with a period  $T_{osc}$  (top two curves). If pump pulse 2 excites the sample  $\sim 1.5T_{osc}$  after pulse 1, magnetization precession is stopped (3rd trace). If the time delay between the pulses is  $\sim T_{osc}$ , the magnetization precession is amplified (last trace). (c) [145] The spin angular momentum of the excited photo-carriers exerts an optical spin-torque on the magnetization, whose sign depends on the circular polarization of the pump beam.

At INSP, we arrived fairly “late” on the topic, the main effects having already been published, many of them by the trail-blazing Prague groups of T. Jungwirth (Institute of Physics/Nottingham University) and P. Němec (Charles University): magnetization precession, excitation of standing spin waves, optical spin-orbit<sup>1</sup> and spin-transfer<sup>2</sup> torques, coherent control of precession (see for instance Refs. [214, 144, 145, 189, 165], and reviews such as [215, 99, 42]). We focused rather on bridging the gap with (static) domain studies, and understanding precessional effects, whose description remained up to then mostly phenomenological.

In 2011, we started building **a new experimental tool in the group**<sup>3</sup>, a fairly standard “pump-probe” set-up but that would prove indispensable to our later magnetoacoustics studies (Chap. IV). The output of a Ti:Sapphire laser emitting femtosecond pulses at 75 MHz is split in two beams of very different powers. They are modulated at two different frequencies (50 kHz or 520 Hz), and focused on the sample by a wide lense (or microscope objective). A set of waveplates controls independently the polarization of the two beams (linear for the probe, linear/elliptical or circular for the pump). The probe beam is mechanically delayed by a 12 ns line. After reflecting off the sample in the cryostat, a balanced bridge detector analyses the polarization rotation induced by the dynamic/static magnetization and sends it to a lock-in amplifier. A double demodulation of the signal (at 50 kHz then 520 Hz) gives access to the pump-induced magnetization dynamics, whereas the single demodulation at 520 Hz gives the static magnetization. By varying the incoming polarization of the probe beam, the reflected signal contains a varying proportion of polar Kerr and magnetic linear dichroism effects (sensitive resp. to out-of-plane and in-plane components), a strategy initially developed by the group of P. Němec [145, 144]. In this way, a genuine vectorial detection of the magnetization can be obtained, both static ( $\theta_0, \varphi_0$ ) and dynamic ( $\delta\theta(t), \delta\varphi(t)$ ).

Please refer to the PhD thesis of Sylvain Shihab for a detailed description of the specifications and a diagram of the set-up [179] (Chapter 4).

## 2 Influence of the phosphorus content on the exchange constant

As explained in Chap. I, out-of-plane magnetized (Ga,Mn)As is obtained when the layer is in tensile strain. This was initially done by growing the film over a relaxed  $\text{In}_y\text{Ga}_{1-y}\text{As}$  buffer. The misfit dislocations at the (In,Ga)As/GaAs interface however often led to a cross-hatch pattern at the surface of the layer, and threading dislocations popping up on the (Ga,Mn)As layer as strong pinning centers, so that dynamics ended up being governed by these extrinsic defects [200]. A breakthrough came when the tensile strain was induced in a less traumatizing fashion, by modifying the magnetic layer itself, not the substrate: co-doping the As sublattice with smaller Phosphorus atoms naturally led to a smaller lattice constant, and a tensile strain over GaAs [34, 115, 185]. This gradually pulls the easy axis

<sup>1</sup>Driven by out-of-equilibrium non-polarized photo-holes [189].

<sup>2</sup>Driven by out-of-equilibrium spin-polarized photo-electrons [145].

<sup>3</sup>We greatly benefited from the “pump-probe” expertise of C. Testelin (INSP) to mount this set-up.

out of the plane of the sample.

The reduction in lattice parameter (i.e. cell volume) was initially predicted to be accompanied by an increase of the Mn-hole exchange integral  $J_{pd} \propto A_{ex}$  in (Ga,Mn)(As,P) due to the more efficient overlap of anion  $p$  orbitals with Mn  $d$  orbitals [132]. Several interesting consequences motivated the search for a higher exchange constant: a potential increase of the Curie temperature (up to then limited to 190 K), (ii) a widening of the domain-walls ( $\Delta = \sqrt{\frac{A_{ex}}{K_u}}$ ) and thus an increase of their speed (see Chap. II), and finally (iii) a tuning of the exchange-magnon dispersion curve ( $\omega \propto A_{ex}k^2$ ). The PhD thesis of S. Haghighi at INSP had already deduced a weak variation of  $A_{ex}$  with phosphorus concentration from the self-organization period of magnetic domains in out-of-plane magnetized samples [65], as could have been anticipated by the equally small variation of  $T_c$ . The thesis of S. Shihab followed another approach, not limited to out-of-plane anisotropy: measuring the frequency splitting between exchange-related modes excited optically using short laser pulses (Fig. III.2b).

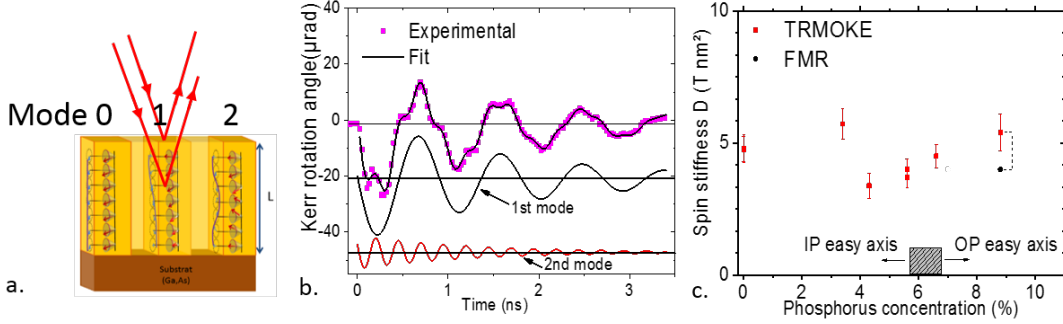


Figure III.2: [176] (a) Schematic profile of optically excited standing spin-waves. (b) Time-resolved Kerr effect: 2 frequencies. (c) Evolution of the spin stiffness ( $D = \frac{2A_{ex}}{M_s}$ ) as a function of the phosphorus concentration.

The exchange stiffness is extracted from the splitting between optically detected spin waves (Fig. III.2b):

$$\omega(k) = \gamma \sqrt{\frac{F_{\theta\theta}F_{\varphi\varphi}}{M_s^2} \pm \frac{(F_{\theta\theta} + F_{\varphi\varphi})Dk^2}{M_s} + D^2k^4}$$

$F_{ij}$  are the energy derivatives with respect to coordinates  $i, j$ , and  $k_{z,n} = \frac{n\pi}{L}$  is the quantized standing spin-wave-vector,  $L$  being the thickness of the layer. The  $\pm$  sign corresponds to bulk/surface modes varying as  $\cos(kz)/\sin(kz)$  or  $\cosh(kz)/\sinh(kz)$ . Correctly indexing the modes (and hence their symmetry via  $n$ ) is therefore critical for a correct estimate of  $A_{ex}$  [57], and required a study of its own. By comparing  $A_{ex}$  obtained by pump-probe, domain self-organization and FMR data (taken by J. von Bardeleben at INSP), we concluded that the excited mode was very probably an *even* mode (with respect to the center of the layer,  $n = 2$  in Fig. III.2a).

The study of about ten samples with varying manganese and phosphorus content concluded that the variation of  $A_{ex}$  with phosphorus was indeed rather weak [176] (Fig. III.2c). Two reasons were put forward as to why experiments fell short of Mašek's forecast [35, 176]: (i) the volume decrease had been quite overestimated [132] because the (Ga,Mn)(As,P) layer had been assumed fully relaxed, instead of strained on its substrate; (ii) co-doping with Phosphorus also increases the gap of the material, bringing it closer to that of GaP and possibly lowering the density of delocalized carriers. This effect would counterbalance negatively any minor increase of the exchange  $J_{pd}$ . The gradual transition of (Ga,Mn)(As,P) from a metallic to an impurity band conduction regime observed upon Phosphorus doping makes this explanation quite likely [35].

### 3 The magneto-optical illusion

The two non-uniform modes ( $n = 1, 2$  in Fig. III.2a) should however have a *zero* total dynamic component across the layer, and should therefore not be detectable by Kerr effect, if one supposes it to detect merely the average of the magnetization! The question of why we could nevertheless observe them had simply not been considered. To explain it, a multi-layer Kerr detection formalism was developed by C. Gourdon. Known for metals and the

static magnetization of (Ga,Mn)As [78], it had not been applied to magnetization dynamics. This model evidenced that it is the optical phase delay experienced by the light penetrating the layer that allows the observation of the spin-waves (Fig. III.3, bottom). This effect is all the more stronger that the layer is *weakly absorbing*, as is the case for (Ga,Mn)As. An intriguing prediction of the model is that the first two modes should appear to “turn” in opposite directions, which we indeed observed experimentally, thanks to our full  $\delta\theta(t), \delta\varphi(t)$  reconstruction (Fig. III.3, top). A momentous (so to speak..) consequence of this result is that we had improperly indexed the optical modes in the 2015 paper [176], and thus underestimated by a factor of 4 the spin-stiffness. Its variation with phosphorus content however remained undisturbingly flat...

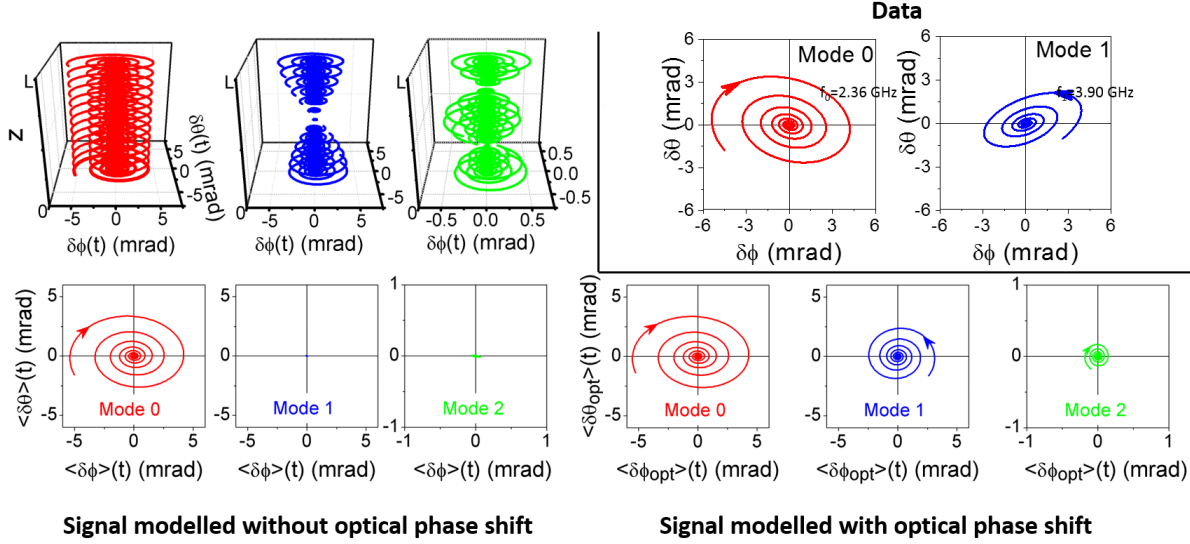


Figure III.3: [178] **Data:** by separating the polar Kerr effect from the linear dichroism in the time-scans, we can extract the  $\delta\theta, \delta\phi(t)$  trajectory of the dynamics for each observed frequency (here 2.36 GHz and 3.90 GHz). **Simulation/Modelling:** [top-left] depth-dependence of the spin waves obtained by numerically solving the LLG equation. Summing the signal over the whole layer with and without optical dephasing demonstrates that the former condition is necessary to observe higher modes [bottom-left and right]. The apparent change of rotation sense for the excited mode unambiguously identifies it as mode “1” rather than mode “2” (modelling of phase-shift effects by C. Gourdon).

## 4 Pump-driven transient and stationary heating

### 4.1 Role of transient heating in precession

An (unpublished) by-product of the spin-stiffness study was to understand rigourously the conditions leading to the triggering of precession, in particular the influence of the initial magnetization position. While it may now seem trivial to observe coherent magnetic oscillations when shining laser pulses on a (Ga,Mn)As layer, many of the first “pump-probe” articles reported either demagnetizing effects [101, 232], or photo-induced electron spin polarization [98, 158].

Tuning the static magnetization either by an applied field or by choosing the right phosphorus doping, Sylvain concluded that the precession was excited only if the magnetization was initially *disaligned* with respect to the high symmetry axes of the sample, and that the pump beam mainly affected the in-plane uniaxial and biaxial anisotropies  $K_{2||}, K_{4||}$ . What governed the transient modification of these 2 constants ? The precession amplitude/phase was in the vast majority of cases independent of the pump beam’s polarization, ruling out optical spin-transfer torque. On the other hand, for most of the samples studied, the initial carrier density was too high to be modified substantially by photo-generated carriers ( $\Delta p_{photo} \lesssim 10^{19} \text{ cm}^{-3}$ ) making optical spin-orbit torque equally unlikely [189]. Instead it was simply the transient heating of the layer that gave the necessary  $\delta K_{2||}(t), \delta K_{4||}(t)$ . Sylvain modelled this effect and concluded that a temperature rise of about 10 Kelvins following the arrival of the pump beam was necessary to account for the observed precession amplitude [179].



## 4.2 Magnetism reversal driven by optical pulses

Instead of looking at the *dynamical* aspects on in-plane magnetized samples, we then looked at *static* modifications (as in “before” and “after” the pulse) on an out-of-plane magnetized sample. Studying the effect of pump pulses on the coercivity of a weakly perpendicular layer was the first step towards a fast, all-optical writing of magnetic bits. This effect is now well studied in garnets and rare-earth alloys [127, 184], but had not been fully explored in (Ga,Mn)As. Several teams had however evidenced a lowering of the coercive field - reversible or not - attributed to a temperature rise, or to a so called “photo-coercitive effect” of unclear origin [161]...Using the spin-torque induced by circularly polarized photons absorbed by the layer was also a promising route, reported to assist the propagation of domain-walls in (Ga,Mn)(As,P) tracks [159]. Note that this effect has since been shown to be effective in metallic Pt/Co/Ni/Co/Pt layers [235].

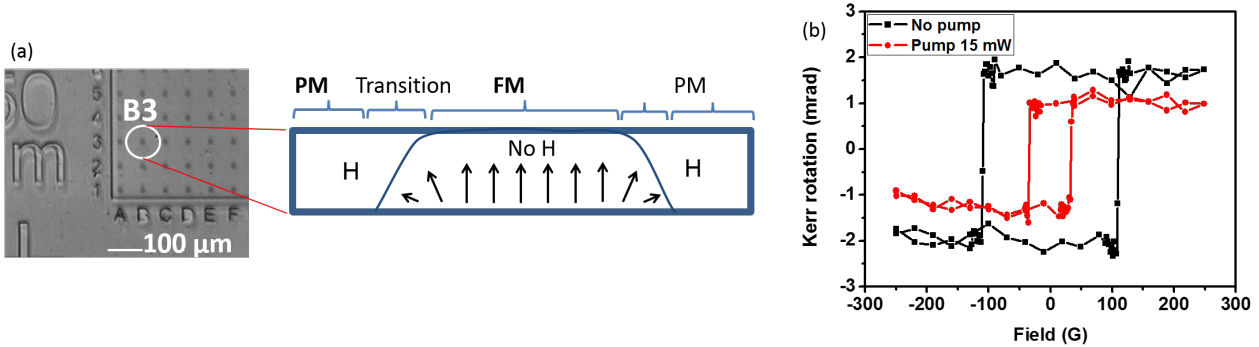


Figure III.4: (a) Kerr microscopy of an array of  $15\mu\text{m}$  diameter dots patterned by hydrogenation spaced by  $50\mu\text{m}$ , schematics (not to scale) of the cross-section of a dot, with paramagnetic (PM) and ferromagnetic regions (FM) separated by a  $\sim 100$  nm transition [201]. (b) Reduction of the static coercivity under pump beam. These effects are mainly of thermal origin.

Here we chose to work on a sample hydrogen-patterned into a dilute array of  $\varnothing 15\mu\text{m}$  dots, in order to control the localisation of the laser-assisted nucleation [201]. With this patterning technique, the edge of the structures is known to have a weaker hole doping level, and a slightly in-plane magnetization (Fig. III.4b). We hope this could be exploited via optical spin torque with circularly polarized light (Fig. III.4a), or at least a local modification of the carrier concentration capable of reducing substantially the coercivity. P. Kuszewski (PhD) and H. Bakr (M2) both spent a lot of energy and enthusiasm studying in detail the effects of the laser power, focusing and polarization on the reversal of these dots. We concluded on a clear dominance of thermal effects which lowered domain nucleation/propagation barriers (Fig. III.4c). Minute effect of circular polarization were crushed by thermal effects. A large part was clearly due to stationary heating, which could only be partially minimized by reducing the duty cycle of the pump laser <sup>4</sup>. By nature stochastic, these effects were poorly reproducible, and were not published.

## 4.3 Steady-state thermal gradient induced by the pump beam

These results prompted us to put some numbers on the *stationary* temperature rise induced by the pump beam, which often “polluted” our experiments. For this, we used the amplitude and switching fields of static magnetic linear dichroism hysteresis cycles as a “thermometer”, to relate the power of the pump-beam to the effective temperature of the sample, under the spot, or in its vicinity (Fig. III.5).

<sup>4</sup>This was done by playing with the ON/OFF time of the acousto-optic modulation. At the time we did not have a “pulse-selector” (reduction of the laser repetition rate to  $f_L/n$ ), which would have allowed us to see the effect of just a single pulse and test the effect of transient heating.

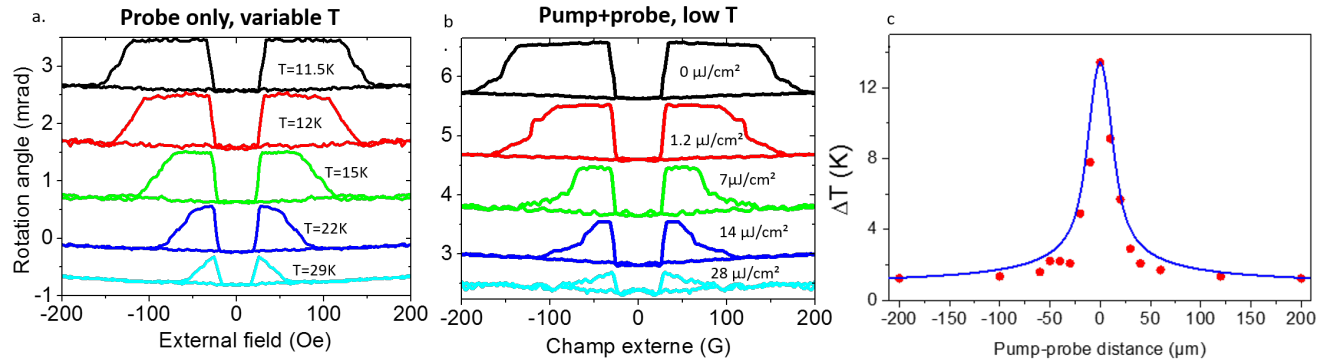


Figure III.5: [177] (a,b) Linear dichroism cycles taken with the probe beam only (varying the temperature), or in the presence of the pump beam (at low temperature). (c) Radial profile of the temperature rise induced by a pump beam of  $1.5 \mu\text{J}/\text{cm}^2$  fluence: experiment and modelling (collaboration with J.-Y. Duquesne, INSP) taking into account a thermal contact resistance.

Knowing the effective temperature of the layer, we could inject the right FMR-determined anisotropy constants in our models.

\* \* \*

Whilst analyzing in depth the polarization-dependent data of Sylvain, we came to understand more finely the many artefacts of time-resolved Kerr effect experiments, but also their power, such as the possibility to put credible numbers on the amplitude of the precession cone. Despite the disappointingly low number of publications that came out of quite a large volume of data, the experimental, numerical, and theoretical tools developed during Sylvain's thesis provided invaluable for the dynamic magnetoacoustic studies (Chap. IV).

The extreme temperature-sensitivity of the magnetic anisotropy and saturation magnetization of (Ga,Mn)As and (Ga,Mn)(As,P) was the source of many experimental issues, false hopes, or last-minute frights. Moving on to acoustic excitations was in that respect quite comforting.

# Chapter IV

## Magneto-acoustics

> **Students/post-doc involved:** Piotr Kuszewski (PhD, 2015-2018), Nicolas Biarrotte (M2, 2016), Ibrahima Camara (post-doc 2015-2016), Meriam Kraimia (PhD 2016-2020)

> **Related publications:**

- *Effect of picosecond strain pulses on thin layers of the ferromagnetic semiconductor  $(Ga,Mn)(As,P)$* , L. Thevenard, E. Perronne, C. Testelin, C. Gourdon, M. Cubucku, S. Vincent, E. Charron, A. Lemaître, B. Perrin, *Physical Review B* 82,104422 (2010)
- *Irreversible magnetization switching using surface acoustic waves*, L. Thevenard, J.-Y. Duquesne, E. Peronne, H. J. von Bardeleben, H. Jaffres, S. Ruttala, J.-M. George, A. Lemaître, and C. Gourdon, *PRB* 87, 144402 (2013)
- *Surface-acoustic-wave-driven ferromagnetic resonance in  $(Ga,Mn)(As,P)$  epilayers*, L. Thevenard, C. Gourdon, J.Y. Prieur, H. J. von Bardeleben, S. Vincent, L. Becerra, L. Largeau, J.Y. Duquesne, *PRB* 90, 094401 (2014)
- *Precessional magnetization switching by a surface acoustic wave*, L. Thevenard, I. S. Camara, S. Majrab, M. Bernard, P. Rovillain, A. Lemaître, C. Gourdon, and J.-Y. Duquesne, *Phys. Rev. B* 93, 134430 (2016)
- *Strong reduction of the coercivity by a surface acoustic wave in an out-of-plane magnetized epilayer*, L. Thevenard, I. S. Camara, J.-Y. Prieur, P. Rovillain, A. Lemaître, C. Gourdon, and J.-Y. Duquesne, *Phys. Rev. B* 93, 140405(R) (2016)
- *Laboratory X-ray characterization of a surface acoustic wave on GaAs: the critical role of instrumental convolution*, L. Largeau, I. Camara, J.-Y. Duquesne, C. Gourdon, P. Rovillain, L. Thevenard, B. Croset, *J. Applied Cryst.*, 49, 1 (2016)
- *Vector network analyzer measurement of the amplitude of an electrically excited surface acoustic wave and validation by X-ray diffraction*, I. S. Camara, B. Croset, L. Largeau, P. Rovillain, L. Thevenard, and J.-Y. Duquesne, *J. Appl. Phys.* 121, 044503 (2017)
- *Resonant magneto-acoustic switching: influence of Rayleigh wave frequency and wavevector*, P. Kuszewski, I. S. Camara, N. Biarrotte, L. Becerra, J. von Bardeleben, W Savero Torres, A. Lemaître, C. Gourdon, J.-Y. Duquesne, and L. Thevenard, *Journal of Physics: Condensed Matter* 30 244003 (2018)
- *Optical probing of Rayleigh wave driven magnetoacoustic resonance*, P. Kuszewski, J.-Y. Duquesne, L. Becerra, A. Lemaître, S. Vincent, S. Majrab, F. Margaillan, C. Gourdon, and L. Thevenard, *Physical Review Applied*, 10 (2018)
- *Field-Free Magnetization Switching by an Acoustic Wave*, I.S. Camara, J.-Y. Duquesne, A. Lemaître, C. Gourdon, and L. Thevenard, *Physical Review Applied* 11 014045 (2019)
- *The 2019 surface acoustic waves roadmap*, P. Delsing, C. Gourdon, M. Marangolo, J.-Y. Duquesne, L. Thevenard *et al.*, *Journal of Physics D: Applied Physics*, 52 353001 (2019)
- *Time- and space-resolved nonlinear magnetoacoustic dynamics* M. Kraimia, P. Kuszewski, J.-Y. Duquesne, A. Lemaître, F. Margaillan, C. Gourdon, & L. Thevenard, *Physical Review B*, 101 144425 (2020)

# 1 Context

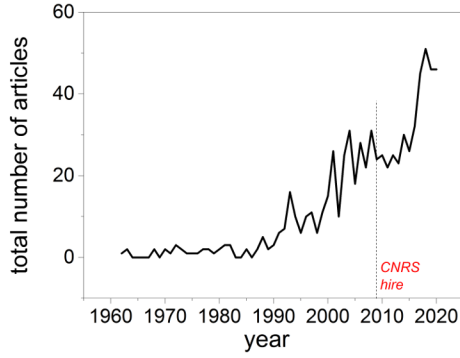
The magnetic anisotropy of (Ga,Mn)As varies strongly with strain, via the dependence of the heavy-hole/light-hole band splitting on strain (see Chap. **I**). It can thus be tuned post-growth by using a piezoelectric transducer to apply stress [166, 16, 151], or micropatterning to make the epitaxial strain relax anisotropically [70] for instance. Beyond these static aspects, magneto-elastic *dynamics* started to stir interest. In 2010, two groups endeavored in parallel to use instead picosecond *strain pulses* to trigger the magnetization dynamics in (Ga,Mn)As (at INSP, following a suggestion of A. Lemaitre, and A. V. Scherbakov at the Ioffe Institut of St. Petersburg, in collaboration with M. Bayer of Dortmund University). Much like what had been done in pump-probe experiments (see Chap. **III**), the idea was to put the magnetization out of equilibrium by a strain-induced transient modification of its anisotropy. Whereas light pulses generate a broadband population of carriers and phonons, strain (acoustic) waves held the promise of a resonant coupling to the magnetization, since their frequency and wavevector can be made close to that of spin-waves, an opportunity realized over sixty years ago by Kittel [100]. It would thus enable a GHz control of magnetization dynamics, without any rf fields, or the cumbersome management of heat that comes with light pulses [177] (Chap. **III**, Sec. **3**).

Realizing that the frequency spectrum of picosecond strain waves was actually too high and broad to couple efficiently to the low lying frequencies of (Ga,Mn)As, we turned in the summer of 2012 towards sub-GHz surface acoustic waves (SAWs). Whilst we were initially more interested in how these waves could be used to switching magnetization precessionally [194], a much-cited article by the group of S. Goennenwein (Walter Meissner Institut, Garching) demonstrated SAWs driving ferromagnetic resonance (FMR) in Nickel layers [219]. Although similar acoustic-FMR had been obtained half a century ago with bulk acoustic waves [157, 21, 156], the clear demonstration that this could be done with SAWs contributed to launching a renewed interest in the topic.

Using SAWs to excite precession presents several interesting features. While the rf field produced by antennas or coplanar waveguides has a polarization that varies strongly in space and decays rapidly, the *effective* magnetic field induced via magnetoelasticity by the elliptically polarized weakly damped surface acoustic waves is identical at any point on the SAW path, making magnetization actuation by strain potentially much more reliable. With their low attenuation, and power-flow confined to the surface, they can be made to interfere, diffract and focus on and have thus proved over the last couple years to be a relevant tool to manipulate many different degrees of freedom, electronic, elastic or magnetic [40]. The magnetoacoustics work done at INSP since 2012 illustrates the novelty of what can be done using SAWs, and the not-so-new physics of magnetostriction. The following main results, detailed in the coming sections, were obtained:

- concomitant magnetic and acoustic SAW-driven resonance in (Ga,Mn)As, detected optically and electrically [196, 111, 109]
- resonant (precessional) SAW-induced switching in planar and out-of-plane (Ga,Mn)As and (Ga,Mn)(As,P), including in zero applied field [111, 192, 24]
- acousto-magneto-optical effects induced by a picosecond acoustic strain wave in thin layers of (Ga,Mn)(As,P) [202]
- experimental determination of the surface acoustic wave amplitude, electrically and using a laboratory diffractometer [23, 113]

For these studies, we benefited from a very fruitful intra-INSP collaboration with members of the Acoustics team, in particular Emmanuel Perrone, Jean-Yves Duquesne, Jean-Yves Prieur and Laurent Belliard, and regular interaction with X-Ray diffraction specialists, L. Largeau (former LPN, now C2N) and B. Croset (INSP).



Web of Knowledge publication statistics with “ferromagnetic” and “acoustic” in the topic.

## 2 Acoustic waves

There is a very rich physics exploiting the coupling between spins and *incoherent* phonons that I will not detail [39, 94]. I will instead focus on acoustic waves, with frequencies ranging from the sub-Hz to THz regimes. They are characterized by a generally linear dispersion relationship, i.e. a velocity that depends only weakly on wave-vector, in stark contrast with generally dispersive spin-waves. Their velocity is much lower than the speed of light, so they are routinely used to delay electromagnetic waves (SAW filters). When propagating on a layer, their velocity is extremely sensitive to the surface, so they are also ideal for sensing applications.

### 2.1 Wave equations

- Let us recall the main tensor quantities and relationships governing linear elasticity, as a function of the displacement  $u_i$  along coordinate  $i$  :

$$\text{strain} \quad S_{ij} = \frac{1}{2} \left( \frac{\partial u_i}{\partial x_j} + \frac{\partial u_j}{\partial x_i} \right) \quad (\text{IV.1})$$

$$\text{stress} \quad \sigma_{ij} = c_{ijkl} S_{kl} = \frac{\partial f_{el}}{\partial S_{ij}} \quad (\text{IV.2})$$

$$\text{elastic energy} : \quad f_{el} = \frac{1}{2} \sigma_{ij} S_{kl} \quad (\text{IV.3})$$

$c_{ijkl}$  is the stiffness tensor, which, together with the density  $\rho$  are the material parameters that truly govern the acoustic wave dynamics. For the cubic GaAs, there are only 3 independent components, so that the elastic energy reads in Einstein notation:

$$f_{el, GaAs} = \frac{1}{2} c_{11} S_{ii}^2 + 2c_{44} S_{ij}^2 + c_{12} S_{i,i+1}$$

Note that the expression of the stress is modified when the material is piezoelectric. This is the case of GaAs (and therefore (Ga,Mn)As), but we have neglected this effect. It essentially leads to a so-called “hardening” of the elastic constants, i.e. a static renormalization that does not depend on the magnetization.

- The elastic wave equation reads:

$$\rho \frac{\partial^2 u_i(\vec{r}', t)}{\partial t^2} = \frac{\partial \sigma_{ij}}{\partial x_j} = c_{ijkl} \frac{\partial f_{el}}{\partial x_j S_{kl}}. \quad (\text{IV.4})$$

In a **bulk geometry**, injecting harmonic solutions of the form  $u_i(\vec{r}', t) = U_i \exp[i(\vec{k} \cdot \vec{r}' - \omega t)]$  in this equation leads to a determinant, which cancelled out yields the bulk longitudinal and transverse velocities: in GaAs,  $V_L = \sqrt{\frac{c_{11}}{\rho}}$  (4700 m.s<sup>-1</sup>) and  $V_T = \sqrt{\frac{c_{44}}{\rho}}$  (3400 m.s<sup>-1</sup>). Pure longitudinal modes only exhibit displacement along the wave-vector, while the two pure transverse modes have atoms oscillating in the plane perpendicular to  $\vec{k}$ .

When a **semi-infinite substrate** is considered instead, the presence of the surface imposes boundary conditions (no surface stress surface,  $\sigma_{iz} = 0$  in  $z = 0$ ) that modify the modes allowed to propagate. They are now harmonic Rayleigh plane wave solutions  $u_i(x, t) = U_i e^{-\beta z} \exp i(kx - \omega t)$  travelling on the surface ( $\vec{k} \parallel x$ ), and  $z$ -damped down to a little over a wavelength  $\lambda = \frac{2\pi}{k}$ . Plugging this form into Eq. IV.4 leads to a new determinant, which cancelled out gives implicitly the new mode's velocity,  $V_R = \frac{\omega}{k}$  (Eq. IV.5). This mode is again non-dispersive. For a surface acoustic wave (SAW) travelling in GaAs along  $\langle 110 \rangle$ , the velocity  $V_R \sim 2700 \text{ m.s}^{-1}$  is obtained from the equation<sup>1</sup> :

$$(c_{44} - \rho V_R^2)(c_{11}c_{33} - c_{13}^2 - c_{33}\rho V_R^2)^2 = c_{44}c_{33}(c_{11} - \rho V_R^2)(\rho V_R^2)^2 \quad (\text{IV.5})$$

The allowed displacements modes are now longitudinal along  $\vec{k} \parallel x$ , and out of the plane ( $u_x$  and  $u_z$ ), giving three components of strain:  $S_{xx}$ ,  $S_{zz}$  and  $S_{xz}$ :

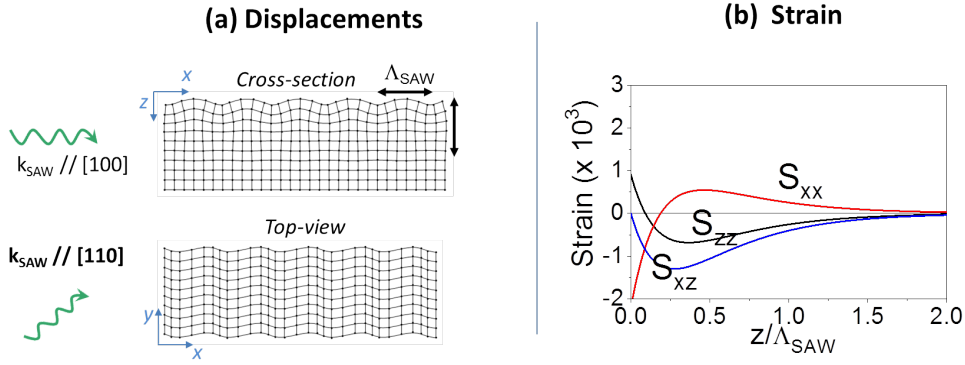


Figure IV.1: Surface acoustic wave in GaAs. (a) Displacements, viewed either from the cross-section of the semi-infinite substrate, or in top view for a wave travelling along  $[110]$ . In that case, unequal  $S_{xx}$  and  $S_{yy}$  strains are generated, thereby modifying the shear strain felt by the GaAs lattice. (b) Depth dependence of the strain. At the surface  $S_{xx}$  and  $S_{zz}$  are maxima and of opposite sign, while the shear strain  $S_{xz}$  is zero. For the 50 nm-thick layer used,  $z/\Lambda_R < 1\%$ , so the strain is considered constant through the magnetic layer depth.

## 2.2 Different transduction mechanisms

We have used two different transduction mechanisms to generate bulk or surface acoustic waves, both relying on the creation of a time-varying stress. Their specifications, advantages and inconvenients are summarized in Fig. IV.2.

<sup>1</sup>This is all very well detailed in the excellent reference textbook of D. Royer and E. Dieulesaint, *Elastic Waves in Solids: Free and Guided Propagation*, Springer

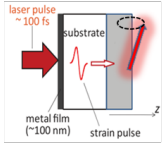
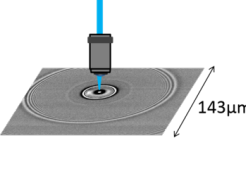
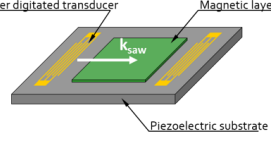
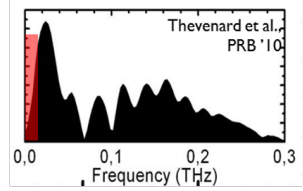
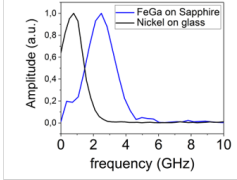
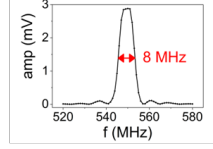
	Optical generation BAWs	Opticals generation SAWs	Electrical generation- SAWs
Mechanism			
	thermoelasticity via a metallic film (which can be the magnetic layer itself)		piezoelectric substrate (GaAs, LiNbO <sub>3</sub> ) or overlayer (ZnO)
Strain components	$S_{zz}$	$S_{rr}, S_{zz}, S_{rz}$ , 360° emission	$S_{xx}, S_{zz}, S_{xz}, x//k_{saw}$
Bandwidth / max frequency	 Wide / THz (solitons) at high power	 $f_{max} = V_R/\phi$ dependent on substrate and laser spot diameter	 narrow (inversely proportional to the number of digits) / $f_{max} = V_R/4d_{min} \sim$ dependent on substrate and minimum digit width ( $\sim 5$ GHz for $d \sim 200$ nm)
Power required	high power femtosecond laser		RF power between 0 and +40dBm (1mW to 10 W)
Pros	no need of any lithography, straightforward synchronization between (optical) excitation and detection		Very well mastered technology, quasi- monochromatic plane-wave
Cons	Frequencies generally too high for (Ga,Mn)As	very tight focusing ( $<1$ $\mu\text{m}$ ), large N.A objective generally incompatible with working with a cryostat	Need of lithography steps, and of a piezoelectric material. Complex synchronization with optical detection.

Figure IV.2: Bulk (BAW) and surface (SAW) acoustic wave excitation mechanisms.

- **thermoelasticity**: a laser pulse impinging on a metallic thin film induces a transient temperature rise  $\Delta T$ , usually dominantly along a particular direction (e.g. along the sample normal, or radially  $\Delta T|_z, \Delta T|_r$ ). The resulting stress is proportional to the thermal expansion coefficient  $\xi$ :  $\sigma_{ij} = c_{ijkl}\xi\Delta T\delta_{kl}$ . Plugging this in Eq. IV.4 with the appropriate boundary conditions shows that a bulk or surface acoustic wave is then generated. A temperature gradient perpendicular to the surface (laser spot size large with respect to the acoustic wavelength) causes longitudinal waves to appear, with a broad frequency spectrum. A very focused laser beam (diameter of the order of  $\lambda_{SAW}$ ) producing a dominantly lateral temperature gradient will give instead shear or surface waves. The frequency content is then centered around  $f_{SAW,opt} = \frac{V_R}{\text{spot diameter}}$ . These waves can be probed optically using a pump-probe set-up to perform either interferometry (surface displacement measurement) or differential reflectivity (strain measurement via photoelasticity). The strain amplitude ranges from a few  $10^{-5}$  to  $10^{-3}$  (soliton regime [154]).
- **inverse-piezoelectricity**: an oscillating electric field  $\vec{E}$  applied between two metallic surfaces (parallel plates of a capacitor, or parallel digits on a surface) generates a time-varying mechanical stress:  $\sigma_{jk} = c_{jklm}S_{lm} - e_{ijk}E_i$ , where  $e_{ijk}$  is the piezoelectric tensor. Constructive interferences between waves whose wave-lengths are proportional to the spacing between plate/digit generate an acoustic wave (fundamental and harmonics, Fig. IV.3). We have been working in the surface geometry, with Rayleigh frequencies between 140

MHz and almost 1 GHz. This corresponds to SAW wave-lengths 5 to 20  $\mu\text{m}$ , i.e. a minimum digit width of 1.25  $\mu\text{m}$  conveniently adapted to INSP's optical lithography equipment. GHz transducers made using ebeam lithography are also routinely made and studied at INSP [164].

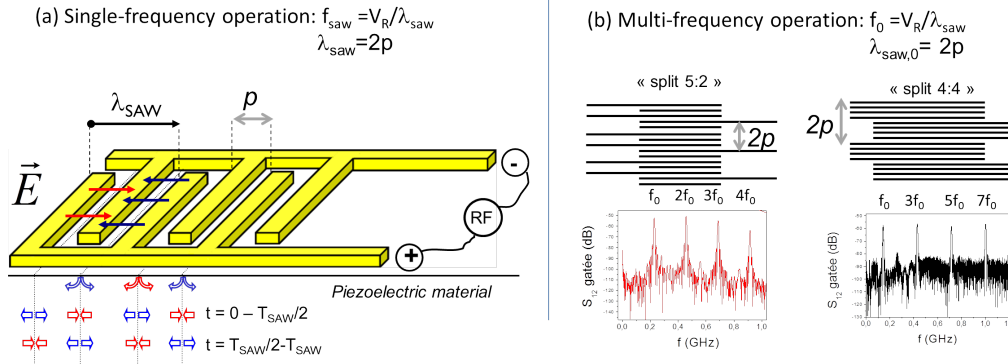


Figure IV.3: (a) Electrical generation of SAWs: a sinusoidal field generates a strain that changes sign every half time and spatial period. The interferences of the generated waves are all destructive except for the one whose wavelength is twice the digit period  $d$ , with a bandwidth that sharpens when the number of digits increases. (b) More complex interdigitated transducer (IDT) design to excite harmonics with equivalent efficiency [174]. Vector network analyzer (VNA) transmission measurement using a second, identical IDT.

It is more challenging to measure precisely the strain amplitude of these waves. We have performed it on an epi-ready GaAs substrate following two procedures, whose results perfectly coincided [23, 113]: (i) **X-Ray diffraction** in presence of a CW SAW makes new  $k_{\text{SAW}}$ -spaced peaks appear symmetrically of the Bragg peak (Fig. IV.4b). Correct modelling of these peaks gives the modified lattice constant of the substrate, and therefore the surface displacement and strain. (ii) **Vector network analyzer measurement of scattering parameters**  $S_{11}, S_{12}$ . At  $f = f_{\text{SAW}}$ , a slight dip appears in the reflection coefficient  $S_{11}$  due to the power being lost in the SAW emission (Fig. IV.4a). By careful characterization of the fixtures and of the admittance of the transducers via Coupling-of-Modes (COM) theory, a precision equivalent to that of XRD could be obtained on the strain estimation (Fig. IV.4c).

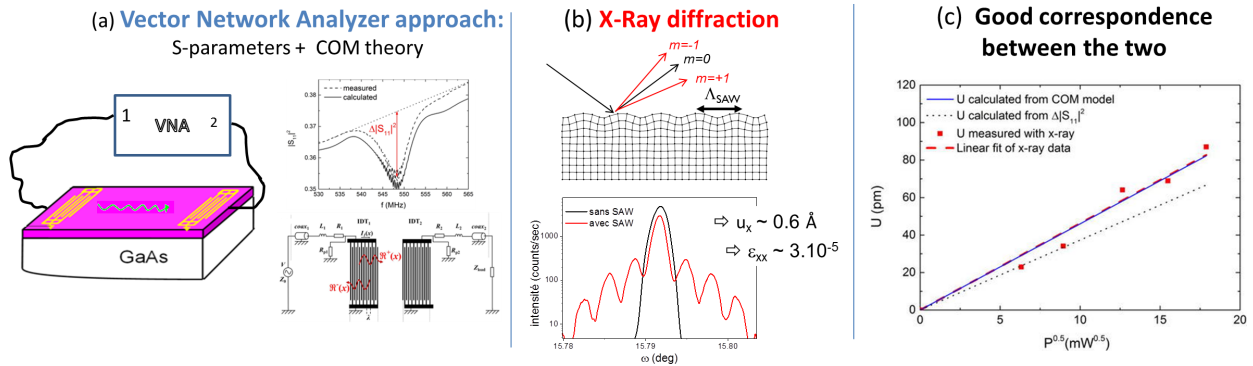


Figure IV.4: Two ways of measuring the amplitude of an electrically generated SAW: (a) [23] Using a vector network analyzer (VNA). This approach is difficult to implement at low temperature (i.e. in relevant conditions for (Ga,Mn)As) as it requires a characterization of the fixtures up to the cooled-down sample holder, in the cryostat. (b) [113] Using X-ray diffraction (XRD). While similar measurements had been done on synchrotron [207], this work was the first demonstration that a good enough resolution could be obtained on a *lab* diffractometer to extract this type of information. (c) With a correct modelling of both VNA and XRD scans, an excellent agreement is obtained between the two, and the  $\sqrt{P_{\text{rf}}}$  dependency of the displacement well reproduced.



### 3 Experimental developments

The strong point of our experimental studies in the various acoustic geometries has been from the start the possibility to measure both the acoustic and the magnetization dynamics. In all configurations, the latter were detected using magneto-optical effects, i.e a rotation of the light polarization induced by the varying magnetization. In (Ga,Mn)As this rotation depends on both the in-plane (Voigt effect) and out-of-plane (Kerr effect) components of the magnetization, so that the full dynamics trajectory can be reconstructed, as done in the pump-probe experiments described in Chap. III. In metals, the Kerr effect is dominant (very weak magnetic linear dichroism, and no longitudinal Kerr effect since the probe beam arrives at normal incidence).

- For **optically generated waves**, we worked on the modified “pump-probe” set-ups of E. Péronne and B. Perrin (BAWs) and L. Belliard (SAWs). The pump beam hits the metallic transducer on the back side of either, the substrate (BAWs) or the magnetic layer itself (SAWs, through a transparent substrate), and generates longitudinal bulk or Rayleigh surface acoustic waves. A weaker probe beam scans the magnetic layer, and monitors the surface displacement by interferometry (Sagnac or Michelson). A flip-mirror selects whether the beam goes through the interferometer, or to the polarization rotation detection bridge. The pump and probe objectives are on XYZ piezo stages. In the SAW set-up, pump and probe beams came from the same laser beam, split in two, and are thus naturally synchronized. In the BAW set-up, an original asynchronous detection scheme was used: the two beams come from two separate Ti:Sa lasers of very close repetition frequencies ( $f_{rep} \sim 80$  MHz,  $\Delta f_{rep} \sim 1$  kHz). The time step is then given by  $\frac{\Delta f_{rep}}{f_{rep}(f_{rep} + \Delta f_{rep})}$ . This stroboscopic effect yields shorter acquisition times (better signal/noise ratio) and easier independent tuning of pump and probe colors [202].

Note that other groups studying optically generated acoustic waves measure both magnetic and elastic dynamic components, relying for the latter on transient diffraction [83, 29, 82], differential reflectivity [225] or solely on the polarization rotation (Ref. [167], mechanism not explicated, probably “leaks” in the bridge balancing).

- For **electrically generated SAWs**, a typical experiment consists in exciting  $IDT_{exc}$  with a 100-1000 MHz RF voltage, modulated into square pulses of a few hundreds of ns. With a detecting  $IDT_{det}$  placed far enough (a few mm) and hooked up to an oscilloscope, the electromagnetic radiation (“antenna”-like signal that arrives at the speed of light) can be separated in the time-domain from the acoustic wave travelling much slower at  $V_R$ . The latter is converted back into a voltage when passing under  $IDT_{det}$ . The amplitude and phase of this signal are then extracted - either by a direct sinusoidal fit (rapid sampling), or by first multiplying it to the carrier wave (home-made lock-in detection in Fig. IV.5) - and monitored as a function of field for instance. In this scheme, and as long as exciting and detecting IDTs are identical, only the homodyne response at  $f_{saw}$  can be picked up.

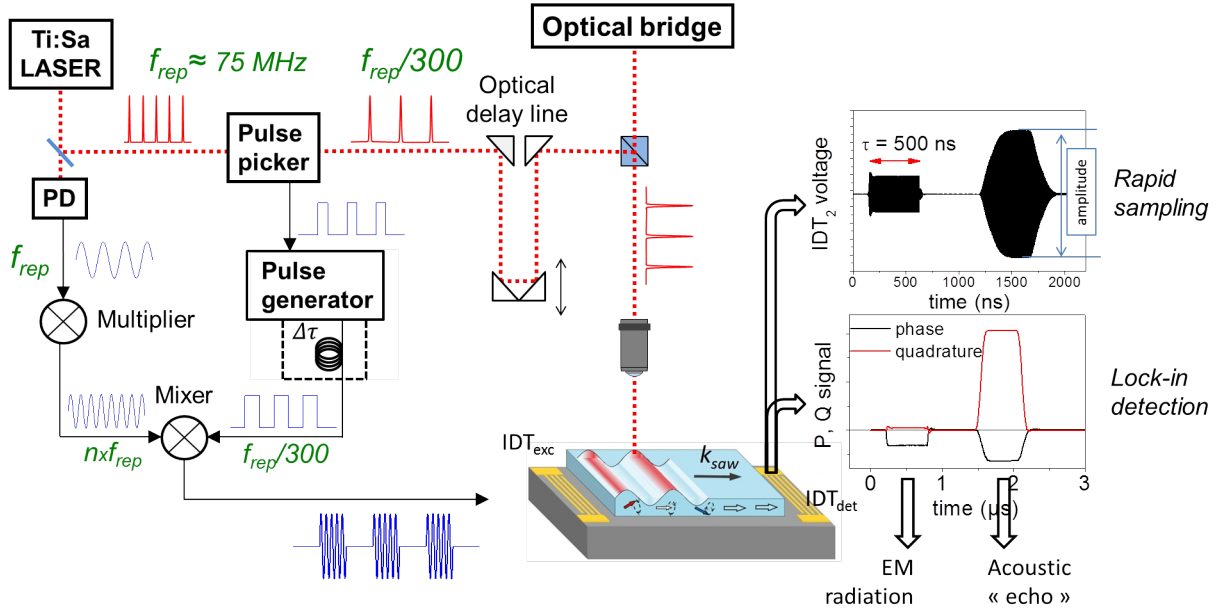
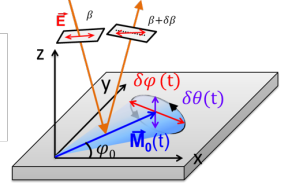


Figure IV.5: Detecting magnetic and acoustic dynamics for electrically generated SAWs [110, 109]. The RF voltage exciting the transducer is generated from the laser itself. The acoustics are monitored electrically, or optically via the photoelastic effect. While the electrical part of this set-up was essentially reproduced from Jean-Yves Duquesne's lab, mounting the optical part took the better part of Piotr Kuszewski's PhD thesis (2015-2018).

To monitor the magnetization dynamics, the laser pulses need to be synchronized to the RF voltage, which cannot be done straightforwardly when using a synthesizer as a source. The elegant solution we ended up using, proposed by C. Gourdon, was to create this RF voltage from the laser itself, using a photodiode followed by a series of filters and multipliers. More specifically: a small portion of the  $f_{rep} \sim 75$  MHz laser pulses is picked up by a slow photodiode+low pass filter in order to create a 75 MHz sinusoidal. This signal can then be multiplied+amplified by  $n=2,4,6$  to generate an RF voltage that can run at several hundreds of MHz, and power the IDTs to generate the SAW. The rest of the beam is sent to a pulse selector which divides the repetition rate by about 300 to reach 250 kHz. This is the frequency of the probing beam, that is by construction perfectly locked to the “pump” exciting the transducers. It is also used to trigger the emission of square pulses with which to modulate the  $n f_{rep}$  carrier wave (Fig. IV.5). The main draw-back of this approach is that the SAW frequency can only be a multiple of the laser repetition rate, imposing power-greedy multiplying+amplifying for the higher frequencies. Another factor limiting the maximum frequency lies in the optics detecting  $M(t)$ : the laser spot diameter of around  $1 \mu\text{m}$  (FWHM) needs to remain much smaller than the SAW wavelength if we don't want to average out the signal to zero [the magnetization dynamics are directly proportional to the strain, see further Eq. IV.11]. Choosing a high acoustic velocity substrate can only partially compensate for this limit. Typically, we have been able to see dynamics up to 900 MHz [105], corresponding to a wave-length of about  $3 \mu\text{m}$  in GaAs, i.e. already heavily convoluted by the laser spot size.

Moreover, in (Ga,Mn)As we were fortunate to have the polarization rotation ( $\delta\beta(x,t)$ ) depend not only on in-plane and out-of-plane magnetization components ( $\delta\theta(x,t), \delta\varphi(x,t)$ ) via the Kerr ( $K$  constant) and Voigt ( $V$  constant) effects, but also on the in-plane strain  $S_{xx}(x,t)$ , via the photo-elastic effect ( $P_E$  constant). Because each of those three optical effects has a different dependency on the incoming light polarization  $\beta$ , and static magnetization direction  $\varphi_0$ , magnetic and elastic dynamic components can be determined independently [109, 105].

$$\delta\beta(x, t) = K\delta\theta(x, t) + 2V\delta\varphi(x, t)\cos[2(\beta - \varphi_0)] + P_E S_{xx}(x, t)\sin 2\beta$$



Finally, the objective is mounted on a 300/300/300 $\mu\text{m}$  three-directional stage, with which we could for instance convince ourselves that the acoustic waves generated by the IDT were indeed plane-waves, and that they diffracted very weakly at the edge of the transducers (Fig. IV.6):

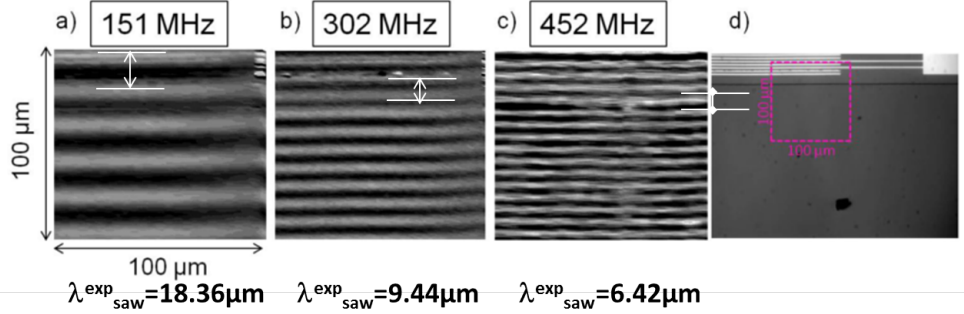


Figure IV.6: [110] Photoelastic effect maps of surface acoustic waves of frequency  $f_{\text{saw}} = n f_L$  ( $n = 1, 2, 3$ ) taken at room temperature on (Ga,Mn)As, at the edge of the IDT (last image: photo of the sample).

To my knowledge, this is the only set-up capable of measuring in the time-domain the magnetic precession amplitude triggered by electrically generated SAWs, and the concomitant field-dependent elastic behavior.

## 4 Magneto-acoustic ferromagnetic resonance (SAW-FMR) in (Ga,Mn)As

### 4.1 Magneto-elasticity and magnetostriction

Magnetoelasticity is the coupling between strain and magnetic components. It originates microscopically from the modification of the shape of atomic orbitals in the presence of magnetization, due to both anisotropic exchange interaction and crystal field effects, both of which varying strongly with interatomic distances. In (Ga,Mn)As, it is directly related to the modification of the valence band structure by the strain, and the resulting anisotropy of the magnetic energy (see Chap. I). Different formulations are used in the literature, depending on whether the crystal is free or strained, but also depending on communities. A short paragraph to clarify this [77]:

- In a cubic material free from any external stress cubic material, the magnetoelastic energy density is expressed by Eq. IV.6:

$$f_{ME} = B_1(m_x^2 S_{xx} + m_y^2 S_{yy} + m_z^2 S_{zz}) + 2B_2(m_x m_y S_{xy} + m_z m_y S_{zy} + m_x m_z S_{xz}) \quad (\text{IV.6})$$

$$\triangleright f_{ME} = -\frac{3}{2}\lambda_{100}(c_{11} - c_{12})(m_x^2 S_{xx} + m_y^2 S_{yy} + m_z^2 S_{zz}) - 3c_{44}\lambda_{111}(m_x m_y S_{xy} + m_z m_y S_{zy} + m_x m_z S_{xz}) \quad (\text{IV.7})$$

where  $m_i$  are the normalized coordinates of the magnetization and  $B_1, B_2$  the **anisotropic magnetoelastic constants**. From an elasticity point of view, the equilibrium is reached by minimizing the total elastic energy  $f_{ME} + f_{el}$  (Eqs. IV.6 and IV.3) with respect to the strain, for a given magnetic configuration. In (Ga,Mn)As, the resulting magnetostrictive strain is minute, much smaller than the epitaxial strain. With this equilibrium strain and reference dimensions taken in the completely demagnetized state, the relative elongation of the material  $\lambda = \frac{\delta l}{l}$  can be computed for the magnetization lying along different directions. These are the **magnetostriction coefficients**  $\lambda_{100}, \lambda_{111}$ , with which one can re-write the magnetoelastic energy as Eq. IV.7, using the elastic constants  $c_{ij}$ .

- In (Ga,Mn)As, the strained crystal is not free. The magnetoelastic energy is then expressed as a function of stresses of non-magnetic origin (e.g. epitaxy, internal stress coming from dislocations):

$$f_{ME} = -\frac{3}{2}\lambda_{100} \sum_i \sigma_{ii}(m_i^2 - \frac{1}{3}) - 3\lambda_{111} \sum_{i>k} \sigma_{ik}m_i m_k \quad (\text{IV.8})$$

$$\triangleright f_{ME} = f_0 + \left[ \frac{3}{2}\lambda_{100} \frac{(c_{11} - c_{12})(c_{11} + 2c_{12})}{2c_{11}} S_{xx,0} + 3c_{44}\lambda_{111} S_{xy,0} \right] m_z^2 + 3c_{44}\lambda_{111} S_{xy,0} (m_x^2 - m_y^2) \quad (\text{IV.9})$$

This non magnetic *stress* can be expressed as a function of the corresponding static *strain*  $S_{ij,0}$ , with  $S_{zz,0} = -\frac{c_{12}}{c_{11}}(S_{xx,0} + S_{yy,0})$  so that one can rewrite the magneto-elastic energy as Eq. IV.9.

- This expression only accounts for uniaxial in-plane and out-of-plane anisotropies. In (Ga,Mn)As, there are also higher order cubic anisotropy components, tetragonal more specifically, with a distinction between in-plane and out-of plane coefficients  $K_{4\parallel}$  and  $K_{4\perp}$  (see Chap I). The phenomenological expression generally used, e.g. for ferromagnetic resonance is then:

$$f_{FMR} = -\mu_0 \vec{M} \cdot \vec{H} + \left( \frac{\mu_0 M_s^2}{2} - K_{2\perp} \right) \cos^2\theta - \frac{K_{4\perp}}{2} \cos^4\theta - \frac{K_{4\parallel}}{8} (3 + \cos 4\varphi) \sin^4\theta - K_{2\parallel} \sin^2\theta \sin^2(\varphi - \frac{\pi}{4})$$

- Finally, the following correspondence - somewhat partial since cubic components are lost - can be established between  $B_i$  magnetoelastic constants,  $K_i$  FMR coefficients and magnetostriction coefficients  $\lambda_{100}, \lambda_{111}$  :

$$B_1 = -\frac{3}{2}\lambda_{100}(c_{11} - c_{12}) = \frac{-K_{2\perp} + K_{2\parallel}/2}{S_{zz,0} - S_{xx,0}}$$

$$B_2 = -3\lambda_{111}c_{44} = \frac{K_{2\parallel}}{2S_{xy,0}}$$

Typical values of magnetostriction for (Ga,Mn)As are not so far from nickel [133, 104, 110], larger than YIG, but much smaller than Co, or very magnetostrictive materials like terfenol or galfenol FeGa:

$B_1 \sim 0.6 \text{ MJ.m}^{-3}$	$\lambda_{100} \sim -30 \text{ ppm}$	$K_{2\perp} \sim -8500 \text{ J.m}^{-3}$
$B_2 \sim 0.2 \text{ MJ.m}^{-3}$	$\lambda_{111} \sim -30 \text{ ppm}$	$K_{2\parallel} \sim 1000 \text{ J.m}^{-3}$

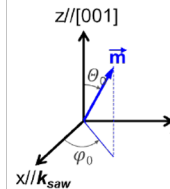
## 4.2 Coupled magnetic and elastic equations

To predict the dynamic coupling between magnetization and strain, one needs to solve simultaneously the Landau-Lifshitz-Gilbert and the elastic dynamics equation, with the total energy given by  $f_{tot} = f_{el} + f_Z + f_{MC} + f_{ME}$  (Zeeman and magneto-crystalline anisotropy terms have been added to the magneto-elastic contribution):

$$\begin{cases} \frac{\partial \vec{m}}{\partial t} &= -\gamma \vec{m} \wedge \mu_0 \vec{H}_{eff} + \alpha \vec{m} \wedge \frac{\partial \vec{m}}{\partial t} & \text{with } \mu_0 \vec{H}_{eff} = -\vec{\nabla}_m f_{tot} \\ \rho \frac{\partial^2 u_i}{\partial t^2} &= \frac{\partial \sigma_{ik}}{\partial x_k} = \frac{\partial^2 f_{tot}}{\partial x_k \partial S_{ik}} \end{cases} \quad (\text{IV.10})$$

The time- and space-dependent strain in  $f_{ME}(\vec{r}, t)$  modifies dynamically the anisotropy of the magnetic layer, and the dynamic magnetization modifies the elastic constants. A maximum coupling is expected at the crossing of magnon and phonon relationships, i.e. equating both frequency and wave-vector. Whatever the type of acoustic wave considered, because its frequency content is fixed (by the laser spot size and pulse duration for optics, and by the IDT geometry for piezo transduction), magnetoacoustic resonance is reached by acting on the magnetic system, e.g. using a magnetic field or temperature to tune eigenfrequencies. A last requirement lies in the initial static magnetization position  $\theta_0, \varphi_0$  for a given strain configuration. Indeed, simplifying, the torque acting on the magnetization contains different terms:

$$\begin{aligned} &\propto B_1 \sin 2\theta_0 [S_{zz}(z, t) - S_{xx}(z, t)] \\ &\propto B_1 \cos 2\theta_0 \sin 2\varphi_0 S_{xx}(z, t) \\ &\propto B_2 \cos 2\theta_0 \cos \varphi_0 S_{xz}(z, t) \end{aligned}$$



### 4.3 Magnetoacoustics with optically excited BAWs

When using a (001) GaAs substrate, only longitudinal  $S_{zz}$  acoustic waves travelling along the growth axis are generated optically. They couple to spin-waves with a wave-vector perpendicular to the surface of the sample, i.e. exchange-driven perpendicular standing spin-waves (PSSW), so that the exchange energy must be added in the total magnetic energy. The only efficient torque varies like  $\propto B_1 \sin 2\theta_0 S_{zz}(z, t)$ : a magnetization lying either fully in-plane or fully out-of-plane will not see its effective field modified by the strain. One must work with an in-plane (resp. out-of-plane) magnetized layer under a hard-axis out-of-plane (resp. in-plane) field.

Solving the LLG equation then gives the small varying components of the magnetization  $\delta M_i(\vec{r}, t)$  as a superposition of the magnetic standing eigenmodes of frequency  $\omega_n$ , with a weight  $C^n$  that reflects the spatial overlap of the  $n^{\text{th}}$  spin wave mode of amplitude  $A_i^n$  and the  $\omega_n$  Fourier component of the strain  $S_{zz}^n(z)$  [20]:

$$\delta M_i(z, t) = \sum_i C^n A_i^n(z) \cos(\omega_n t + \alpha_i^n)$$

$$C^n = \int_{z=0}^d A_i^n(z) S_{zz}^n(z) dz$$

A more explicit illustration of this is shown below, taken from Ref. [20], where the spatial profiles of the first 3 standing spin waves are plotted and compared to the strain profile (Fig. IV.7a,b).

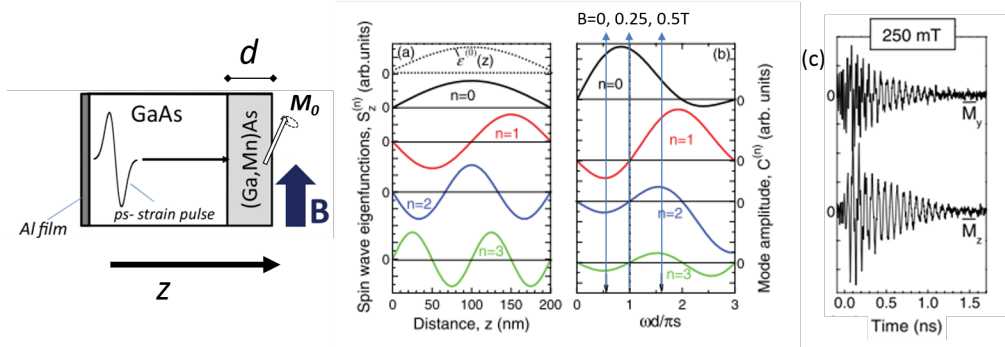


Figure IV.7: From Ref. [20]: (a) Spin wave eigenfunctions (solid lines, pinning boundary conditions assumed) and strain pulse profile (dotted line,  $\omega_0 = 12$  GHz Fourier component of the acoustic wave packet). (b) Dependencies of the  $n^{\text{th}}$ -spin wave mode amplitude on the normalized resonance frequency  $\frac{\omega_0(B)d}{\pi V_L}$ . (c) Experimental time-resolved Kerr rotation trace for  $B = 0.25$  T. In that case only mode  $n = 0$  is excited since  $C_1, C_2, C_3 = 0$  (see b).

In 2010, roughly at the same time as the work started at INSP, the group of A. Scherbakov evidenced magnetization precession triggered by picosecond acoustic waves in a layer of (Ga,Mn)As [171], and refined the optimal coupling conditions in the following years [121, 120, 170, 19]:

▷ high fields to ensure high precession frequencies matching the strain's high frequency content

▷ strong magnetic anisotropy so that the high (hard axis) field does not saturate the layer and cancel out the  $S_{zz}$  torque (or use of high-index substrates to excite *shear* strain components [19], raising some constraints on the static magnetization  $\theta_0, \varphi_0$  for efficient excitation.)

▷ thick enough layers (200 nm) to ensure decent overlap of the strain with the magnetic eigenmodes, or use of a non-magnetic top-layer so that the total strain felt by the layer does not cancel out (see Ref. [81] for FeGa). Indeed, the total strain is the sum of the incident strain pulse and its reflection off the sample/air interface, and thus completely cancels out at the surface.

In that respect, the experimental conditions chosen for our 2009-2010 study[202] could not possibly have been worse: a very weakly anisotropic (Ga,Mn)(As,P) layer (saturation field of 0.006 mT), low precession frequencies (200 MHz), a thickness of 50 nm almost guaranteeing no strain at the surface, and finally, experimental conditions tuned to favor high frequency/wave-vector acoustic solitons. Yet, we observed clear magneto-optical oscillations (Fig. IV.8). Their time-dependence mimicked very closely that of the strain pulse monitored by interferometry (see set-up Sec. 3), and their amplitude did not cancel out, but saturated when the magnetization was aligned to the hard axis ( $\theta_0 = 0$ ). We however demonstrated that the observed traces were in fact a non-resonant *magneto-acousto-optical artifact*: strain-induced reflectivity changes due to the photo-elastic effect are slightly different for  $\sigma_+$  and  $\sigma_-$  components of a linearly polarized light, because the optical indices are different in a magnetic material ( $n_+ \neq n_-$ ). This results in a polarization rotation of a few microradians that is not a Kerr rotation - yet cancels out above the Curie temperature - and that we could pick up with the great sensitivity of our detection bridge.

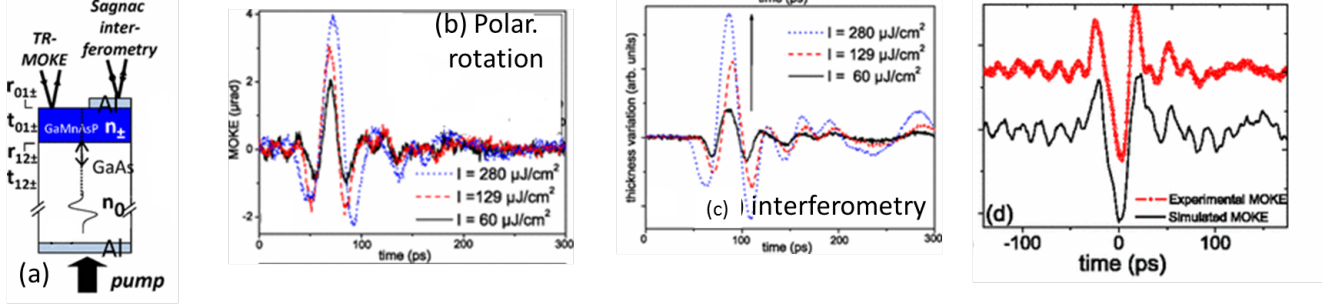


Figure IV.8: [202]: (a) Experimental configuration. (b,c) Polarization rotation and interferometry measurement of the surface displacement show very similar time-profiles. (d) That is not by coincidence: the former can be directly calculated by injecting the latter in the formula of  $\sigma_+$  and  $\sigma_-$  reflectivities leading to the polarization rotation, without invoking any strain-driven torque on the magnetization.

While this negative result was obviously a disappointment, it highlighted the care that needs to be taken in analyzing this type of data. Picosecond acoustic wave excitation of ferromagnetic metals and magnetic dielectrics actually leads to similar issues, but also to very nice resonant coupling in the right conditions [96, 81, 38, 39]. Yet, these experiments guided us towards a much more efficient non-magnetic stimulus that had not been envisioned for (Ga,Mn)As yet: *surface* acoustic waves.

#### 4.4 Magnetoacoustics with electrically excited SAWs

Surface acoustic waves generated electrically can couple easily to weakly propagating in-plane or uniform modes of a magnetic layer and usually have a small frequency ( $<5$  GHz)/wave-vector. This is typically the precession frequencies of the FMR mode in (Ga,Mn)As, which can be lowered by a hard-axis field, should it be higher than  $f_{saw}$ . We demonstrated the resonant coupling between SAWs and magnetization by the two types of measurements described in Sec. 3, one on the SAWs, the second one on the magnetization precession.

##### Resonance of the acoustic wave absorption and velocity at $f_{prec}(B) = f_{saw}$ :

The amplitude  $A$  and phase  $\psi$  of the SAW arriving on the receiving transducer (Fig. IV.5) are monitored with respect to the hard axis field. Their variations with respect to a reference level ( $A_0, \psi_0$ ) are converted into absorption  $\Delta\Gamma = -20\log\frac{A}{A_0}$ , and velocity variations using  $\frac{dV}{V} = \frac{\psi - \psi_0}{2\pi f_{saw}\tau_0}$ . Both of these quantities evidence a clear resonance at a particular field, identified to be the one for which the precession frequency lies closest to the SAW frequency, so that we call this phenomenon SAW-FMR.

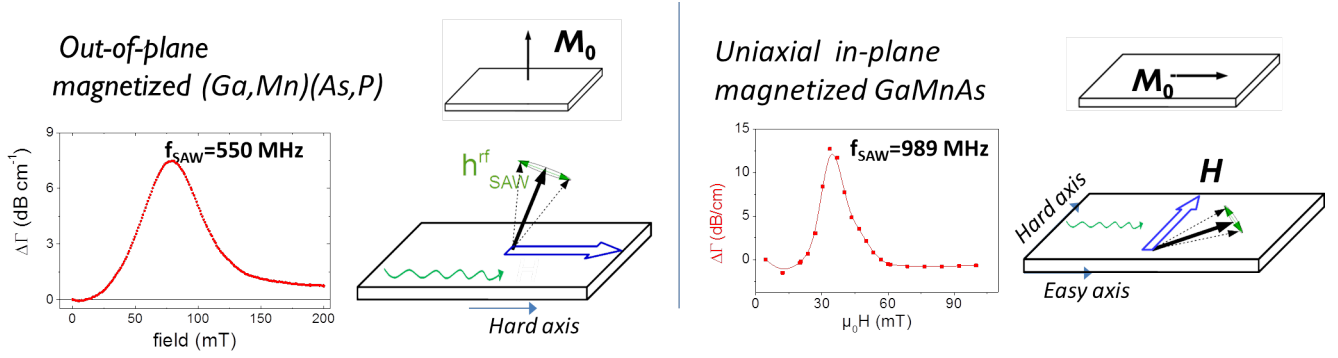
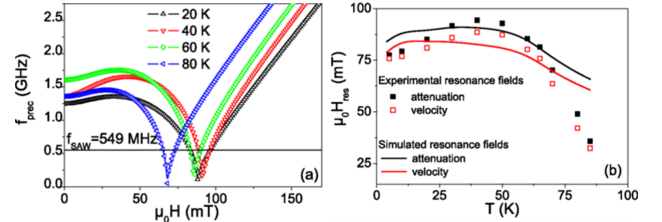


Figure IV.9: [111, 196]: Examples of SAW-FMR curves for (Ga,Mn)As and (Ga,Mn)(As,P) evidencing different anisotropies: for an out-of-plane magnetized layer, the field must be applied in-plane, for an in-plane, uniaxial layer, along the in-plane hard axis (see Eqs. IV.11).

Several features come out:

- **SAW-FMR can be obtained on both in-plane and out-of-plane samples**, provided the field is applied in the direction guaranteeing non-zero torque between magnetization and SAWs (Eqs. IV.11, Fig. IV.9). This result would have been very difficult to obtain on a material other than (Ga,Mn)As, whose anisotropy can be modified keeping other relevant magnetic parameters ( $M_s$ ,  $T_c$ ) identical.

- The **resonance fields can be predicted easily** by calculating the intersection of  $f_{saw}$  with the field variations of the precession frequency  $f_{prec}$ , using the anisotropy constants determined by cavity FMR (J. von Bardeleben). When the field is applied along the hard axis,  $f_{prec}$  decreases, up to the point when the magnetization is saturated along the field.

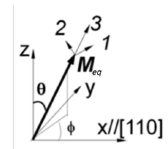


- The **absorption at resonance increases with the SAW frequency**, as does the absorbed power in a cavity FMR experiment [219]  $P_{abs} = -\frac{\omega_{saw}}{2} \Im \left( \mathbf{h}_{rf}^* [\bar{\chi}] \mathbf{h}_{rf} \right)$  where  $\bar{\chi}$  is the susceptibility tensor. The maximum attenuation obtained was of the order of -27 dB/cm ( $\Delta\Gamma=5$  dB, i.e. almost half of the SAW amplitude has been lost to the interaction with the magnetization) and maximum delays of 560ps ( $dV/V=8.10^{-4}$ ) [24]. Considering the moderate magneto-elasticity of (Ga,Mn)As, and that its thickness is about 1% of the SAW penetration depth, these values are quite remarkable and rival those found in nickel at comparable frequencies [219].

- The **shape of the absorption curve can be reproduced by a relatively simple model**, adapted from Refs. [219, 45]:

The LLG equation is first linearized and solved to give the small oscillations components of the magnetization,  $m_1, m_2$  around the static position  $\vec{M}_{eq}(H) // \vec{m}_3$ :

$$\begin{pmatrix} m_1 \\ m_2 \end{pmatrix} = \bar{\chi} \begin{pmatrix} \mu_0 h_1 \\ \mu_0 h_2 \end{pmatrix}$$



$\bar{\chi}$  is the susceptibility tensor. It depends solely on the derivatives of the total static energy with respect to the directions 1, 2, 3. In the SAW-FMR geometries exposed here, only the diagonal components of this tensor,  $\chi_{11}, \chi_{22}$

intervene.  $\mu_0 h_1, \mu_0 h_2 = -\frac{\partial f_{ME}^{SAW}}{\partial m_i}$  are the effective SAW-induced fields, calculated from the time-dependent part of the magneto-elastic energy,  $f_{ME}^{SAW}(x, t)$ .

Then the derivation of the SAW velocity in the magnetic layer is done as in Sec. 2, but counting this time the total elastic energy:

$$\begin{aligned} \rho \frac{\partial^2 u_i(\vec{r}, t)}{\partial t^2} &= c_{ijkl} \frac{\partial (f_{el} + f_{ME})}{\partial x_j S_{kl}} \\ u_i(x, t) &= U_i e^{-\beta z} \exp^{i(kx - \omega t)} \end{aligned} \quad (IV.12)$$

Solving this equation as above leads to an equation linking  $\omega$  and  $k$  very similar to Eq. IV.5, but where most of the elastic constants have been modified by the magnetoelastic interaction. For an out-of-plane magnetized layer for instance [196]:

$$(c_{44} - \rho V_R^2)(c_{11}^* c_{33}^* - c_{13}^{*2} - c_{33}^* \rho V_R^2)^2 = c_{44} c_{33}^* (c_{11}^* - \rho V_R^2) (\rho V_R^2)^2 \quad (IV.13)$$

$$(IV.14)$$

$$\left\{ \begin{array}{l} c_{13} \mapsto c_{13}^* = c_{13} + M_s A_{2\varepsilon}^2 \sin^2 2\theta_0 \chi_{11} / 2 \\ c_{11} \mapsto c_{11}^* = c_{11} - M_s A_{2\varepsilon}^2 \sin^2 2\theta_0 \chi_{11} / 4 \\ c_{33} \mapsto c_{33}^* = c_{33} - M_s A_{2\varepsilon}^2 \sin^2 2\theta_0 \chi_{11} \end{array} \right. \quad (IV.15)$$

$A_{2\varepsilon}$  is roughly proportional to the  $B_1$  magnetoelastic coefficients introduced above. Because the susceptibility tensor is complex and field-dependent, so are the new elastic constants, and wave-vector solutions that result from them:  $k \mapsto k^* = k + \Delta k(B)$ . Intuitively,  $\Re[\Delta k(B)]$  can be understood as the *phase* variations of the SAW under field, whereas the imaginary part  $\Im[\Delta k(B)] < 0$  will instead reflect on the *amplitude* variations that are measured.

Because  $\chi_{11} \propto \frac{1}{\omega_{prec}^2 + 2i\omega\Gamma_0 - \omega^2}$ , these variations will peak at  $\omega_{prec} = \omega_{saw}$ , and be broadened by a quantity proportional to the Gilbert damping ( $\Gamma_0 \propto \alpha$ ). Finally, plotting  $\exp[\Im[\Delta k(B)].l]$  where  $l$  is the length of the delay line reproduces quite well the shape and frequency dependence of the experimental absorption curve (Fig. IV.10b,c).

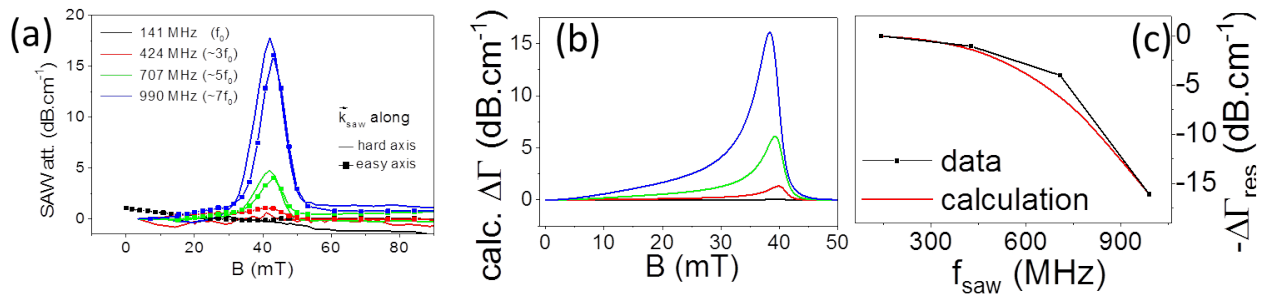


Figure IV.10: [111]: (a) The SAW-FMR absorption increases with  $f_{saw}$ . (b,c) The dynamic delta- $E$  model reproduces decently the shape and amplitude of the experimental curves.

The main addition of our approach was to take explicitly into account the depth-dependence of the SAW amplitude necessary to describe a genuine Rayleigh wave, instead of taking the attenuation  $\beta = 0$  in Eq. IV.12 as in Refs. [45, 80]. It is the resulting coupling of  $u_x$  and  $u_z$  displacements components that leads to an analytical expression of the modified elastic constants, which we named “dynamic delta- $E$  effect”. This is indeed an extension of the static “delta- $E$ ” model published over thirty years ago, in which magnetostriction was demonstrated to lead to a static modification of Young’s constant [88].



Its clear limitation is that, as in Refs. [45, 80], the magnetic sample is considered to be a semi-infinite substrate, not a thin layer on a magnetic substrate..whilst assuming at the same time a strain constant in the depth of the layer, and equal to its surface value.... To take into account the first point and reproduce quantitatively the absorption observed experimentally, one must renormalize the magnetoelastic constants by a “filling factor”, typically about 3 for a 50nm thick layer excited by a 550 MHz SAW( $\lambda \sim 5\mu\text{m}$ ). When the magnetic layer is acoustically matched to its substrate - as is the case of (Ga,Mn)As or (Ga,Mn)(As,P) over GaAs - this approach is legitimate. For heterostructures made of materials presenting very different acoustic impedances, other approaches need to be used: a perturbative “layer-over-substrate” model [62], or even a more rigorous transfer matrix approach with boundary conditions clearly identified at each interface [238, 51, 25].

### Resonance of the magnetization precession amplitude at $f_{prec}(B) = f_{saw}$

Using the set-up described in Sec. 3, we measured the real-time precession of the magnetization induced by a SAW in the in-plane magnetized (Ga,Mn)As layer shown above. Multiples of the laser frequency ( $nf_L$  with  $n = 2, 4, 6, 8$ ) excite appropriately designed transducers, and the polarization rotation is recorded as a function of the optical delay line position. The time-traces (Fig. IV.11a) show oscillations at the same frequency as  $f_{saw}$ , which disappear above the Curie temperature.

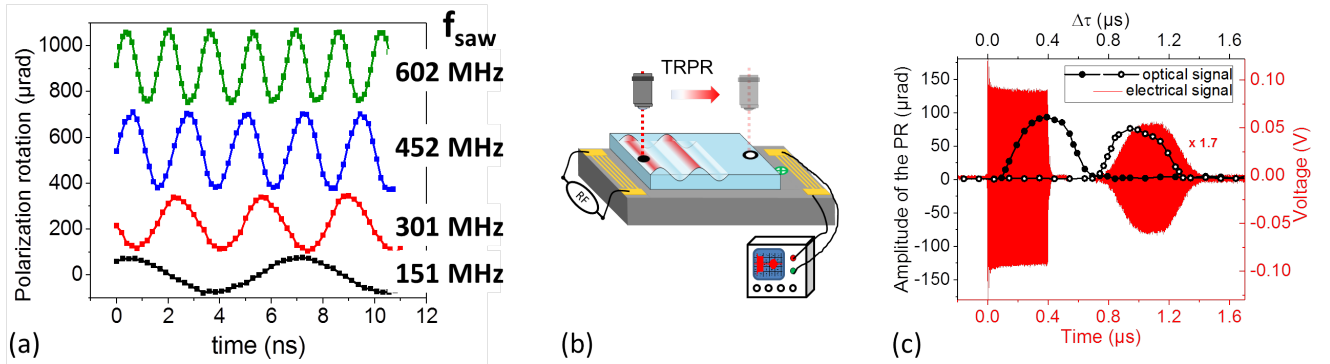


Figure IV.11: [109]: First real-time observation of the magnetization being forced into precession by an electrically generated surface acoustic wave. When the laser spot is shifted by 2mm, the synchronization with RF pulses also needs to be shifted by  $\Delta\tau = \frac{2mm}{V_R} \sim 700\text{ns}$  to recover the signal (full and empty circles in (b,c)).

A further confirmation of the magnetoacoustic origin of the signal was a thorough study of the amplitude of the precession as a function of incoming beam polarization. As shown above, this is a convenient - albeit time-consuming - way of extracting the small oscillating  $\delta\theta, \delta\varphi(x, t)$  components of the magnetization, but also the in-plane strain  $S_{xx}(x, t)$ . Performing this as a function of field and for different frequencies clearly shows the resonant excitation of magnetization precession, at the same fields at which the SAW is critically absorbed (Fig. IV.12).

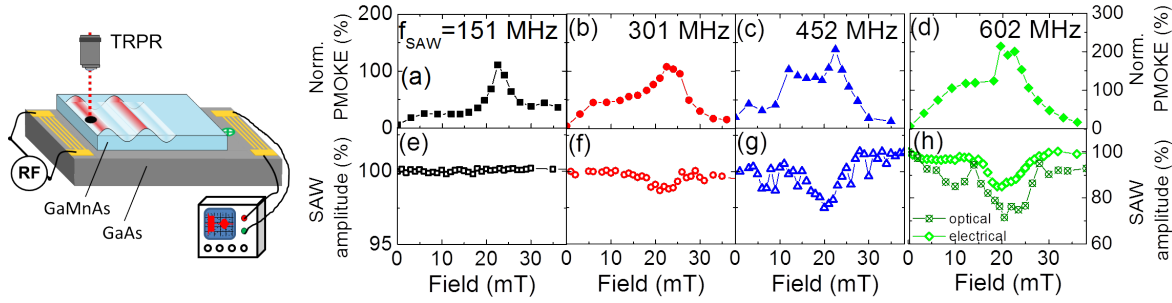


Figure IV.12: **[109]**: *Top panel*: magnetization precession (polar contribution to the magneto-optical signal, proportional to  $\delta\theta(t)$ ). *Bottom panel*: electrical measurement of the SAW FMR. By placing the laser spot on the GaAs, opposite from the exciting IDT, one can also monitor *optically* the SAW FMR using the photo-elastic effect (crossed out squares in panel *h*).

Again, the shape, amplitude and position of the magnetic resonance can be easily reproduced by solving the linearized LLG equation in presence of a time-dependent forcing magneto-elastic field. A SAW propagating along  $x||[110]$  will induce different  $S_{XX} \neq S_{YY}$  components in the GaAs lattice reference frame  $X||[100]$ , and thus change the in-plane anisotropy via the  $B_2$  term. Because exchange-coupled propagating spin waves lie much higher up in energy, the magnetic exchange contribution can be ignored here: the SAW is only coupling to the uniform FMR mode. For an in-plane magnetized layer excited by a SAW propagating along  $x||[110]$ :

$$\delta\theta(x, t) \propto \frac{B_2 |S_{xx}|}{\sqrt{(\omega_{saw}^2 - \omega_{prec}^2)^2 + 4\Gamma_0^2 \omega_{saw}^2}} \sin(\omega_{saw} t - k_{saw} x + \psi) \quad (\text{IV.16})$$

By scanning the objective in the plane of the sample, one can indeed see that the acoustic plane-wave excites locally the precession (Fig. IV.13, top map). The imparted wave-vector is too low and the magnetic damping too high for these waves to interfere, as observed for instance for thermally excited spinwaves in Ref. [8].

### Non-linear magnetization dynamics triggered by SAWs

The amplitude of the magnetization precession is in the vast majority of cases proportional to the SAW amplitude (Eq. IV.16), as is the SAW absorption at resonance. Yet we soon realized that for particular field ranges, temperatures or RF powers, non-linearities appeared in both behaviors: the double frequency  $2f_{saw}$  showed up in the magneto-optical traces (temporal and spatial), and the normalized SAW absorption varied with incoming power (Fig. IV.13). The  $2f_{saw}$  magnetic precession amplitude also showed a clear resonant behavior, at fields close to that of the  $f_{saw}$  resonance (Fig. IV.14c), and its amplitude varied quadratically with SAW amplitude (Fig. IV.15c).

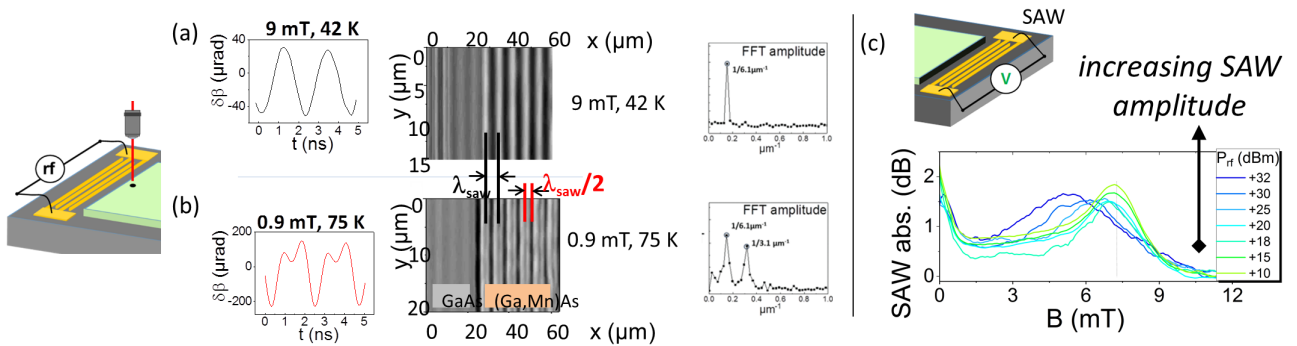


Figure IV.13: **[105]** Uniaxial, in-plane magnetized (Ga,Mn)As layer, excited by  $f_{saw} = 452$  MHz. (a) Linear magnetic response. (b) Non-linear magnetic response. The doubled acoustic frequency appears in the time and space magnetization at certain fields, temperatures and powers. (c) Non-linear acoustic response: the maximum absorption of the SAW at resonance varies and shifts with incoming power.

The conditions for this phenomenon to arise at the resonance field were: (i) large enough RF power to excite larger precession amplitudes, (ii) a dependency of  $f_{prec}$  with magnetic field such as to intersect comfortably both  $f_{saw}$  and  $2f_{saw}$  (Fig. IV.14a).

Adapting the parametric resonance model of Ref. [29], C. Gourdon moreover showed that the resonance of  $f_{saw}$  and  $2f_{saw}$  precession components could be well reproduced by conserving a *linearized* form of the LLG equation (i.e. ignoring small oscillating  $\delta\theta\delta\varphi(x,t)$ ,  $\delta\theta^2(x,t)$ ,  $\delta\varphi^2(x,t)$  components), but taking into account non-linear acoustic driving components (i.e. terms varying as  $\delta\theta S_{xx}(x,t)$ ,  $\delta\varphi S_{xx}(x,t)$ ). In that approach, one finds in addition to the  $\delta\theta_{f_{saw}}(x,t)$  response (Eq. IV.16):

$$\delta\theta_{2f_{saw}}(x,t) \propto \frac{B_2|S_{xx}|^2}{\sqrt{(\omega_{saw}^2 - \omega_{prec}^2)^2 + 4\Gamma_0^2\omega_{saw}^2} \cdot \sqrt{(4\omega_{saw}^2 - \omega_{prec}^2)^2 + 16\Gamma_0^2\omega_{saw}^2}} \sin(2\omega_{saw}t - 2k_{saw}x + \psi_{2f_{saw}}) \quad (IV.17)$$

Because the  $f_{prec}(B)$  is steep when crossing  $f_{saw}$  and  $2f_{saw}$ , only one resonance field is seen at each intersection (around 0.8mT and around 9mT in the 75K data of Fig. IV.14), but one could imagine a configuration where distinct resonance fields would be observable.

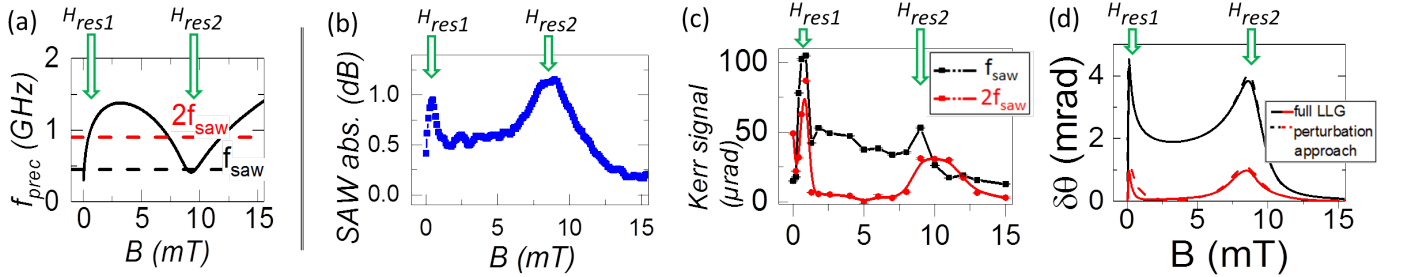


Figure IV.14: [105](a) At certain temperatures (here 75K), the precession frequency intersects twice the acoustic frequency, giving two resonance fields observable in: (b) the SAW absorption and (c) the precession amplitude. (d) This behavior is well reproduced by a parametric resonance model (C. Gourdon).

While this model correctly reproduces the initial quadratic evolution of  $|\delta\theta_{2f_{saw}}|$ , it breaks down at the highest SAW amplitudes, for which the amplitude of  $|\delta\theta_{f_{saw}}|$  also becomes sub-linear (Fig. IV.15), a phenomenon already observed with traditional rf field excitation [11]. This effect is due to genuine magnetic non-linearities, with which the uniform mode loses energy to higher order spin waves. It arises at surprisingly small precession angles (less than  $0.1^\circ$  here), questioning the common use of the linearized form of the LLG equation in most magneto-acoustics papers.

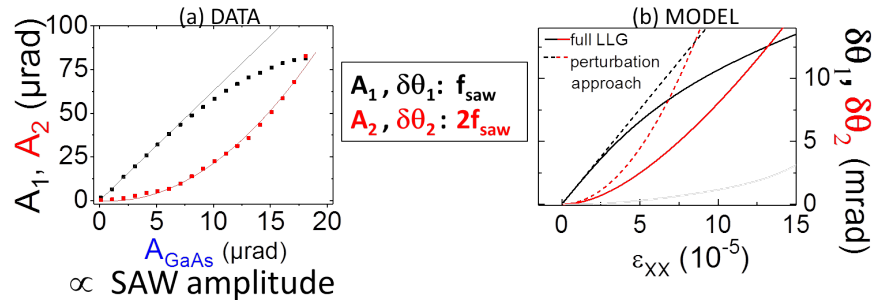


Figure IV.15: [105] At small SAW amplitude,  $f_{saw}$  and  $2f_{saw}$  precession amplitudes vary linearly and quadratically with driving force. Beyond a certain value, they both vary less fast than this linearized LLG prediction (dashed lines), as higher-order magnetic modes become excited.

## 4.5 Magnon-polarons

There are now countless articles reporting a resonant SAW absorption or magnetization precession amplitude at the field where  $f_{prec}(B) = f_{saw}$  [29, 219, 225]. There are a lot less showing a crossing, or anti-crossing of phonon and magnon dispersion curves, a theoretical curve that however often illustrates the introduction of magnetoacoustics presentations. This section is dedicated to the description of the failed attempt to measure (anti-)crossing magnon and phonon dispersion relationships during P. Kuszewski's thesis. While these measurements were essentially inconclusive, an overview of the motivations, the problems we met and the (more successful) experiments that have been published since on the topic seems relevant to this manuscript.

### 4.5.1 Motivations

The coupling of magnetization and lattice dynamics can be seen as that of two oscillators having a set of eigenfrequencies and -vectors. While there are other (non-linear) conditions under which they can interact, their coupling is most efficient when magnetic and lattice vibrations have equal energy (frequency) and wave-vectors, i.e. where their dispersion relationships meet. Depending on the strength of the magnetoelastic coupling,  $\kappa_c$ , they will either simply cross, or avoid each other, opening a gap at the borders of which excitations have both a magnon- and phonon-like behavior, a new quasi-particle called "magnon-polaron" (Fig. IV.16). This is very much like what happens when excitons and photons couple for instance (on the general treatment of frequency splitting induced by strong coupling between two resonators, see the excellent review paper by Novotny *et al.* [146]).

As explained above, for magnons and phonons, this involves solving simultaneously the 5 coupled equations:

$$\begin{cases} \frac{\partial \vec{m}}{\partial t} &= -\gamma \vec{m} \wedge \mu_0 \vec{H}_{eff} + \alpha \vec{m} \wedge \frac{\partial \vec{m}}{\partial t} & \text{with } \mu_0 \vec{H}_{eff} = -\vec{\nabla}_m f_{tot} \\ \rho \frac{\partial^2 u_i}{\partial t^2} &= \frac{\partial \sigma_{ik}}{\partial x_k} = \frac{\partial^2 f_{tot}}{\partial x_k \partial S_{ik}} \end{cases}$$

which can be re-written in the most general case as:

$$[M(\omega)].[U_x, U_y, U_z, m_1, m_2] = [A]$$

$[M(\omega)]$  is a 5x5 matrix and  $[A]$  encompasses all the forcing terms. Already introduced above, the  $U_i$ 's are the displacement amplitudes defined in Eq. IV.12 and the  $m_1, m_2$  are the dynamic magnetization components in the plane perpendicular to the static position  $\mathbf{M}_0$ . Cancelling out the determinant of  $M$  gives in all generality [15]:

$$(\omega^2 - \omega_{ph}^2(k)) [(\omega^2 - \omega_{mag}^2(k)) (\omega^2 - \omega_{ph}^2(k)) - \omega_c^4(k)] = 0 \quad (\text{IV.18})$$

$\omega_c(k)$  has the dimension of a frequency, and accounts for all coupling effects: spin-waves modified by the dynamic effective magneto-elastic field  $\mu_0 h_{eff,i} = -\frac{\partial f_{ME}}{\partial m_i}$ , and displacements modified by the dynamic magneto-elastic stress  $\frac{\partial}{\partial x_k} \sigma_{me,x_i,x_k} = \frac{\partial}{\partial x_k} \left( \frac{\partial f_{ME}}{\partial \varepsilon_{x_i x_k}} \right)$ . When equal to zero, one recovers the uncoupled solutions for phonons and magnons,  $\omega_{ph}$  and  $\omega_{mag}$  (green lines in Fig. IV.16). Otherwise a frequency splitting  $\Delta$  appears at the wave-vector for which  $\omega_{mag} = \omega_{ph}$  (black/red symbols in Fig. IV.16). When  $\omega_c \ll \omega_{mag}, \omega_{ph}$ , solving Eq. IV.18 simply gives  $\Delta = \frac{\omega_c^2}{\omega_{mag}} = \frac{\omega_c^2}{\omega_{ph}}$ . This splitting has been derived analytically by different authors for varying geometries who have expressed it as a function of a coupling constant  $\kappa_c$  [76, 7, 211, 15]. A general formula reads :

$$\kappa_c = \frac{\Delta}{2} = \sqrt{\frac{\gamma}{\rho \omega_{ph} M_{sat}}} \mathcal{F}(B_i, m_i, \varphi)$$

It has the dimension of a frequency, and  $\mathcal{F}(B_i, m_i, \psi)$  is a function translating the overlap ( $\sum_{i,j,k} m_i(\mathbf{r}) \cdot S_{jk}(\mathbf{r})$ ) between acoustic and magnetic modes. It depends on the magnetoelastic coefficients  $B_i$ , the reduced magnetization coordinates  $m_i$  and the angle between the SAW wave-vector and the static magnetization,  $\varphi$ . Because this coupling is highly anisotropic (Eq. IV.11), equating magnon/phonon frequencies/wave-vector is thus not necessarily sufficient

to induce a frequency splitting. Likewise, the coupling can be maximized by choosing the right angle, but the system be quite off resonance, as illustrated in Fig. IV.16.<sup>2</sup>:

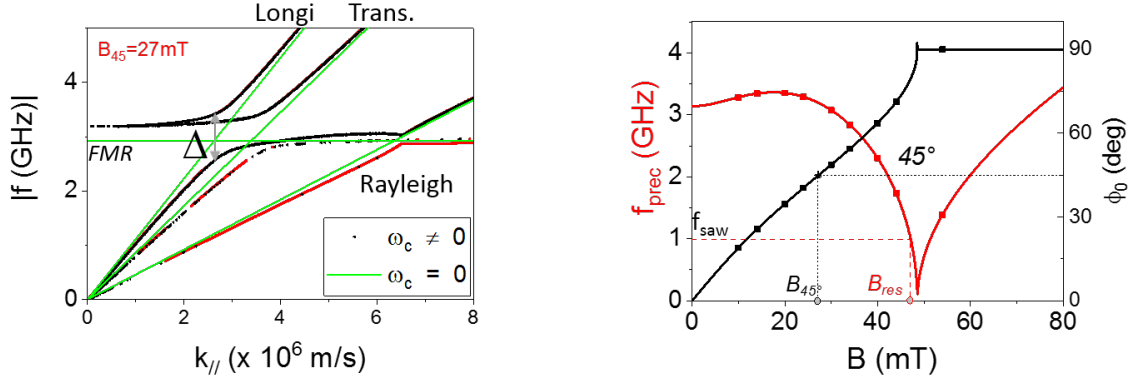


Figure IV.16: An illustration of the crossing of magnon and phonon DRs calculated for a (Ga,Mn)As sample. Solving simultaneously elastic and magnetization dynamics yields the undisturbed dispersion relationship (here: uniform magnetic mode and longitudinal, transverse and Rayleigh acoustic modes). Coupling to the Rayleigh mode is maximum at  $B_{45}$ , when the angle between SAW wave-vector and static magnetization is  $\varphi = 45^\circ$  (see Eqs. IV.11). This field is not necessary the resonance field for which  $\omega_{ph} = \omega_{mag}(B_{res})$  (here  $B_{res} \sim 48mT$  for  $f_{saw} = 1GHz$ ), leading to a very weak anti-crossing for the Rayleigh mode, compared to the longitudinal/transverse modes.

This gap can only be resolved provided it is larger than both acoustic and magnetic damping rates. Otherwise no gap will open, but phonon and magnon resonance linewidths (damping) will be substantially modified [56]. While the acoustic damping rates are typically very low, FMR linewidths  $\Delta\omega_{mag} = \alpha\omega_{mag}$  can reach the GHz with  $\alpha = 0.01 - 0.1$ .

Apart from the fundamental challenge of evidencing these “magnon-polarons”, obtaining a magnetic-field tunable gap could offer exciting possibilities for tunable SAW-based filters for instance: acoustic waves travelling across a delay line could undergo a sizable decrease of their group velocity or amplitude at will for example. In addition, because of the great tunability of spinwave dispersion, one can imagine different original ways to modify phonons: non-reciprocal coupling (IV.32b), tangential coupling (group velocity matching) etc. Another way to see this is to consider the gap opening as a way to excite/modify phonons via magnons or vice-versa, in cases where a direct excitation is not possible, as recently demonstrated very nicely by Godejohann *et al.* [56].

However, seeing any type of crossing or anticrossing has been challenging as it first requires to tune either acoustic or magnetic wave-vector over a broad enough range. Instead of scanning the wave-vector, people have often shown avoided crossing in acoustic/magnetic frequency spectrum versus *field*, for a couple different acoustic wave-vectors (in general, different mode polarizations). This approach is of course equivalent, but will be difficult to implement for magnetic systems whose frequency varies weakly with magnetic field (e.g, antiferromagnets).

<sup>2</sup>Some details on this calculation that has not been published: magnetic parameters of the (Ga,Mn)As sample used in Ref. [111]. No  $k$ -dependence assumed for  $\omega_{mag}$  (FMR mode), frequency-independent filling factor assumed for the SAW.

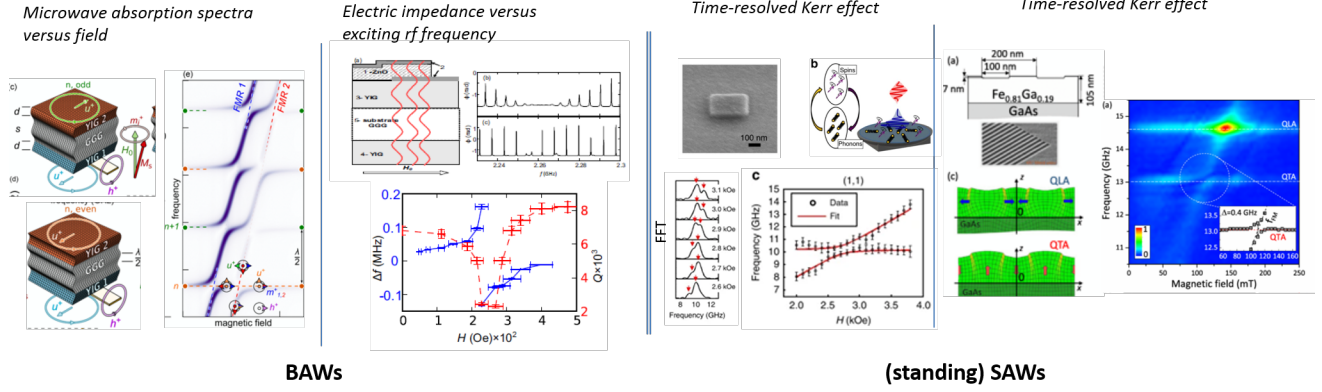


Figure IV.17: **BAWs**: Using a bulk acoustic resonator geometry including a magnetic layer, An *et al.* and Polzikova *et al.* both used the magnetic field to adjust the FMR mode to the standing *bulk* acoustic modes in the thickness of the sample, focusing either on the magnetic or the acoustic response. In both cases, gap openings below 1 MHz were observed. (a) [7]: Periodic modulation of the intensity interpreted as the avoided crossings between the YIG FMR mode at  $\omega_1 = \gamma\mu_0(H_0 - M_1)$ , and the  $n$ th standing (shear) acoustic resonances across the total thickness (horizontal dashed lines) at  $\omega_n = n\pi v/(2d + s)$  and the exchange of phonons between the top and bottom ferromagnetic layers. (b) [155]: fine field-driven shifting of the resonances of a high overtone acoustic resonator through its magnetoelastic coupling to a YIG film. **SAWs**: optical excitation of *standing* acoustic modes ( $k_{x,y} = \frac{n\pi}{l_{x,y}}$ ) on nanostructured samples (Ni or FeGa) to increase the spatial overlap with the magnetic mode, tuned by a magnetic field: (c) Berk *et al.* [15] Probing mainly the magnetization dynamics, they witness the coexistence of two modes over a fairly broad field range. (d) Godejohann *et al.* [56]: very shallow FeGa grating. A gap opening is seen only when crossing magnon and *transverse* acoustic modes because of an ideal spatial overlap, contrary to the longitudinal mode.

Generating the SAWs optically is a more appropriate approach, since their spectral range, given by the Fourier transform of the laser pulse duration and diameter is inherently broader. This is what we and Hashimoto *et al.* [69] attempted to do, the latter successfully as shown further.

#### 4.5.2 Looking for $f(k)$ avoided crossing in FeGa, Nickel and Co

When we started Piotr's thesis there was no demonstration of (anti-)crossing dispersion relationships between Rayleigh waves and spinwaves. We studied different magnetic thin films sequentially: Ni(100nm)|glass (deposited by L. Becerra at INSP), FeGa(90nm)|SrTO<sub>3</sub> and FeGa(120nm)|Al<sub>2</sub>O<sub>3</sub> (sputtered by Rocio Ranchal at Universidad Complutense de Madrid) and finally Co(100nm)|Al<sub>2</sub>O<sub>3</sub> (deposited by S. Suffit at Paris VII), as well as non-magnetic control samples (Ti/Al<sub>2</sub>O<sub>3</sub> and Al/glass). Nickel was rapidly abandoned because of its poor Kerr constant and tendency to melt under the laser pulses. FeGa was eventually swapped for Cobalt because of its larger magnetoelastic coefficient. In the end however, observations varied only weakly from one material to another. The SAWs were excited optically as described in Sec. 3 on Laurent Belliard's set-up (INSP), slightly modified to switch by a single mirror flip from an interferometric detection of the surface displacement to a polarization rotation (PR) detection. For this, thin films were grown over a double-polished and transparent substrate<sup>3</sup> to have pump and probing beams on either side of the magnetic layer (Fig. IV.18).

Broad-band FMR (Fig. IV.18) and a full angular-dependence of the hysteresis loops showed that in the weak magnetic field conditions imposed by the set-up, precession frequencies of around 1-2 GHz could be expected, and switching fields below 20 mT, manageable by a permanent magnet. High numerical aperture objectives (0.95) were used in order to provide a tight focusing to  $d_{min}$ . Combined with the high velocity  $V_R$  substrates used in the latter studies (STO and sapphire), this ensured the highest possible acoustic frequencies ( $f_{max} = \frac{V_R}{4d_{min}}$ ) to match to the FMR mode.

<sup>3</sup>Note that other authors [56] have worked with two synchronized lasers, one of them lying in the infra-red, below the gap of the substrate

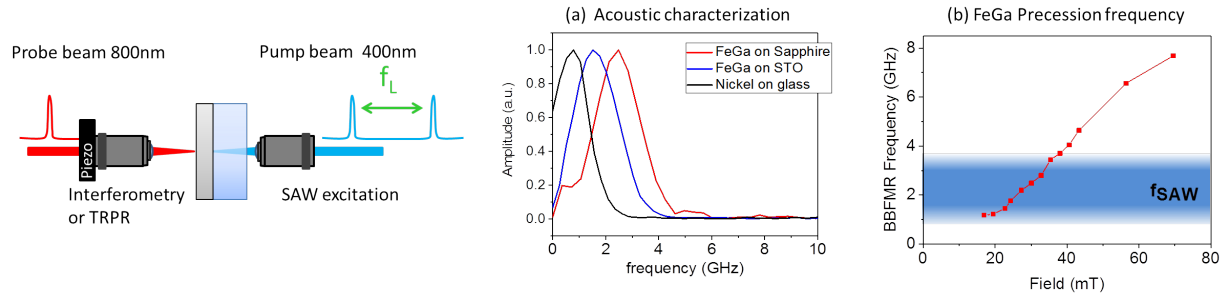


Figure IV.18: [110]: Schematics of the dual interferometry/time-resolved polarization rotation (TRPR) experiment. (a) Frequency content of the Rayleigh waves generated by thermoelasticity (interferometric detection). (b) FMR mode of the FeGa/Al<sub>2</sub>O<sub>3</sub> sample showing a good overlap with acoustic frequency (broad-band FMR on the set-up developed by our post-doc I. Camara).

- Typical interferometry and polarization rotation (PR) maps are shown below in Fig. IV.19 for the FeGa/Al<sub>2</sub>O<sub>3</sub> sample. The signal in the epicenter is generally saturating, so I will rather discuss the contours away from it. A clear hexagonal surface acoustic wave-front appears on both maps due to 3-fold symmetry of the substrate. The ripples evidence a large dispersion of the frequency waves (low frequencies travelling faster than higher ones). The PR map shows a two-fold in-plane symmetry whose main axis did not seem to vary with the incident polarization or the magnetization direction, but rather from day to day..

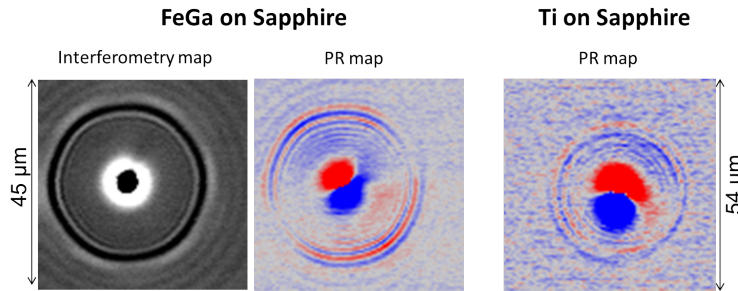


Figure IV.19: [110]: Typical interferometric and polarization rotation (PR) maps recorded on FeGa. Comparative PR map taken on a control non-magnetic Ti sample evidencing weaker signal to noise ratio, but similar features.

Comparing to the expected magnetic PR signatures calculated from the magneto-elastic torques (Fig. IV.20), the only way to reconcile the observed map is to have a dominant contribution of the *shear* strain component. A film-over-substrate calculation however estimated this component to be very small. Moreover, a similar map was obtained on a non-magnetic sample, pointing rather to an elasticity-driven PR. This would not result from photoelasticity which would give a 4-fold symmetry (Fig. IV.20), but possibly from diffraction. This point has not been resolved unfortunately.

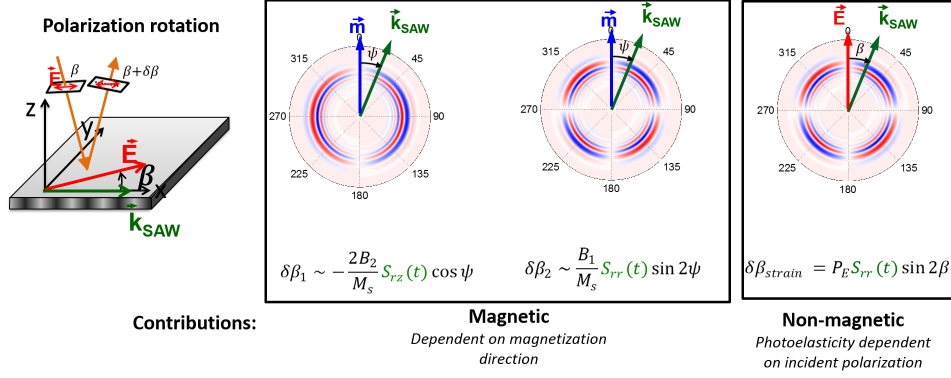


Figure IV.20: [110]: Angular dependence of the polarization rotation  $\delta\beta$  expected from magnetic precession or photoelastic effect: 2-fold with magneto-elastic coupling to the shear strain, 4-fold (never observed) when coupling to the longitudinal component, or when detecting photoelasticity.

- Doing line scans at variable pump-probe delays, in both interferometry and polarization rotation modes, we then obtained dispersion relationships. In the final dispersion map shown in Fig. IV.21, one clearly sees two acoustic modes (surface travelling at 5.7km/s and skimming at 10.6km/s). The dispersion due to the acoustic impedance mismatch between the film and the substrate also shows up as a slightly sub-linear slope of  $f(k)$ .

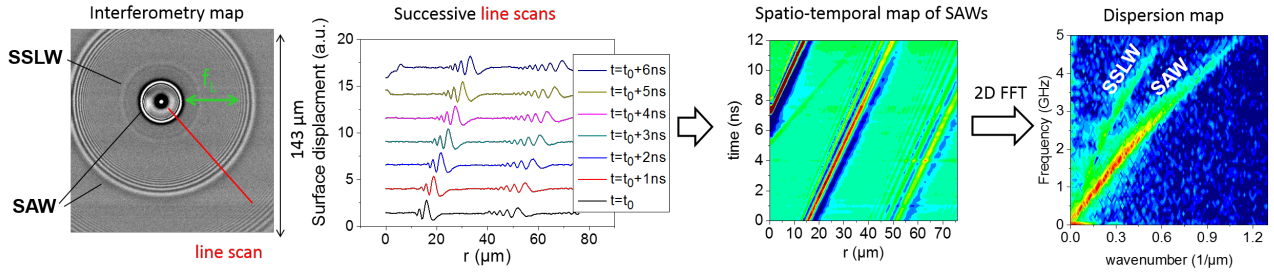


Figure IV.21: [110]: Methodology to obtain dispersion maps from time- and spaced-resolved pump-probe experiments.

A fairly typical set of PR/elastic dispersion relationships (DR) is shown in Fig. IV.22 for the FeGa|sapphire sample, but similar results were obtained on Ni|glass or Co|Al<sub>2</sub>O<sub>3</sub>. The polarization rotation DR seems to follow roughly the SAW of the interferometry DR, except at low frequency/wave-vector where the signal is much weaker. Projecting both Fourier maps onto the frequency axis confirms that the PR data mainly peaks just under 2 GHz, slightly above the FMR frequency, while the interferometry data spreads out more evenly across the spectrum. Although no anti-crossing appeared, this initially seemed like a sign we were indeed seeing the magnons excited by the SAWs.

Various points however went in the wrong direction, such as the insensitivity of this curve to the applied field, or the unexpected two-fold symmetry of the spatial maps. The general absence of tunability of all the features observed with magnetic material, incoming optical polarization or acoustic spectral content all seemed to point to an experimental artefact giving the PR data some of the characteristics we needed, without being of magnetic origin.



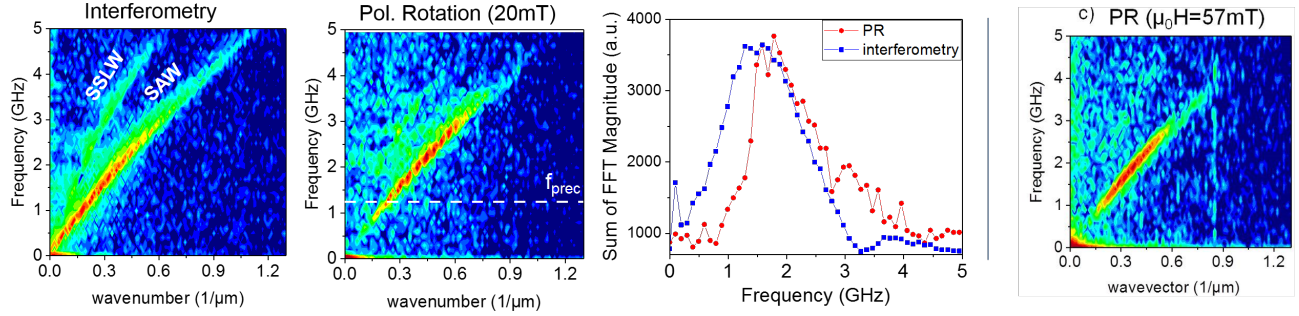


Figure IV.22: [110]: Interferometry and polarization rotation (PR) dispersion maps obtained on the  $\text{FeGa}/\text{Al}_2\text{O}_3$  sample, under 20mT (see corresponding FMR data in Fig. IV.18). The more peaked distribution of PR frequencies, close to the FMR-determined precession frequency could indicate a magneto-acoustic coupling, but the angular dependency of PR maps says otherwise.

I will spare the reader the description of the numerous tests and experiments performed and direct him/her to Piotr's thesis [110]. The general sense was that the data was dominated by an elasticity-driven polarization rotation, and therefore that the magnetic signal was very weak. Since acoustic and magnetic frequencies were overall generally well matched, one could invoke instead:

- a very elliptical precession trajectory resulting from the high magnetization of the materials used, giving a very small polar Kerr dynamics component
- very small elastic strain due to the acoustic power having to spread out over a contour of increasing perimeter (added to the natural acoustic damping, which is quite weak). This could easily be addressed by patterning a linear metallic transducer.
- poor spatial overlap of magnon and phonon modes (see for instance a detailed description of this issue in Babu *et al.* [9])

#### 4.5.3 Successful endeavors of other groups since then

- *Time-domain* observations of magnon and phonon  $f(k)$  curves still remain elusive. With high fluence pulses impinging through the transparent GGG substrate on the back-side of a  $\text{Lu}_{2.3}\text{Bi}_{0.7}\text{Fe}_{4.2}\text{G}_{0.8}\text{O}_{12}$  (LuIG) layer, Hashimoto *et al.* [69] evidence a resonant spin dynamics signal at the crossing point of the acoustic mode dispersion with that of high- $k$  backward volume modes. The success of their approach seems to rely on very strong magneto-optical effect of LuIG, and on the excitation of *bulk* acoustic modes, whose spatial profile favors a strong coupling with magnons [9].
- *Frequency-domain* techniques are naturally better adapted to this topic, in particular Neutron Scattering [124] and Brillouin Light Scattering [22, 9, 237, 76], with their sensitivity to both magnon and phonon excitations. A very nice recent paper measures and explains the (anti-)crossings of magnon and phonon DR of  $\text{CoFeB}/\text{Au}$  multilayers and concludes on the necessity to have not only frequency/wave-vector matching between the two populations, but also a sizable spatial overlap of the modes. This can be seen as a matching of wave-vectors in 3-dimensions (often 2 though), instead of having a simple  $f(k)$  curve with  $k = k \cdot \mathbf{u}$  singling out a unique direction.

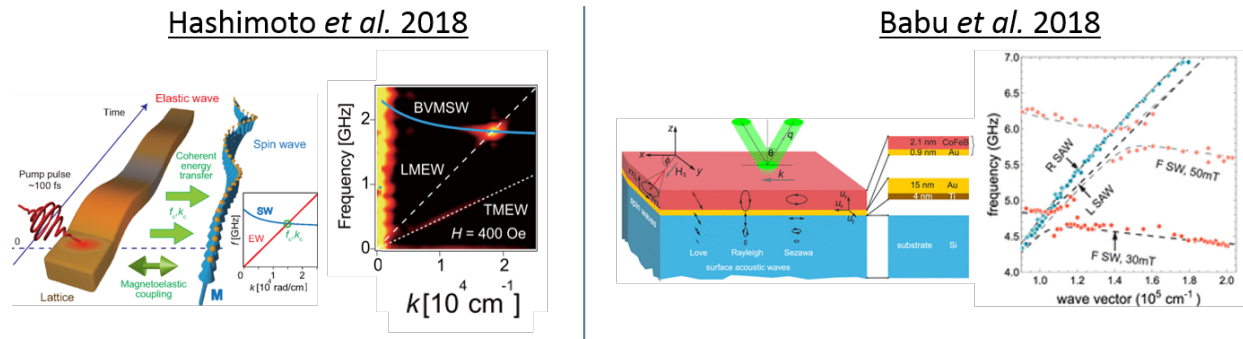


Figure IV.23: [71]: Time- and space-domain detection of the spin-dynamics triggered by optically excited bulk acoustic waves. The mechanism by which they excite these modes is not detailed but might rely on electrostriction (which they seem to call impulse Raman process), or on the thermoelastic effect using the weak absorption of the pump beam in the substrate [148]. [9] Brillouin light scattering evidencing strong (resp. weak) coupling of magnons to Love (resp. Rayleigh, R-SAW) waves and a gap opening of a few 100 MHz for the former.

## 5 SAW-driven or -assisted magnetization switching

### 5.1 Resonant SAW-driven precessional switching

One step beyond the triggering of magnetic resonance with an acoustic wave is the full switching of the magnetization. Again, we first tried with picosecond bulk acoustic waves before realizing that coupling conditions were very poor in this case (Sec. 4.3). We turned instead to SAWs, initiating our collaboration with Jean-Yves Duquesne (INSP, Acoustics Team).

- Principle

As described above, at low SAW amplitude or far from the resonance, the SAW triggers the precession of magnetization around its equilibrium position at  $f_{saw}$ . As the strain is increased,  $2f_{saw}$  components appear in the magnetization dynamics, and the position around which it precesses departs from the SAW-free configuration to drift towards the direction of the applied field [105]. The next step, which we predicted in 2013 [194], is that above a particular SAW amplitude threshold and close to resonance, the precession becomes highly non-linear. Large oscillations at  $f_{saw}/2$  appear, around the applied field this time, with the magnetization oscillating from one energy valley to another (Fig. IV.25). By stopping the SAW at the right moment of this trajectory, we showed numerically that an irreversible magnetization switching could be expected. Note that a similar prediction was published around the same time for picosecond acoustic bulk waves hitting a biaxial film of Terfenol [103].

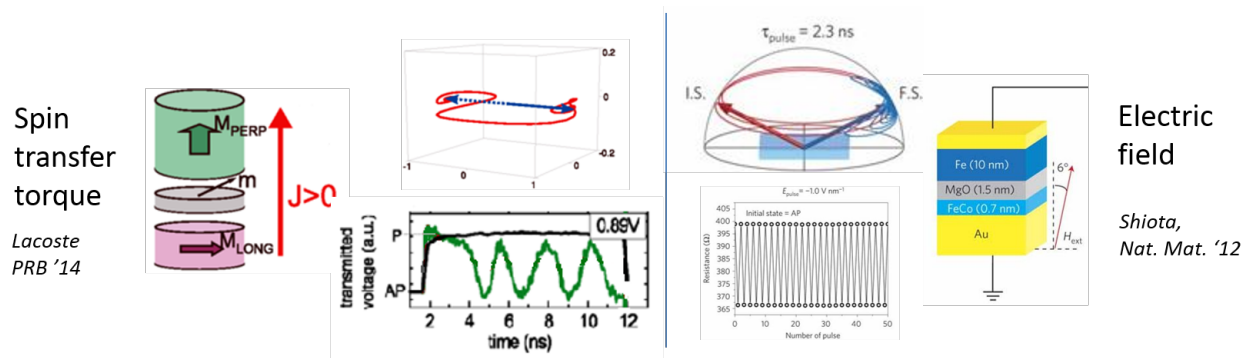


Figure IV.24: Two examples of precessional switching from Refs. [112, 180], using a pulsed polarized current or electric field.

This “precessional switching” mechanism is well-known when triggered by a pulsed field or polarized current, as in magnetic tunnel junctions (Fig. IV.24) [41, 152, 134, 87]. It is of high interest for magnetic storage technology since switching occurs at fields lower than by a classical Stoner-Wohlfarth mechanism, deterministically (at least for short pulses), and at GHz rates of the order of the precession frequency (provided the end phase of the stimulus is well controlled) [122]. In the case of fields/currents, it is the magnetic damping that is particularly critical in determining the magnetic state at the end of the pulse. When using SAWs and in our geometry, it is rather the (slow) decay transient-time of the acoustic wave through the transducers. The final state (e.g. ‘up’ or ‘down’) then depends subtly on the tuning of SAW/magnetic frequencies, and the duration of the SAW pulse, which itself governs the phase of the magnetization dynamics when the SAW amplitude decreases below the large-oscillation threshold (Fig. IV.25). As when using fields/current pulses, SAW-switching is deterministic (Fig. IV.25c). The main foreseen advantage is the remotability of the switching: SAWs are very weakly damped and can travel over millimetric distances. The perspectives of mixing wave-mechanics with spintronics to have acoustic waves address distant bits drove us to initiate the experiments (“SPINSAW” ANR JCJC project 2014-2017).

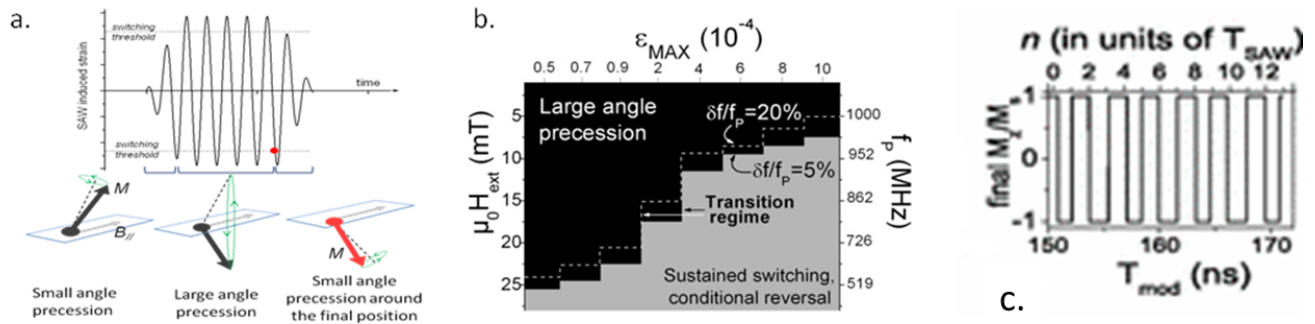


Figure IV.25: [194] Principles of SAW-driven precessional switching and theoretical diagram for applied field/SAW amplitude conditions required to induce precession around the applied field, potentially leading to a full reversal if the SAW pulse is stopped at the right moment.

- **Experimental demonstration of SAW-driven switching**

Using Kerr microscopy to probe initial and final magnetic states in zero field, we demonstrated that we could indeed switch the magnetization of uniaxial *in-plane* or *out-of-plane* magnetized (Ga,Mn)As and (Ga,Mn)(As,P) layers, as summarized in Fig. IV.26. We used SAW pulses of a few hundreds of nanoseconds, or any duration longer than the  $\sim 80$ -100 ns transient. Playing with the wave properties of SAWs, we also showed that standing waves could structure magnetically a layer in  $\lambda_{SAW}/4$ -wide stripes (Fig. IV.27), whose position could be very finally adjusted by varying the relative phase between the two electrical excitation pulses [111].

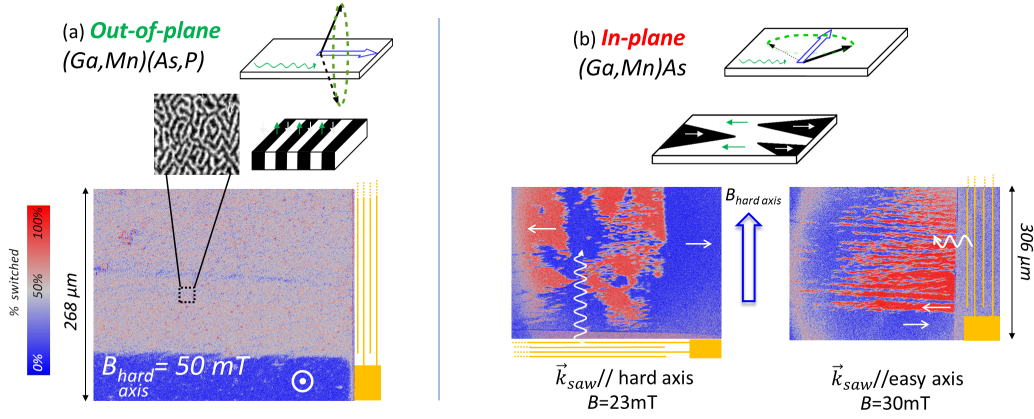


Figure IV.26: **[192, 111]** Resonant switching induced by a 400ns SAW pulse, Kerr microscopy. Reference images taken in opposite saturated states give the percentage of the layer that has switched. No switching is observed out of the SAW path or out of the IDT resonance. (a) Out-of-plane magnetized layer,  $f_{saw} = 549\ MHz$ . After the acoustic pulse, self-organized unresolved domains form, giving an overall 50% switched layer. (b) In-plane magnetized layer,  $f_{saw} = 989\ MHz$ . This time, fully-switched domains can be observed, but on average only about half the layer has switched.

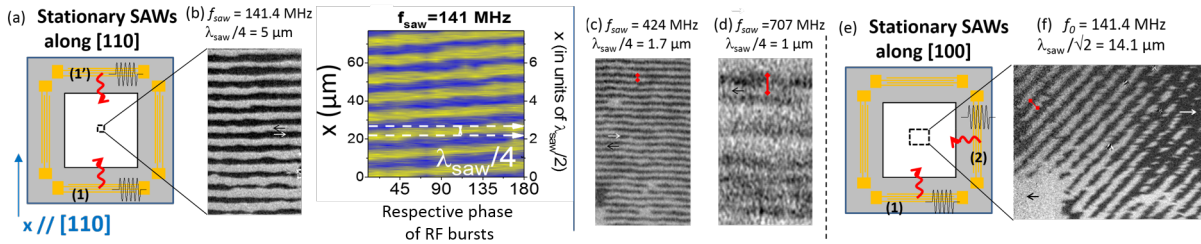


Figure IV.27: **[111]** stationary acoustic waves for magnetic patterning ( $T=40K$ ), created by two acoustic waves interfering with either colinear (a-d) or perpendicular (e-f) wave-vectors. Precise, nanometric positioning of these patterns can easily be obtained by tuning the respective phase of the two RF bursts.

The resonant nature of the switching reversal was proved indirectly by showing it was more efficient:

- at the SAW-FMR resonance field (Fig. IV.28b)
- at RF powers at which non-linear SAW-FMR behaviors appeared (down-shift of the resonance field and non-linear SAW power dependence of the absorption at resonance, Fig. IV.28a)
- as the SAW frequency increased (Fig. IV.28d)
- in geometries maximizing the SAW-induced torques (in particular playing with the angle of the applied field, Fig. IV.28c)

However, we noticed that the duration or phase of the SAW pulse did not seem to have any incidence on the final state, contrary to what is expected of deterministic switching (see for instance the nice data in Fig. IV.24). Moreover, switching was not “reversible”: applying a second SAW pulse on a multi-domain configuration changed only marginally the magnetic configuration.

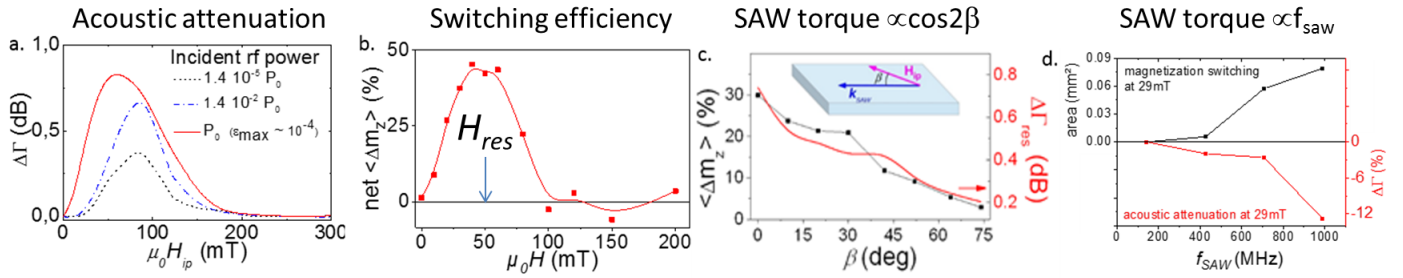


Figure IV.28: [192, 111] Indirect proofs of the resonant nature of the switching by correlating the switching efficiency (area or switching %) and the SAW-absorption at resonance (see text).

Having convinced ourselves of the resonant nature of the switching, we looked for experimental conditions allowing the precession frequency to be resonant with  $f_{saw}$  in *zero field*. This was possible on a particular (Ga,Mn)As layer at  $T = 100\text{K}$ , for which the competition between uniaxial and biaxial anisotropy gives a particular shape to  $f_{prec}(B)$  (Fig. IV.29a). In these conditions, we indeed demonstrated zero-field switching, and even showed reversible toggling between the two equilibrium magnetic states for over 20 consecutive acoustic pulses. This had not been possible for SAW-driven switching under field [192, 111] because any imperfect alignment of the field with the hard axis made  $\leftarrow$  to  $\rightarrow$  switching efficiency very asymmetrical compared to that of  $\rightarrow$  to  $\leftarrow$  (or likewise  $\downarrow$  to  $\uparrow$  and  $\uparrow$  to  $\downarrow$ ), an issue also encountered for current-driven precessional spin-valve switching [152].

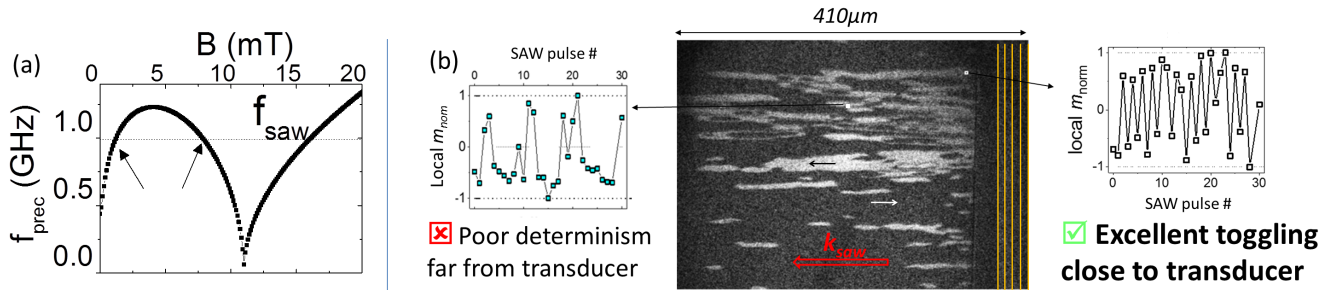


Figure IV.29: [24] Zero-field switching ( $T=100\text{K}$ ): (a)  $f_{prec}(B = 0) \sim f_{saw} = 990 \text{ MHz}$ . (b) Toggling behavior under successive 250 ns-long SAW bursts. It is excellent close to the exciting transducer, but becomes poor away from it, possibly due to incoherent scattering of the wave as it travels over the multi-magnetic domain layer as domain-walls may modify its phase and amplitude.

### • Explaining the shape of the domains

We studied the shape of the domains obtained after SAW-switching, to elucidate why we did not obtain the “fully switched” or “fully unswitched” final state predicted in Ref. [194]. MuMax micromagnetic simulations (see [videos online](#)) showed quite convincingly that it is the spatial dispersion of magneto-elastic constants in the layer that is responsible for the onset of the filamentation: it induces local disparities of the detuning between SAW frequency and precession rate, making the magnetization stop oscillating at different moments of its trajectory when the RF pulse is turned off (Fig. IV.25a). This is also the cause for the insensitivity of the final domain configuration on the SAW pulse duration (Fig. IV.30). As could have been expected, the layer indeed doesn’t behave like a “macrospin”, and tries instead to limit exchange, magnetostatic and domain-wall energies by finding an optimum arrangement: self-organizing into ‘up’/‘down’ domains for the out-of-plane magnetized (Ga,Mn)(As,P) layer, or forming domains several hundreds of  $\mu\text{m}^2$ -wide for in-plane magnetized sample, with the filament shape reducing the magnetostatic energy. Instead, for  $\mathbf{k}_{saw}$  perpendicular to the easy axis (EA), the final domains are larger and less filamented than when  $\mathbf{k}_{saw} \parallel \text{EA}$ , since the SAW wave-front evolves parallel to the magnetic easy axis, a much more comfortable situation from the point of view of magneto-statics.

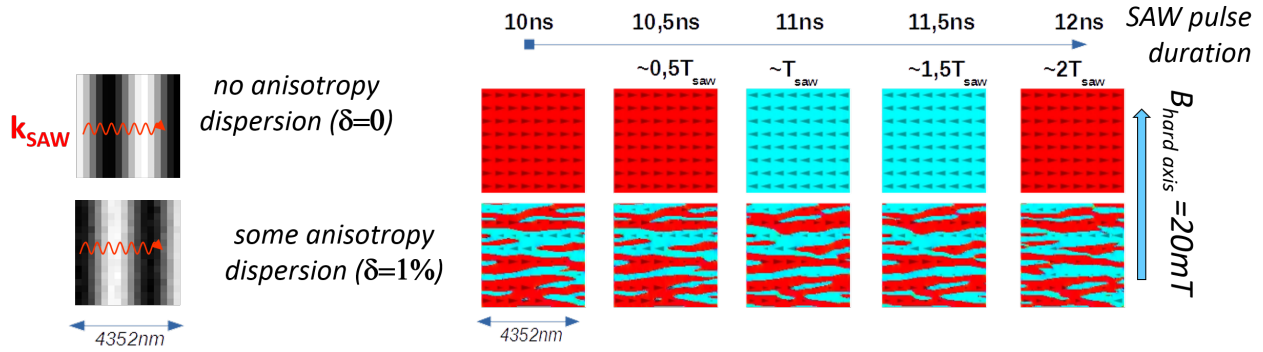


Figure IV.30: [111] Simulations of the final magnetic state after a SAW pulse lasting  $n \frac{T_{saw}}{2}$  including (or not) a phenomenological random dispersion of magnetoelastic constants:  $K_2(x, y, t) = K_{2||,0} + \delta \cdot rand(x, y) \Delta K_{2||,SAW}(x, t)$ .  $B=23$  mT,  $f_{saw} = 989$ MHz,  $\mathbf{k}_{saw}$  along the easy axis. The filament shape of the domains in Fig. IV.26b are well reproduced. For the full movie of the simulations (with/without anisotropy dispersions, for  $\mathbf{k}_{saw}$  parallel or perpendicular to the easy axis), please see [online videos](#).

- Is this really “precessional switching” ?

While these experiments were met with an unexpected success, for both in-plane and out-of-plane layers, several arguments have understandably been put forward by the community to discard the denomination “SAW-driven precessional switching”.

> This term is most generally used in spintronics to signify the use of a hard axis magnetic field combined with a short current or field pulse that reverses the magnetization within half its precession period, rather than within a multiple of  $\frac{T_{precc}}{2}$  as we have done. This may be considered a terminology issue, in which case it would be more appropriate to qualify our experiments as SAW-driven *resonant* switching. Given our geometry, it was not possible to test whether the magnetization could be switched in  $\frac{T_{precc}}{2}$  (or  $\frac{T_{saw}}{2}$ ): the transient of the IDT was much too slow to have reached the SAW-amplitude switching threshold within a fraction of  $\frac{T_{precc}}{2}$ . A better geometry for this would be the use of SAWs generated by femto second pulses illuminating a few-digit IDT. Such optically generated waves have already been shown to excite and control coherently (low angle) magnetization precession in a CoFeB magnetic tunnel junction [231]. A definitive time-domain demonstration of the precessional  $\frac{T_{saw}}{2}$ -periodic trajectory would settle the matter, and was not done for lack of time.

> It has also been argued that it was not the magnetoacoustic torque driving the precession, but the heat generated by the SAW that, combined with applied fields very close to the saturation field would favor the tilt of magnetization towards the opposite potential valley. To adress these remarks, we have repeatedly shown that exciting the IDT at a frequency just off-resonance (no SAW emitted, but identical rf field radiation and heating) gave no switching, and also estimated the temperature-rise due to the SAW itself (thermoelastic effect) as minute [192]. Moreover, the correlation between the depth and field of the SAW absorption resonance with the efficiency and field of the magnetization reversal efficiency does seem to point in the right direction. Because the SAW frequencies were generally quite low, resonance fields (and thus switching field) were indeed often close to the hard axis saturation field. Yet, the demonstration of zero-field switching, with convincing successive toggling between the two states, showed that this mechanism did not require being very close to the saturation field.

## 5.2 Non-resonant SAW-assisted switching

- Principles

Our 2013 calculation [194] also explored another geometry, with a distinct mechanism: the field is this time applied along the *easy* axis, and SAW pulses are applied *continuously* (at 50 Hz repetition rate). Since the domain nucleation energy and domain-wall energy both depend on the easy-axis anisotropy constant -  $K_{2\perp}$  for out-of-plane anisotropy

(OOPA),  $K_{2||}$  for in-plane anisotropy (IPA), see Chap. II, Sec. 2. Both of these parameters are related to *magneto-elastic* constants ( $\propto B_1$  or  $B_2$ , see Sec. 4), so that the SAW pulses can lower the system’s energy sufficiently to facilitate the nucleation/propagation of domains and lower the coercive field. This geometry is “non-resonant” because the torque on the SAW onto the magnetization cancels out when  $\vec{M} \perp \vec{k}_{saw}$  (Eq. IV.11 with  $\theta_0 = 0$  for OOPA, and  $\theta_0 = \frac{\pi}{2}, \varphi_0 = 0$  for IPA), so that we are not trying to equate the SAW and precession frequencies. The anisotropy constants nevertheless feel a  $T_{saw}$ -periodic modulation, hopefully slow enough to substantially decrease the system’s total energy in the appropriate half-period (Fig. IV.31a).

- **Strong reduction of the coercivity by a SAW in out-of-plane magnetized (Ga,Mn)(As,P)**

We showed experimentally that the coercive field  $B_c$  could be divided by 2 by this approach<sup>4</sup>, and over millimetric distances [193], compared to the 11% decrease observed by Li *et al.* [118] in Gallenol or the 5% decrease observed by Edrington *et al.* [47] in Cobalt. A study of the swiching efficiency at fixed field and fixed number of pulses but varying repetition rate seemed to indicate a *cumulative* effect from successive SAW pulses. To reproduce the SAW amplitude dependence of coercive field, we adapted without much success the so-called “droplet” model [10, 139], with the SAW inducing a transient lowering of the energy cost to reverse a single opposite domain. Other phenomena were probably at play, such as the effect of the strain on the propagation/depinning energies, more complex to model (Fig. IV.31b). A more thorough study - impossible technically at the time since we had single-frequency IDTs - would have been to probe the effect of the SAW frequency on the switching efficiency.

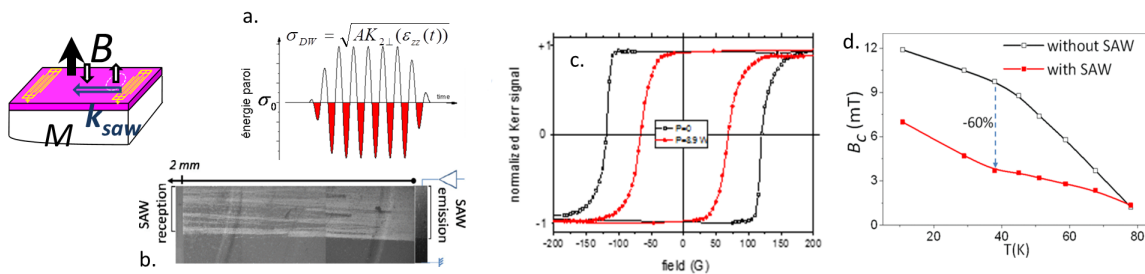


Figure IV.31: [193] (a) Magnetization switching in out-of-plane magnetized (Ga,Mn)(As,P) assisted by SAW, via the transient lowering of the domain-wall energy. (b) Kerr microscopy image at  $B = 0.6B_c$  under a 50 Hz train of high-amplitude SAWs. (c) Full hysteresis cycles measured with/without SAW by averaging the magneto-optical signal in front of the IDT. (d) Dependency of the coercive field  $B_c$  with temperature and rf power.

Finally, a short study of coercivity under SAW pulses was performed on the in-plane magnetized sample used for the magnetoacoustic resonance and switching studies of Refs. [109, 111]. The coercivity decrease proved a lot less spectacular for these layers: about 15% for  $k_{saw}$  parallel to the easy axis, and 30% for  $k_{saw}$  perpendicular to the easy axis (unpublished), the latter probably being more favorable because of the comparatively lower magnetostatic energy cost, as demonstrated for the precessional switching case (Sec. 5.1).

## 6 Comments & Perspectives

Taking a step back from this fairly fundamental work done on (Ga,Mn)As, let’s consider part of the very interesting magnetoacoustics work that has been done across the globe in the past couple years. In 2019 we were kindly asked to contribute a *Straintronics* chapter to the “SAW Roadmap” [40], coordinated by Hubert Krenner from Augsburg University. I will cite below a few of the tendencies we had identified then and that confirmed to emerge as hot topics, as well as some other ideas:

<sup>4</sup>We were in fact limited by the maximum available RF power, and poorly optimized impedance matching of our circuit.

- **Non-reciprocal SAW-FMR:** Waves behaving very differently for opposite wave-vectors are of great technical interests in electronics, to drive elements such as circulators, gyrators, isolators, or non-reciprocal phase shifters. Damon Eshbach-like magnetostatic waves which travel in opposite direction  $+\vec{k}_{DE}/-\vec{k}_{DE}$  at the top/bottom surface of a film have been used for this purpose. The non-reciprocal coupling of SAWs to these waves has also been known for half a century (see excellent review by Camley [26]), usually working at fairly low  $<100\text{MHz}$  frequencies. The non-reciprocity (e.g. eigenfrequency difference for a given  $\vec{k}_{DE}$ ) then scales linearly with film thickness [55], quickly becoming quite negligible for the ultra-thin films currently used in spintronics. Yet other strategies can be used to obtain non-reciprocal SAW propagation or attenuation by playing on chiral magnetic or acoustic effects :

- using magnetic layers presenting a (chiral) Dzyaloshinskii-Moriya interaction or synthetic antiferromagnets with a highly asymmetric magnon dispersion [211, 212, 5]
- using off-diagonal strains components of the SAW, either the symmetric part,  $S_{xz} = \frac{1}{2} \left( \frac{\partial u_x}{\partial z} + \frac{\partial u_z}{\partial x} \right)$  (small, if not zero at the surface, see torque in Eq. IV.11), or the anti-symmetric part  $\omega_{xz} = \frac{1}{2} \left( \frac{\partial u_x}{\partial z} - \frac{\partial u_z}{\partial x} \right)$ . For instance, recent data shows a 77% non-reciprocal ratio in CoFeB excited by SAWs [223].

Note that in the past couple years, there have been close to a dozen experimental or theoretical papers on non-reciprocal SAW-FMR [224, 188, 211, 212, 217, 74, 175].

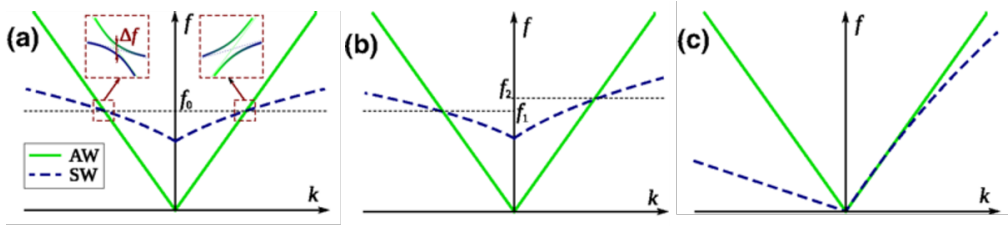


Figure IV.32: [211, 212] An illustration of how playing with the magnon (dashed blue) dispersion can lead to a highly non-reciprocal coupling to phonons (green curve): (a) Reciprocal coupling. (b) Narrow-band nonreciprocity relying e.g. on the Dzyaloshinskii-Moriya interaction, with coinciding and frequency-separated hybridization bands. (c) Wide-band nonreciprocity using synthetic antiferromagnets.

- **Electrical detection of magnetization precession:** the field-tunable SAW attenuation and phase delay of SAW-FMR was understood early on to be of particular interest for tunable delay lines, field sensing and so on. Little was suggested on how to use the magnetic precession that accompanies it. Our studies comfort the understanding of the coupled magnon-phonon interaction, and have provided a credible theoretical framework to put numbers on the amplitude of both in-plane and out-of-plane precession. The fact that SAW-FMR can excite spin-waves of controlled wave-vectors, over long distances, and possibly with non-linear behaviors, could provide a relevant solution to the magnonics community, so far held back by the difficulty to sustain these waves over long distances. An optical detection of this precession is of little technological interest, unlike its conversion into an electrically detected signal, i.e. by pumping the angular momentum towards a neighboring spin-sink and transforming it into a charge current [93]. This was clearly demonstrated on Co/Pt structures (once again early on by the Goennenwein group [220] later by INSP [164]), as well as on Ni/Cu/Bi<sub>2</sub>O<sub>3</sub> [222] and Y<sub>3</sub>Fe<sub>5</sub>O<sub>12</sub>/Pt [222, 208]. Signals remain quite weak, but this approach will surely benefit from the search for high spin-to-charge conversion led by the “spin-orbitronics” community.
- **Shifting away from Rayleigh waves:** while the “rediscovery” of Rayleigh-magnon interaction was clearly motivated by the use of these modes in electronic filters, and the higher frequencies allowed by the progresses of e-beam lithography, these might not always be the best suited:
  - as described above, the magneto-elastic coupling is highly anisotropic. Considering the main Rayleigh strain components  $S_{xx}, S_{zz}$  ( $x||\mathbf{k}_{saw}, z \perp$  plane), the coupling is 4-fold. It goes to zero 4 times across the quadrant (Eq. IV.11) and is maximized for angles that are not necessarily the ones for which the frequency matching is reached. The coexistence of Rayleigh waves with other modes having a different angular dependence would raise this geometrical constraint. Love waves might be a good candidate, evidencing a 4-fold, but  $\pi/4$ -shifted dependency [9, 135].



- Rayleigh waves are the natural modes existing at the surface of a semi-infinite substrate, they decay down to a depth of about  $\lambda_{\text{SAW}}$ . This implies that most of the acoustic energy is “wasted” when we have a thin ( $<50\text{nm}$ ) magnetic layer topping the substrate. Moreover, the dominant strain components of this mode go to zero (and change sign) fairly close to the surface (Fig. IV.1). This implies that the overlap with some of the magnetic modes might simply average out to zero [9]. One option is to bury the magnetic layer to exploit the Rayleigh wave’s shear  $S_{xz}$  component [188], which becomes non-zero away from the surface, but remains weak. Another solution would, again, be to work with Love waves, whose transverse displacement decays monotonously with the same sign in the thickness (Fig. IV.33), or to engineer the acoustic parameters to have the waves strongly guided in the magnetic layer. This approach was implemented successfully in  $TbCo_2/FeCo$  multilayers by Mazzamurro *et al.* [135]. An alternative used recently is to pattern the films enough to generate standing waves in the element, that decay very little in the thickness [56].

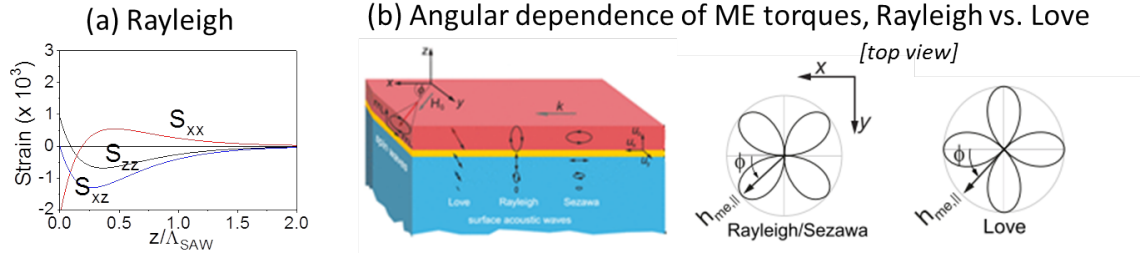


Figure IV.33: (a) [194] Reminder of the depth dependence of the strain components of a Rayleigh wave. (b) [9] Angular dependence of the magnetoelastic torque driven by Rayleigh or Love waves.

\* \* \*

These exciting ideas, already partially implemented on ferromagnetic metals, do not invalidate the work started at INSP on a low-temperature, technologically “irrelevant” material at the onset of this revival. To sum up, what made the success of these magnetoacoustic studies in (Ga,Mn)As was:

- the temperature- and field-tunable lower-GHz precession frequencies of (Ga,Mn)As that brought resonant behavior within easy reach. Resonant coupling is of course possible for any ferromagnetic layer precessing in the more usual 5-10 GHz range softened to low value under a hard axis field, but the constraint is then on the direction of the field, which must be perfectly aligned with the hard axis (see SAW-FMR study in Fe by Duquesne *et al.* [46] for instance).
- the low  $M_s$  that meant it was sufficient to consider the uniform mode, and not worry about magnetostatic modes [62, 69, 9]
- the rich and sizable magneto-optical effects that made it easy to detect the magnetization precession and switching. The excellent sensitivity to e.g. the out-of-plane precession component  $\delta\theta$  was also favored by the low saturation magnetization of (Ga,Mn)As which kept the precession cone a lot less elliptical, squished in the plane, than for higher  $M_s$  metals.

The switching study however falls a bit short of the initial aspirations. The idea was that with their weak attenuation, and power-flow confined to the surface, they could be made to interfere, diffract and focus on magnetic elements, opening a new route toward “straintronics” [7][40]. Once “proofs-of-concept” obtained on unpatterned layers of a low-temperature ferromagnet, one should move on to e.g. studying single-domain structures, working on the IDT design to improve the impedance matching and reduce the transient duration, or implement complex wave-shaping or focusing to selectively address a single “bit”, and of course branch out to room-temperature ferromagnets. Instead, I have made the choice of moving towards antiferromagnets, as will be detailed in Chap. V.

# Chapter V

## Future work: acoustics for antiferromagnets

- Students involved: Antoine Rignon-Bret (L3, 2019), Ali Kassem (M2, 2020), Anthony Chavatte (M1, 2020)

In the coming years, my goal is to study magnetoacoustic interaction in antiferromagnets. This shift is driven in part by the desire to (i) work closer to room-temperature, on more technologically relevant materials, (ii) exploit the “magnetoelasticity” experimental and theoretical knowledge accumulated on ferromagnets on systems (comparatively) less studied so far, (iii) explore these fascinating materials in which the antiferromagnetic order can be native, or created “synthetically”, yielding incredibly tunable properties [91, 68, 6, 119]. While antiferromagnets are well-known for their very high precession frequencies, and would thus appear poorly adapted to SAWs, we have chosen some systems on which they may be relevant.

One of these projects has recently been funded by the French Research Agency (ANR, 2020 call). ACAF (“Acoustics for Antiferromagnets”) is a collaboration between INSP, the Laboratoire de Physique des Solides (LPS, Orsay, A. Mougin & João Sampaio), the Laboratoire des Sciences des Procédés et des Matériaux (LSPM, Villetaneuse, Y. Roussigne, M. Belmeguenai, M. Cherif), CEITEC (Brno, Czech Republic, V. Ulhir) and University of Mainz (Olena Gomonay). I am copying/pasting in extenso the short version of this proposal.

### 1 Context, scientific objectives and research hypothesis

This experimental project aims to understand and harness the role of dynamic strain (surface acoustic waves, SAWs) to control antiferromagnetic (AF) states using magnetoelasticity. The main objective will be to gauge the possibilities SAWs offer as opposed to the traditional excitation of AF dynamics with radio-frequency (rf) fields, in terms of coupling efficiency, frequency, tunability, or zoology of excited modes. SAW-driving of AF dynamics, and the resulting possible manipulation of AF static states will be explored on two very different well-chosen systems, both bypassing in a different way the main bottleneck of addressing collinear antiferromagnets: their near-total lack of macroscopic stray field and magnetization. Magnetic coding of information has so far relied on bistable ferromagnetic (FM) states. Easily manipulated with magnetic fields, they are also prone to cumbersome bit-to-bit interactions via stray fields. Typical operating frequencies are capped to the GHz range by the magnetic anisotropy energy. There is thus now a keen interest in using collinear antiferromagnets [89]. They are composed of two sub-lattices of magnetizations  $\mathbf{M}_1 = -\mathbf{M}_2$ , with  $\mathbf{M}_1 - \mathbf{M}_2 = \mathbf{L}$  the Néel vector, and  $\mathbf{M}_1 + \mathbf{M}_2 \sim 0$ . In an AF with biaxial anisotropy, the two possible orthogonal directions of  $\mathbf{L}$  would code for “0” and “1” bits. AF bits are expected to be very robust against cross-talk and environmental magnetic fields, having zero net magnetization. The dynamics are this time ruled by both anisotropy and exchange energies, which rockets accessible frequencies to a few GHz, up to the THz.

Antiferromagnetic resonance is obtained using rf magnetic fields in very much the same way as for ferromagnetic resonance (FMR), i.e. by tuning the frequency of the drive field to the magnetic eigenfrequency. In this project we will implement an alternative approach, radiation-free, electric-field driven and travelling wave-like: SAWs will create an effective rf field via magneto-elasticity [111, 45] and induce AF resonance when phonon and magnon dispersion curves meet, i.e. for energy/wave-vector matching conditions. Because this effective field is different on each magnetic sub-lattice, we expect the SAW-torque to be more efficient than a global rf field, and to introduce

more tunability and efficiency in AF magnon excitation. In the longer term this scheme would limit Joule dissipation (and associated spurious temperature-gradient related effects) as strain will be excited by electrical fields, and allow alternative AF data storage design using focusing, interference, wave-front shaping and waveguiding effects, or remote accessing of bits, thanks to the weak attenuation of SAWs. Implementing these effects into a novel device however requires a deep understanding of strain-driven AF dynamics, in particular: how resonance (and therefore large precession angles) can be obtained, which strain components and frequencies are most efficient, what types of magnon modes are excited and with which efficiency compared to rf field excitation, how does the coexistence of ferro- and anti-ferromagnetic phases hinder or boost AF dynamics, and finally, could SAWs even induce  $L$ -vector switching? The aim of the project is thus to lay the foundational physics to harness acoustic wave-driven AF dynamics.

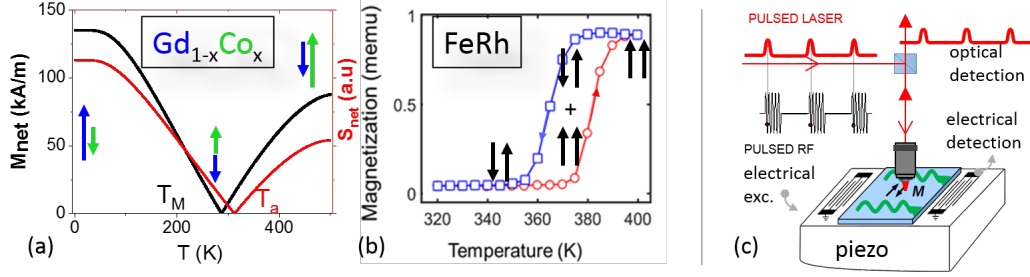


Figure V.1: (a) Net magnetization (cancelling at  $T_m$ ) and spin density (cancelling at  $T_a$ ) calculated in  $Gd_{0.2}Co_{0.8}$ . (b) Hysteretic magnetization of FeRh (CEITEC). (c) Envisionned measurement of AF dynamics under SAW excitation (INSP). Different piezoelectrics will be used: ZnO, LiNbO<sub>3</sub>, AlN/Si or Lead Magnesium Niobate-Lead Titanate.

## 2 Innovative and ambitious nature of the project, state of the art

The interaction of electrically excited SAWs with magnons has been evidenced in ferromagnetic metals [45], insulating ferrimagnets [183], and magnetic semiconductors, on which INSP has shown that SAWs can drive FMR, and magnetization switching [109, 192]. Controlling antiferromagnets with strain has instead been very little explored, although their magnetoelasticity is well documented [59]. This is partly due to the experimental difficulties encountered when studying these materials: (i) preparing/detecting a given static AF state and (ii) detecting the AF dynamics, which both result from the near-absence of macroscopic stray field and magnetization in these materials. The project’s innovative approach is to use SAWs on two systems chosen to bypass these bottle-necks by reintroducing a finite magnetization: the ferrimagnet  $Gd_{1-x}Co_x$  which can behave dynamically as an antiferromagnet but maintains a detectable magnetization and a field sensitivity, and a particular antiferromagnet, **FeRh**, transitioning via strain to a FM phase around room temperature. The project is thus naturally divided into two fairly independent but complementary parts:

\*) The perfect anti-alignment of sublattices in conventional collinear AFs limits probing techniques to those of even parity in local magnetization (e.g. magnetic linear dichroism, anisotropic magnetoresistance - AMR), effects whose multiple origins complicate interpretation. To circumvent this, we propose to study ferrimagnets at varying temperature. These materials are made of two AF-coupled uncompensated sublattices of magnetization  $M_{1,2} = S_{1,2}\mu_B g_{1,2}$ , where  $S_i$  and  $g_i$  are the total spin density and Landé factor [84]. Two particular temperatures stand out (Fig. a): magnetic compensation at  $T_m$  ( $M_1 = -M_2$ ) and angular compensation at  $T_a$  ( $S_1 = -S_2$ ). At  $T_a$ , a simplified picture shows the effective gyromagnetic ratio ( $\gamma_{eff} = \frac{g_{eff}\mu_B}{\hbar} \propto \frac{1}{S_1+S_2}$ ) diverges, rendering the dynamics effectively AF-like [27] whilst keeping them easily detectable since the magnetization remains non-zero. This diverging  $\gamma_{eff}$  has so far mainly been exploited to increase domain-wall propagation velocities [27], including by members of the consortium [67] (LPS), but the “macrospin” behavior at  $T_a$  remains to be explored, in particular under acoustic excitation. The ferrimagnet we will focus on is  $Gd_{1-x}Co_x$ , well mastered by LPS. On this unique system, we will study in depth the interaction of SAWs with magnetic sublattices, varying smoothly from a FM-like to a AF-like dynamical behavior with temperature, and establishing the optimum conditions for a

resonant excitation of the dynamics. This ambitious plan will require careful optimization of the magnetic layers, and modelling of the coupling of uncompensated lattices. For the latter we will benefit from the support of an AF dynamics and magnetoelasticity expert[59, 58], Prof. O. Gomonay (Mainz). This will be uncharted territory as there is no precedent that we know of this type of study, most reports of SAW-driven AF resonance having either focused on non-collinear AFs with incommensurate helical ordering [168], ferrimagnets in the FM-like phase[183] or the acoustic leg of the resonance[18].

\*) The robustness of AFs against typical external magnetic fields also makes it very challenging to toggle between two AF states [89], requiring instead exchange-coupled FM layers or electrical current-induced effective fields acting synchronously on both sublattices, an efficient but rare instance (e.g. in CuMnAs[89]). Their high precession frequencies also renders precessional (resonant) switching[192] very difficult. Another strategy is to rely on the proximity of a magnetic phase transition to ease the switching. We will apply this to the antiferromagnet Iron Rhodium, **FeRh**, a material known as a temperature sensor which exhibits an unusual first order transition from AF to FM states around  $T_{AF-FM} \sim 370$  K, with a broad temperature window seeing both phases coexist (Fig. 1b).  $T_{AF-FM}$  can be tuned by magnetic and electric fields [141, 30, 221], but also by static strain, since the magnetostructural nature of the transition is responsible for an impressive 0.7% isotropic increase of the lattice at  $T_{AF-FM}$ . So the application of strain is essentially equivalent to that of temperature. So far, the most significant results concerning L-switching in FeRh[141, 130] relied on temperature cycling under large fields (0.3-9T) with a mechanism reminiscent of thermally-assisted magnetic recording: a temperature rise above  $T_{AF-FM}$  places the system in the mixed AF-FM state, where a field makes the spins rotate by 90°. A temperature decrease then returns it back to a 90°-rotated AF state. This approach is particularly energy-inefficient because essentially static; we wish instead to implement an ambitious new strategy, with SAWs inducing a transient resonant and localized AF-FM transition. While several groups have studied static strain-driven  $T_{AF-FM}$  tuning[141, 30, 221, 28], none has used it to realize **L**-vector switching. Yet dynamic strain such as SAWs are well-known to be extremely sensitive to phase transitions, and in particular magnetostructural ones like in MnAs[128] or FeRh. This implies conversely, that in FeRh the phase transition may be triggered by SAWs, with effects possibly amplified at the resonance in the AF or mixed AF/FM phase. Beyond the challenging goal of manipulating **L**-vector, this study will offer a unique opportunity to test the resonance of a mixed AF/FM phase, in particular what happens at domain boundaries, where different modes and lower frequencies are expected, and to confront this with what will have been understood from SAW-driven AF dynamics on ferrimagnets.

### 3 Methodology

Over 4 years, ACAF will provide optimized FeRh and GdCo nanometric films and reliable procedures to generate dynamic strain, have evidenced strain-magnetization coupling, and achieved strain-assisted Néel vector switching. To this end, the project is organized into 3 packages involving 3 national partners (INSP, LSPM, LPS) and 2 foreign ones (Mainz, CEITEC):

- WP1: Generating SAWs electrically on thin optimized FeRh and GdCo layers : WP leader Alexandra Mougin (LPS). Months 1-36. Risk: low to medium.
- WP2 Evidencing magnetization-strain coupling WP leader Yves Roussigné (LSPM). Months 12-48. Risk: medium-high.
- WP3: Strain-assisted antiferromagnetic switching in FeRh WP leader L. Thevenard (INSP). Months 12-48. Risk: high.

The project will be driven by a balance of state-of-the art experiments (time-resolved Kerr effect, Brillouin Light Scattering, anomalous Hall effect, Kerr microscopy, electrical SAW-FMR, broad-band FMR), phenomenological modelling and micromagnetic simulations. It will rest on the synthesis of high quality FeRh and GdCo samples by our colleagues from CEITEC (Brno) and LPS (Orsay).

# Chapter VI

## Carrier overview

### 1 CV

#### 1.1 Academic training

- 2004 - 2007: PhD Thesis delivered by Université Pierre et Marie-Curie, done at the Laboratoire de Photonique et Nanostructures (Marcoussis), Director Y. Guldner, Co-director and Supervisor A. Lematre
- 2003-2004 : DEA ( $\leftrightarrow$ Master 2) "Material Science", Université Pierre et Marie-Curie (Paris)
- 2000 - 2003: Engineer Diploma from Ecole Polytechnique (Palaiseau), double physics major

#### 1.2 Professional experience

- 2014 : Promoted CR1 ( $\leftrightarrow$ 1st class research assistant) at the Institut des Nanosciences de Paris (INSP)
- 2009 : Hired CR2 ( $\leftrightarrow$ 2nd class research assistant) at INSP in the team of C. Gourdon with the research project "*Ferromagnetic semiconductors : magnetic domains and magnetization manipulation*"
- 2007 - 2009 : Post-doc at Imperial College London in the team of Russel Cowburn with the research project: "*Study of novel nanostructures for magnetic data storage*"
- 2004 - 2007: PhD Thesis at the Laboratoire de Photonique et Nanostructures (Marcoussis) in the team of Aristide Lematre, on the topic "*Study of the ferromagnetic properties of (Ga,Mn)As using hydrogen*"
- Summer 2003 : Research Internship at LAM Research (Fremont, CA, USA) in the team of Andrew Wilson on the topic "*Feasability study of an in-situ infrared temperature sensor for Silicon wafers*"

### 2 Research credentials

#### 2.1 Research topics and main experimental techniques

- (Ga,Mn)As, MnAs, FeGa, magnetic domains and domain-walls, current- and field-driven domain-wall propagation, magnetoacoustics, magnetization dynamics, magneto-optics
- Kerr microscopy, time- and space-resolved magnetization and elastic dynamics, magneto-transport, micro-magnetic simulations

## 2.2 Contracts

The Agence Nationale de la Recherche (ANR) is the main French national funding agency. C’Nano is a Paris Region funding agency. The Partenariat Hubert Curien (PHC) is a program funding short research stays for experienced or early-stage researcher from selected countries (in our case, Tunisia). Finally, my institute, INSP, is under the dual management from the CNRS (National Research Center) and Sorbonne Université (previously called Université Pierre et Marie Curie, or Paris VI)

- 2021 - 2024: **ANR ACAF** “*Acoustics for Antiferromagnets*” P.I. L. Thevenard, collaborations LPS (Orsay), LSPM (Villetaneuse), CEITEC (Czech Republic), University of Mainz
- 2021 - 2024: **ANR MAXSAW** “*MAGneto-elastic coupling eXploitation for tunable and non-reciprocal rf Surface Acoustic Wave devices*” P.I. T. Devolder, collaborations C2N and CEA SPEC (Orsay), Femto-St (Besançon) and the company Freq|n|Sys
- 2016 - 2019 : **PHC Utique**, P.I. C. Gourdon - funding three 4 months stays of Meriam Kraimia for her Franco-Tunisian PhD thesis
- 2014-2017: **ANR JCJC SPINSAW** “*Generation of spinwaves by surface acoustic waves in ferromagnetic films*” P.I. L. Thevenard. This is a “young researcher” contract funding only intra-lab projects
- 2012 - 2016 : **C’NANO MURAS** - “*Ultrafast manipulation and switching of the magnetization in the diluted magnetic semiconductor (Ga,Mn)AsP*” P.I. L. Thevenard, collaboration with LPN (Marcoussis)
- 2012 - 2015: **Emergence Contract** (“young researcher” project of Université Pierre et Marie Curie), PhD fellowship for S. Shihab on the topic “*Excitation and detection optical processes of the magnetization dynamic in the diluted magnetic-semiconductor (Ga,Mn)(As,P)*”
- 2010 - 2014: **ANR MANGAS** - “*Exploring new techniques for magnetization manipulation in (Ga,Mn)As*” - P.I. A. Lemaître, collaborations with LPN, LPS and IEF, UMR CNRS-Thalès
- 2010 - 2014 : **C’NANO Spin(Ga,Mn)As** - “*(Ga,Mn)As-based spintronics*” P.I. A. Lemaître, collaboration with LPN, IEF and LPS, UMR CNRS-Thalès

Unsuccessful proposals (as P.I. or collaborator): STRAIN (International Training Network, P.I. H. Krenner, 2019 and 2020 calls), ANRs (2009 and 2019 calls), IRONMAG (FET-OPEN European project, P.I. V. Temnov, 2020 call), Sorbonne Université Emergence (2019 call)

## 2.3 Main collaborations

### • France

My main collaborator for the (Ga,Mn)As studies has been **A. Lemaître** (Laboratoire de Photonique et Nanostructures, then merged with IEF into the Centre de Nanosciences et Nanotechnologies, C2N). He has cosigned most of my articles. He has not only provided us with high quality (Ga,Mn)As and (Ga,Mn)(As,P) samples, but been a constant source of ideas and feedback. Among other things, he foresaw early on the interest in using acoustic waves (at the time, picosecond bulk longitudinal waves) to trigger magnetization precession, which was part of my initial CNRS project. I have also interacted a lot with **Ludovic Largeau**, X-Ray specialist at C2N [106, 196, 113]. **A. Thiaville** and **V. Jeudy** (LPS, Orsay), **N. Vernier** and **J.-V. Kim** (IEF) have been active collaborators in domain-wall propagation studies [197, 85, 191], some of them within ANR projects. Finally, it is probably within INSP that I have developed the strongest collaboration, with **J.-Y. Duquesne**, **M. Marangolo** and **P. Rovillain**. In the framework of - but not limited to - the SPINSAW project, we have together created a magneto-acoustics team.

### • Abroad

There is a long-standing collaboration of INSP with two groups in Tunisia (**M. Maaref** at the University of Carthage, la Marsa), and **K. Boudjaria** (Faculté des Sciences de Bizerte). This has allowed several research stays of a student (**H. Riahi** [162, 163, 176, 226]), and the completion of a joint PhD thesis (**M. Kraimia** [106, 105]). Likewise, INSP was involved in a short-lived joint franco-argentinian laboratory, the LIFAN, with strong ties to the magnetism groups of the Centro Atomico Bariloche and of the University of Buenos Aires. In this framework, we have welcomed **M. Tortorolo** for two research stays dealing with the study of MnAs [206].

## 2.4 Full list of publications and talks

51 publications in peer-reviewed journals (among which 8 conference proceeding papers mainly dating from collaborations during my thesis) - 14 as first, 5 as last author, 1275 citations, h index 21 (Jan. 2021, Google Scholar, not checked):

- **Publications :**

- [1] “*Time- and space-resolved nonlinear magnetoacoustic dynamics*”, M. Kraimia, P. Kuszewski, J.-Y. Duquesne, A. Lemaître, F. Margailan, C. Gourdon, and L. Thevenard, Phys. Rev. B 101, 144425 (2020)
- [2] “*Exploring the shear strain contribution to the uniaxial magnetic anisotropy of (Ga,Mn)As*”, M. Kraimia, L. Largeau, K. Boudjaria, B. Croset, . Mocuta, A. Lemaître, C. Gourdon, and L. Thevenard, J. Applied Phys. 127, 093901 (2020)
- [3] “*The 2019 surface acoustic waves roadmap*”, P. Delsing et al, Journal of Physics D: Applied Physics, 52 353001 (2019)
- [4] “*Field-Free Magnetization Switching by an Acoustic Wave*”, Camara, I.S., Duquesne, J.-Y., Lemaître, A., Gourdon, C. and Thevenard, L., Physical Review Applied 11 014045 (2019)
- [5] “*Optical probing of Rayleigh wave driven magnetoacoustic resonance*”, P. Kuszewski, J.-Y. Duquesne, L. Becerra, A. Lemaître, S. Vincent, S. Majrab, F. Margailan, C. Gourdon, and L. Thevenard, Physical Review Applied, 10 1 (2018)
- [6] “*Resonant magneto-acoustic switching: influence of Rayleigh wave frequency and wavevector*”, P. Kuszewski, I. S. Camara, N. Biarrotte, L. Becerra, J. von Bardeleben, W Savero Torres, A. Lemaître, C. Gourdon, J.-Y Duquesne, L.Thevenard, Journal of Physics: Condensed Matter 30 244003 (2018)
- [7] “*Counter-rotating standing spin waves: A magneto-optical illusion*” S. Shihab, L. Thevenard, A. Lemaître, and C. Gourdon, Physical Review B 95 144411 (2017)
- [8] “*Magneto-optical Kerr spectroscopy of (Ga,Mn)(As,P) ferromagnetic layers: Experiments and k.p theory*”, M. Yahyaoui, H. Riahi, M. A. Maaref, K. Boujdaria, A. Lemaître, L. Thevenard, and C. Gourdon, Journal of Applied Physics, 121, 125702 (2017)
- [9] “*Spin transfer and spin-orbit torques in in-plane magnetized (Ga,Mn)As tracks*”, L. Thevenard, B. Boutigny, N. Günsken, L. Becerra, C. Ulysse, S. Shihab, A. Lemaître, J.-V. Kim, V. Jeudy, C. Gourdon, Physical Review B 95 054422 (2017)
- [10] “*Acoustic solitons : A robust tool to investigate the generation and the detection of ultrafast acoustic waves*”, E. Péronne, N. Chuecos, L. Thevenard, and Bernard Perrin, Physical Review B 95 064306 (2017)
- [11] “*Vector network analyzer measurement of the amplitude of an electrically excited surface acoustic wave and validation by X-ray diffraction*”, I. S. Camara , B. Croset , L. Largeau, P. Rovillain, L. Thevenard, and J.-Y. Duquesne, J. Appl. Phys. 121, 044503 (2017)
- [12] “*Laboratory X-ray characterization of a surface acoustic wave on GaAs: the critical role of instrumental convolution*”, L. Largeau, I. Camara, J.-Y. Duquesne, C. Gourdon, P. Rovillain, L. Thevenard, B. Croset, J. Applied Cryst., 49, 1 (2016)
- [13] “*Precessional magnetization switching by a surface acoustic wave*”, L. Thevenard, I. S. Camara, S. Majrab, M. Bernard, P. Rovillain, A. Lemaître, C. Gourdon, and J.-Y. Duquesne, Phys. Rev. B 93, 134430 (2016)
- [14] “*Steady-state thermal gradient induced by pulsed laser excitation in a ferromagnetic layer*”, S. Shihab, L. Thevenard, A. Lemaître, J.-Y. Duquesne and C. Gourdon, J. Appl. Phys. 119, 153904 (2016)
- [15] “*Strong reduction of the coercivity by a surface acoustic wave in an out-of-plane magnetized epilayer*”, L. Thevenard, I. S. Camara, J.-Y. Prieur, P. Rovillain, A. Lemaître, C. Gourdon, and J.-Y. Duquesne, Phys. Rev. B 93, 140405(R) (2016)
- [16] “*Optimizing magneto-optical effects in the ferromagnetic semiconductor (Ga,Mn)As*”, H. Riahi, L. Thevenard, M. Maaref, B. Gallas, A. Lemaître, C. Gourdon, Journal of Magnetism and Magnetic Materials 395, 340 (2015)
- [17] “*Systematic study of the spin stiffness dependence on phosphorus alloying in the ferromagnetic semiconductor (Ga,Mn)As*”, S. Shihab, H. Riahi, L.Thevenard, H. J. von Bardeleben, A. Lemaître, C. Gourdon, Appl. Phys. Lett. 106 142408 (2015)
- [18] “*Surface-acoustic-wave-driven ferromagnetic resonance in (Ga,Mn)(As,P) epilayers*”, L. Thevenard, C. Gourdon, J.Y. Prieur, H. J. von Bardeleben, S. Vincent, L. Becerra, L. Largeau, J.Y. Duquesne, Phys. Rev. B 90, 094401 (2014)
- [19] “*Domain-wall flexing instability and propagation in thin ferromagnetic films*”, C. Gourdon, L. Thevenard, and S. Haghgoo, A. Cebers, Phys. Rev. B 88, 014428 (2013)
- [20] “*Annealing effect on the magnetization reversal and Curie temperature in a (Ga,Mn)As layer*”, H. Riahi, W.

- Ouerghuia, L. Thevenard, C. Gourdon, M.A. Maarefa, A. Lemaître, O. Mauguin, C. Testelin, Journal of Magnetism and Magnetic Materials 342, 149 (2013)
- [21] “*Coupling and induced depinning of magnetic domain walls in adjacent spin valve nanotracks*”, J. Sampaio, L. O’Brien, D. Petit, D. E Read, E.R Lewis, H.T. Zeng, L. Thevenard, S. Cardoso, R. P. Cowburn, Journal of Applied Physics 113, 133901 (2013)
- [22] “*Irreversible magnetization switching using surface acoustic waves*”, L. Thevenard, J.-Y. Duquesne, E. Peronne, H. J. von Bardeleben, H. Jaffres, S. Ruttala, J-M. George, A. Lemaître, and C. Gourdon, Physical Review B 87, 144402 (2013)
- [23] “*Fast domain wall dynamics in MnAs/GaAs films*”, M. Tortarolo, L. Thevenard, H. J. von Bardeleben, M. Cubukcu, V. Etgens, M. Eddrief, C. Gourdon, Applied Physics Letters 101, 072408 (2012), “research highlight”
- [24] “*High domain wall velocities in in-plane magnetized (Ga,Mn)(As,P) layers*”, Thevenard, L., Hussain, S. von Bardeleben, H. Bernard, M. Lemaître, A. Gourdon, C., Physical Review B 85 064419 (2012)
- [25] “*Domain wall propagation in ferromagnetic semiconductors: Beyond the one-dimensional model*, L. Thevenard, C. Gourdon, S. Haghgoo, J-P. Adam, J. von Berdeleben, A. Lemaître, W. Schoch, A. Thiaville, Physical Review B 83, 245211 (2011)
- [26] “*Effect of picosecond strain pulses on thin layers of the ferromagnetic semiconductor (Ga,Mn)(As,P)*”, L. Thevenard, E. Perronne, C. Testelin, C. Gourdon, M. Cubucku, S. Vincent, E. Charron, A. Lemaître, B. Perrin, Physical Review B 82, 104422 (2010)
- [27] “*Exchange constant and domain wall width in (Ga,Mn)(As,P) films with self-organization of magnetic domains*”, S. Haghgoo, M. Cubukcu, H. J. von Bardeleben, L. Thevenard, A. Lemaître, and C. Gourdon, Phys. Rev. B 82 041301 (2010)
- [28] “*Macrospin limit and configurational anisotropy in nanoscale permalloy triangles*”, L. Thevenard, H. T. Zeng, D. Petit, and R. P. Cowburn, Journal of Magnetism and Magnetic Materials 322, 2152 (2010)
- [29] “*Six-fold configurational anisotropy and magnetic reversal in nanoscale Permalloy triangles*”, L. Thevenard, H. T. Zeng, D. Petit, and R. P. Cowburn, J. Appl. Phys. 106, 063902 (2009)
- [30] “*Macrospin behavior and superparamagnetism in (Ga,Mn)As nanodots*”, J.-P. Adam, S. Rohart, J. Ferré, A. Mougou, N. Vernier, L. Thevenard, A. Lemaître, G. Faini, and F. Glas, Phys. Rev. B 80, 155313 (2009)
- [31] “*Magnetic domain wall pinning by a curved conduit*”, E. R. Lewis, D. Petit, L. Thevenard, A. V. Jausovec, L. O’Brien, D. E. Read, and R. P. Cowburn, Appl. Phys. Lett. 95, 152505 (2009)
- [32] “*Nonadiabatic spin-transfer torque in (Ga,Mn)As with perpendicular anisotropy*”, J.-P. Adam, N. Vernier, J. Ferré, A. Thiaville, V. Jeudy, A. Lemaître, L. Thevenard, and G. Faini, Phys. Rev. B 80, 193204 (2009)
- [33] Kh. Khazen, H. J. von Bardeleben, M. Cubukcu, J. L. Cantin, V. Novak, K. Olejnik, M. Cukr, L. Thevenard and A. Lemaître, Phys. Rev. B 78 195210 (2008)
- [34] Kh. Khazen, H. J. von Bardeleben, J. L. Cantin, L. Thevenard, L. Largeau, O. Mauguin, and A. Lemaître, Phys. Rev. B, 77, 165204 (2008)
- [35] “*Magnetic patterning of (Ga,Mn)As by hydrogen passivation*”, Laura Thevenard, A. Miard, L. Vila, G. Faini, A. Lemaître, N. Vernier, et J. Ferré, Appl. Phys. Lett. 91 142511, (2007)
- [36] “*Evolution of the magnetic anisotropy with carrier density in hydrogenated Ga<sub>1-x</sub>Mn<sub>x</sub>As*”, Laura Thevenard, L. Largeau, O. Mauguin, A. Lemaître, K. Khazen, H. J. von Bardeleben, Phys. Rev. B 75, (2007)
- [37] “*Universal Conductance Fluctuations in Epitaxial (Ga,Mn)As Ferromagnets: Dephasing by Structural and Spin Disorder*” L. Vila, R. Giraud, L. Thevenard, F. Pierre, et al. Phys. Rev. Lett. 98, 027204 (2007)
- [38] A. Doulat, V. Jeudy, C. Testelin, F. Bernardot, K. Khazen, C. Gourdon, L. Thevenard, L. Largeau, O. Mauguin: J. Appl. Phys. 102 023913 (2007)
- [39] M. Elsen, H. Jaffres, R. Mattana, L. Thevenard, A. Lemaître, and J.-M. George, Phys. Rev. B 76, 144415 (2007)
- [40] Dependence of Magnetic Anisotropies and Critical Temperatures on the Hole Concentration in Ferromagnetic (Ga,Mn)As Thin Films, K. Khazen, H. J. von Bardeleben, J. L. Cantin, L. Thevenard, L. Largeau, O. Mauguin, A., IEEE Transactions on Magnetics, 43 3028 (2007)
- [41] C. Gourdon, A. Doulat, V. Jeudy, K. Khazen, and H. J. von Bardeleben, L. Thevenard and A. Lemaître, Phys. Rev. B 76, 241301(R) (2007)
- [42] “*Magnetic properties and domain structure of (Ga,Mn)As films with perpendicular anisotropy*”, Laura Thevenard, L. Largeau, O. Mauguin, G. Patriarche, A. Lemaître, N. Vernier, J. Ferré: Phys. Rev. B 73, 195331 (2006)
- [43] “*(Ga,Mn)As layers with perpendicular anisotropy: a study of magnetic domain patterns*”, A. Doulat, C. Gourdon, V. Jeudy, L. Thevenard, A. Lemaître et al., Physica status solidi (c) 3, 4074 (2006)
- [44] “*Voltage-controlled tunneling anisotropic magnetoresistance of a ferromagnetic p[<sup>sup</sup> ++]- (Ga,Mn)As/n[<sup>sup</sup> +-]-GaAs Zener-Esaki diode*”, R. Giraud, M. Gryglas, L. Thevenard, A. Lemaître, and G. Faini; Appl. Phys. Lett.



87, 242505 (2005)

- [45] “*Tuning the ferromagnetic properties of hydrogenated (Ga,Mn)As*”, Laura Thevenard, L. Largeau, O. Mauguin, A. Lemaitre, B. Theys, Appl. Phys. Lett. 87, 182506 (2005)
- [46] “*Dependence of Magnetic Anisotropies and Critical Temperatures on the Hole Concentration in Ferromagnetic (Ga,Mn)As Thin Films*”, K. Khazen, H. J. von Bardeleben, J. L. Cantin, L. Thevenard, L. Largeau, O. Mauguin et A. Lemaitre, IEEE Trans. Mag. 43, n° 6 (2007)
- [47] “*(Ga,Mn)As layers with perpendicular anisotropy: a study of magnetic domain patterns*”, A. Dourlat, V. Jeudy, C. Testelin, C. Gourdon, L. Thevenard, A. Lemaitre ; Phys. Stat. Sol. (c) 3, 4074 (Actes PASPS-IV 2006).
- [48] “*Tuning the ferromagnetic properties of hydrogenated (Ga,Mn)As*”, A. Lemaitre, L. Thevenard, M. Viret, L. Largeau, O. Mauguin, B. Theys, F. Bernardot, R. Bouanani-Rhabi, B. Clerjaud, et F. Jomard, AIP Conf. Proc. 772, 363 (Actes ICPS 2005)

34 oral contributions among which 5 “invited” talks:

- **5 invited talks in national/international scientific events.**

- [1] GDR Optomeca (2018, Paris) ,”Magnetization Dynamics Driven By Surface Acoustic Waves”
- [2] ICM2018 (2018, San Francisco), “Magnetization Dynamics Driven By Surface Acoustic Waves”
- [3] Plenary talk at the Condensed Matter Conference (2016, Bordeaux), “ Contrôle Magnétoacoustique de l’aimantation”
- [4] Journées Surface et Interface (2016, Marseille) : “Contrôle Magnétoacoustique de l’aimantation”
- [5] Magnetism & Magnetic Materials (2014, Hawaii), “Surface acoustic wave driven ferromagnetic resonance and magnetization switching in a magnetic semiconductor”

- **Invitations to seminar/workshops**

- [6] General seminar at LP-ENS (2019, Paris) “Ultrasonic drive of magnetization dynamics”
- [7] General seminar at C2N (2019, Orsay) “Ultrasonic drive of magnetization dynamics”
- [8] Invited talk at MATE day (franco-argentinian magnetism workshop, INSP, Feb. 2018)
- [9] Seminar at the “Waves & matter” day of INSP (Nov. 2016)
- [10] Seminar at the “Spin & Magnetism group” of INSP (April 2016) “Contrôle Magnétoacoustique de l’aimantation”
- [11] Invited talk at the Indo-French Workshop organised by the MATISSE LabEX MATISSE (UPMC, 2015), "Contrôle et renversement d’aimantation dans un semiconducteur: (Ga,Mn)As"
- [12] Invited talk at the the C’Nano days (UPMC, 2011), “Propagation de paroi de domaines sous champ: au delà du modèle unidimensionnel”
- [13] Invited talk at the yearly LabEX MATISSE days (UPMCn 2015), "Contrôle et renversement d’aimantation dans un semiconducteur: (Ga,Mn)As"
- [14] Seminar (Grenoble, Feb. 2008)
- [15] Seminar at the Walther Weissner Institut (Garching, 2007)
- [16] Seminar at the UMR CNRS-THALES (Palaiseau, 2006)

- **Other interventions** (that I have presented - 8 others presented by students or C. Gourdon)

- [18] MMM (online, 2020) “Time and space-resolved non-linear magnetoacoustic dynamics”
- [19] JEMS (Uppsala, 2019) “Time and space-resolved non-linear magnetoacoustic dynamics”
- [20] Physics of magnetism (Poznan, 2017): “Spin transfer and spin-orbit torques in (Ga,Mn)As”
- [21] Intermag (Dublin, 2017) : “Surface acoustic waves for magnetization switching in precessional geometry: effect of the wave frequency”
- [22] Condensed Matter Division days (CMD, Paris, 2014): “ Surface acoustic wave driven ferromagnetic resonance in a magnetic semiconductor”
- [23] MMM (2013), “Field-induced domain-wall propagation in in-plane (Ga,Mn)As(P) in-plane”
- [24] Spintech (Japan, 2011), “Field-induced domain wall propagation: beyond the one dimensional model”
- [25] APS March Meeting (New Orleans, 2008)
- [26] Colloque Louis Néel (Lyon, 2006)

### 3 Activities not directly related to research

#### 3.1 Expertise

- **PhD examiner** in 9 PhD defenses: P. Colson (2011), R. Soucaille (2016), T. Parpiiev (2017), T. de Guillebon (2018), L. Soumah (2019), M. Riou (2019), A. Kyianytsia (2019), Jérémy Létang (2020), A. Mazzamurro (2020), examiner for many Master 2 internship defenses
- **Reviewer** for ANR, Foundation for Polish Science, CNRS-MOMENTUM, Royal Academy of Science projects
- **Reviewer** for articles in Phys. Rev. Applied, B, and Letters, Applied Physic Letters, Journal of Applied Physics, Nature Communications, Scientific Reports etc.
- **Member of the selection committee** for a section 28 Lecturer-Researcher position at Université Paris-Sud (2019)
- **Spintronics expert** at the Micro- and Nanosciences Technology Observatory (OMNT, 2012-2016). This was a consortium of researchers in charge of doing a scientific watch in their respective field of expertise. Short summaries were redacted regularly, compiled into a large volume then sent out to industries and laboratories.

### 3.2 Lab responsibilities

- **Member of the INSP scientific committee** (2019-), in charge of giving a scientific feedback on the projects submitted by members of the laboratory, doing scientific watch and fostering intra-lab interactions in our respective fields of expertise (in my case, the “Spin and Magnetism” { } axe transverse), selecting noteworthy lab publications for the website’s “Highlights” section etc.
- Organizer of **team seminar**, **webmistress** of team website (2009-2012)
- **Member of the “Open Science” study group** (4 people, 2020- ), in charge of analyzing the situation and proposing concrete actions to encourage an open science mindset at INSP

### 3.3 Other responsibilities

- 2016: co-organisation of a “Magnetoacoustics” mini-colloquium at the CMD-EPS conference 2016 (Gröningen, international)
- 2015-2018: member of the Consulting Committee of Universities (CCSU) of the Université Paris-Saclay, section 28-30, in charge of giving a scientific opinion on various internal university affairs (promotions, derogation of teaching for research, emeritus requests etc.)
- 2015-: member of the scientific committee of the Colloque Louis Néel, the national Magnetism workshop that takes place every 18 months (200 people). Co-organizer of the 2017 edition in Paris.

### 3.4 Teaching

- 2019- : intervention on magnetization dynamics in the “Spintronics” class of Agnès Barthelemy for the international Master 2 SMNO-Nanomat program (Sorbonne Université, 8h/year)
- 2018- : tutoring in Solid State Physics at the engineering school ESPCI (16h/year)
- 2011-2018: Kerr microscopy practical for the international Master2 Nanomat program (Paris VI, 18h/year)
- 2013-2015 : in charge of organizing and following the final internship of the students of the international Master2 Nanomat program (Paris VI)

### 3.5 Outreach

- 2018-: Presentation of the CNRS, and what a researcher does at the Physics & Applications Master 1 program (Sorbonne Université)
- 2016 : Participation in the « Histoires Courtes » project of Dars&Papillault
- 2016 : Participation in the CNano projet « Outlook on Nanosciences »: following a high-school for a year, with talks and mini-projects related to nanosciences
- 2010: Participation in the project “1000 researchers” (Pierre Maraval)

## 4 Supervising responsibilities

In my ten years or so at the CNRS, I have (co-)supervised four 3rd year (L3) students, two “master 1”(M1) students, six ”master 2”(M2) students, three PhD students, and one post-doc. Some details on the PhD theses and post-doc:

- Co-supervision at 50% from Sept. 2012 to December 2015 of the thesis of **Sylvain Shihab** (director C. Gourdon) entitled “Ultra-fast control of magnetization in ferromagnetic semiconductors” , funded by a UPMC Emergence contract. The goal of this thesis was to mount a state-of-the art time-resolved Kerr effect set-up, and then to perform an exhaustive study of the optical triggering of magnetization dynamics in (Ga,Mn)AsP. It gave rise to 3 publications on the topic [176, 177, 178], and one on current-driven domain wall propagation [191].
- Co-supervision at 80% of **Ibrahima Camara** (post-doc Jan. ’15-sept. 2016), funded by the ANR JCJC “SPINSAW” (P.I. L. Thevenard). His project consisted in mounting and optimizing a set-up capable of exciting/detecting surface acoustic wave, coupled to a cryogenic Kerr microscope. He was also instrumental in a study aiming to determine the precise displacement generated by the SAWs. His stay gave rise to 7 publications with our group [23, 24, 111, 108, 113, 192, 193].
- Co-supervision at 60% of the PhD thesis of **Piotr Kuszewski** (Oct’15-Sept. ’18, director C. Gourdon), funded by the Ecole Doctorale 397 : “Optical detection of magneto-acoustic dynamics”. This thesis was the natural convergence of the work of S. Shihab (mounting of the pump-probe, all-optical set-up) and of our work on magnetoacoustics. The idea was to resolve spatially and temporally the magnetization dynamics triggered by an acoustic wave. Two generation mechanisms were considered: piezoelectric and thermoelastic effects. His work gave rise to 3 publications [105, 111, 109].
- Co-supervision at 20% of the PhD thesis of **Meriam Kraimia** (Sept. 2016-Sept. 2020), funded by the PHC Utique : “Magnetoelasticity and magnetoacoustics in (Ga,Mn)As”, a joint program between INSP and the Material Physics Laboratory of Bizerte (directors C. Gourdon for France and Kais Boudjaria for Tunisia). Periods in Tunisia (about two thirds of the time) were dedicated to the numerical estimation of the magnetostrictive coefficients of (Ga,Mn)As by k.p. band structure calculations. Parisian stays were reserved for the magnetic characterization of magnetostrictive layers, and the (unsuccessful) attempt to evidence a shear strain in (Ga,Mn)As layers with strong in-plane magnetic anisotropy. Her work gave rise to two publications [105, 106].

Student	Level	Topic	Last known position (2020)
<b>Sanaz Haghgoo</b>	PhD Thesis (2008-2012)	Domains and domain-walls in (Ga,Mn)AsP	Khatam University (Teheran)
<b>Hassen Riahi</b>	M1 2010 then short stays during his PhD ('11,'13 et '14)	Magneto-optical effects in (Ga,Mn)As	Post-doc (Chinese Academy of Science, Beijing)
<b>Asad Syed Hussain</b>	M2 (2011)	Field-driven DWP in (Ga,Mn)As	Assistant-professor (Oxford)
<b>Colin Delfaure</b>	M1 (2011)	Mounting a pump-probe set-up	Product engineer (3SP, lasers)
<b>Sylvain Shihab</b>	M2, then PhD thesis (2012-2015)	Current-driven DWP in (Ga,Mn)As, pump-probe dynamics	Certification engineer (Altroad)
<b>Benoit Boutigny</b>	M2 (2013)	Current-driven DWP in (Ga,Mn)As	?
<b>Nicholas Gusken</b>	M2 (2014)	Current-driven DWP in (Ga,Mn)As	Post doc (Imperial College London)
<b>Hazem Bakr</b>	M2 (2015)	Laser-pulse-driven magnetization reversal	PhD (University of Bayreuth)
<b>Dylan Cadiou</b>	L3 (2016)	Characterization of optical components	Study of wind-turbine activities on biodiversity (Boralex)
<b>Chahrazed Benabid</b>			Electrochemical modelization of lithium-ion batteries (Altran)
<b>Nicolas Biarrotte</b>	M2 (2016)	SAW-driven magnetization reversal in (Ga,Mn)As	?
<b>Ibrahima Camara</b>	Post-doc (2015-2016)	All-electrical magnetoacoustics in (Ga,Mn)As	banking
<b>Piotr Kuszewski</b>	PhD thesis (2015-2018)	Magnetoacoustics dans (Ga,Mn)As et métaux	Post-doc at IMEC
<b>Meriam Kraimia</b>	PhD thesis (2016-2020)	Magnetoelasticity and magnetoacoustics in (Ga,Mn)As	Looking for work
<b>Jian Caoj</b>	L3 (2019)	Characterization of optical & electrical components	Institute of Optics Graduate School
<b>Antoine Rignon-Bret</b>	L3 (2019)	IDT design on MgO	Theoretical Physics Master 2 (ENS)
<b>Antony Chavatte</b>	M1 (2020)	Probing FeRh transition using reflectivity	Optics & Engineering Master 2 (SU)
<b>Ali Kassem</b>	M2 (2020)	Analytical description of antiferromagnetic dynamics	Looking for a PhD thesis

[DWP = domain wall propagation]

# Bibliography

- [1] M Abolfath, Tomáš Jungwirth, J Brum, and A H Macdonald. Theory of magnetic anisotropy in III. *Physical Review*, 63:1–14, 2001.
- [2] Jean-Paul Adam, N. Vernier, Jacques Ferré, André Thiaville, V. Jeudy, A. Lemaître, Laura Thevenard, and G. Faini. Nonadiabatic spin-transfer torque in (Ga,Mn)As with perpendicular anisotropy. *Physical Review B*, 80(19):193204, nov 2009.
- [3] Amikam Aharoni. Demagnetizing factors for rectangular ferromagnetic prisms. *Journal of Applied Physics*, 83(6):3432–3434, 1998.
- [4] Fernando Ajejas, Viola Káizáková, Dayane de Souza Chaves, Jan Vogel, Paolo Perna, Ruben Guerrero, Adrian Gudin, Julio Camarero, and Stefania Pizzini. Tuning domain wall velocity with Dzyaloshinskii-Moriya interaction. *Applied Physics Letters*, 111(20):202402, nov 2017.
- [5] Edoardo Albisetti, S. Tacchi, Raffaele Silvani, Giuseppe Scaramuzzi, Simone Finizio, Sebastian Wintz, Christian Rinaldi, Matteo Cantoni, Jörg Raabe, Giovanni Carlotti, Riccardo Bertacco, Elisa Riedo, and Daniela Petti. Optically Inspired Nanomagnonics with Nonreciprocal Spin Waves in Synthetic Antiferromagnets. *Advanced Materials*, 32(9):1906439, mar 2020.
- [6] Edoardo Albisetti, Silvia Tacchi, Raffaele Silvani, Giuseppe Scaramuzzi, Simone Finizio, Sebastian Wintz, Christian Rinaldi, Matteo Cantoni, Jörg Raabe, Giovanni Carlotti, Riccardo Bertacco, Elisa Riedo, and Daniela Petti. Optically Inspired Nanomagnonics with Nonreciprocal Spin Waves in Synthetic Antiferromagnets. *Advanced Materials*, 32(9):1906439, mar 2020.
- [7] Kyongmo An, Artem N. Litvinenko, R. Kohn, Aufa A. Fuad, Vladimir V. Naletov, Laurent Vila, Ursula Ebels, Grégoire de Loubens, Hervé Hurdequint, Nathan Beaulieu, J. Ben Youssef, Nicolas Vukadinovic, Gerrit E. W. Bauer, Andrei N. Slavin, Vasil S. Tiberkevich, and Olivier Klein. Coherent long-range transfer of angular momentum between magnon Kittel modes by phonons. *Physical Review B*, 101(6):060407, feb 2020.
- [8] Y. Au, Mykola Dvornik, T. Davison, E. Ahmad, P. S. Keatley, Arne Vansteenkiste, B. Van Waeyenberge, and V. V. Kruglyak. Direct Excitation of Propagating Spin Waves by Focused Ultrashort Optical Pulses. *Physical Review Letters*, 110(9):097201, feb 2013.
- [9] Nandan K P Babu, Aleksandra Trzaskowska, Piotr Graczyk, Grzegorz Centała, Szymon Mieszczak, Hubert Głowiński, Miłosz Zdunek, Sławomir Mielcarek, and Jarosław W. Kłos. The Interaction between Surface Acoustic Waves and Spin Waves: The Role of Anisotropy and Spatial Profiles of the Modes. *Nano Letters*, page acs.nanolett.0c03692, nov 2020.
- [10] Bernard Barbara. Magnetization processes in high anisotropy systems. *Journal of Magnetism and Magnetic Materials*, 129(1):79–86, jan 1994.
- [11] Hans G. Bauer, Peter Majchrak, Torsten Kachel, Christian H. Back, and Georg Woltersdorf. Nonlinear spin-wave excitations at low magnetic bias fields. *Nature Communications*, 6(1):8274, nov 2015.
- [12] Geoffrey S.D. Beach, Corneliu Nistor, Carl Knutson, Maxim Tsoi, and James L Erskine. Dynamics of field-driven domain-wall propagation in ferromagnetic nanowires. *Nature materials*, 4(10):741–4, oct 2005.
- [13] N. Bergeard, M. Hehn, Stéphane Mangin, G. Lengaigne, F. Montaigne, M. L. M. Laliou, B. Koopmans, and G. Malinowski. Hot-Electron-Induced Ultrafast Demagnetization in CoPt Multilayers. *Physical Review Letters*, 117(14):147203, sep 2016.

- [14] L. Berger. Low-field magnetoresistance and domain drag in ferromagnets. *Journal of Applied Physics*, 49(3):2156–2161, mar 1978.
- [15] Cassidy Berk, Mike Jaris, Weigang Yang, Scott Dhuey, Stefano Cabrini, and Holger Schmidt. Strongly coupled magnon-phonon dynamics in a single nanomagnet. *Nature Communications*, 10(1):2652, dec 2019.
- [16] C. Bihler, M. Althammer, A Brandlmaier, S. Geprägs, Mathias Weiler, M Opel, W Schoch, W Limmer, R Gross, M. S. Brandt, and Sebastian T.B. Goennenwein. GaMnAs/piezoelectric actuator hybrids: A model system for magnetoelastic magnetization manipulation. *Physical Review B (Condensed Matter and Materials Physics)*, 78(4):45203, 2008.
- [17] M. Birowska, C. Śliwa, J. Majewski, and Tomasz Dietl. Origin of Bulk Uniaxial Anisotropy in Zinc-Blende Dilute Magnetic Semiconductors. *Physical Review Letters*, 108(23):237203, jun 2012.
- [18] M. Boiteux, P. Doussineau, B. Ferry, J. Joffrin, and A. Levelut. Acoustical faraday effect in antiferromagnetic Cr<sub>2</sub>O<sub>3</sub>. *Physical Review B*, 4(9):3077–3088, 1971.
- [19] M. Bombeck, J. V. Jäger, A.V. Scherbakov, T.L. Linnik, D. R. Yakovlev, X. Liu, Jacek K. Furdyna, A. V. Akimov, and Manfred Bayer. Magnetization precession induced by quasitransverse picosecond strain pulses in (311) ferromagnetic (Ga,Mn)As. *Physical Review B*, 87(6):060302, feb 2013.
- [20] M. Bombeck, a. S. Salasyuk, B. Glavin, A.V. Scherbakov, C. Brüggemann, D.R. Yakovlev, V. F. Sapega, X. Liu, Jacek K. Furdyna, Aki, and Manfred Bayer. Excitation of spin waves in ferromagnetic (Ga,Mn)As layers by picosecond strain pulses. *Physical Review Letters*, 85(19):195324, may 2012.
- [21] H Bömmel and K Dransfeld. Excitation of hypersonic waves by ferromagnetic resonance. *Phys. Rev. Lett.*, 3:83, 1959.
- [22] Dmytro A. Bozhko, Peter Clausen, Gennadii A. Melkov, Victor S. L’vov, Anna Pomyalov, Vitaliy I. Vasyuchka, Andrii V. Chumak, Burkard Hillebrands, and Alexander A. Serga. Bottleneck Accumulation of Hybrid Magnetoelastic Bosons. *Physical Review Letters*, 118(23):237201, jun 2017.
- [23] Ibrahima Sock Camara, B Croset, Ludovic Largeau, Pauline Rovillain, Laura Thevenard, and Jean-Yves Duquesne. Vector network analyzer measurement of the amplitude of an electrically excited surface acoustic wave and validation by X-ray diffraction. *Journal of Applied Physics*, 121(4):044503, jan 2017.
- [24] Ibrahima Sock Camara, Jean-Yves Duquesne, A. Lemaître, Catherine Gourdon, and Laura Thevenard. Field-Free Magnetization Switching by an Acoustic Wave. *Physical Review Applied*, 11(1):014045, 2019.
- [25] R. E. Camley. Magnetoelastic waves in a ferromagnetic film on a nonmagnetic substrate. *Journal of Applied Physics*, 50(8):5272–5284, 1979.
- [26] R.E. Camley. Nonreciprocal surface waves. *Surface Science Reports*, 7(3-4):103–187, jul 1987.
- [27] Lucas Caretta, Maxwell Mann, Felix Büttner, Kohei Ueda, Bastian Pfau, Christian M. Günther, Piet Helsing, Alexandra Churikova, Christopher Klose, Michael Schneider, Dieter Engel, Colin Marcus, David Bono, Kai Bagschik, Stefan Eisebitt, and Geoffrey S.D. Beach. Fast current-driven domain walls and small skyrmions in a compensated ferrimagnet. *Nature Nanotechnology*, 13(12):1154–1160, 2018.
- [28] A. Ceballos, Zhanghui Chen, O. Schneider, C. Bordel, Lin-Wang Wang, and F. Hellman. Effect of strain and thickness on the transition temperature of epitaxial FeRh thin-films. *Applied Physics Letters*, 111(17):172401, oct 2017.
- [29] C. L. Chang, A. M. Lomonosov, J. Janušonis, V. S. Vlasov, Vasily V. Temnov, and R. I. Tobey. Parametric frequency mixing in a magnetoelastically driven linear ferromagnetic-resonance oscillator. *Physical Review B*, 95(6):060409, feb 2017.
- [30] R. O. Cherifi, V. Ivanovskaya, L. C. Phillips, A. Zobelli, I. C. Infante, E. Jacquet, V. Garcia, S. Fusil, P. R. Briddon, N. Guiblin, Alexandra Mougin, A. A. Ūnal, F. Kronast, S. Valencia, B. Dkhil, A. Barthélémy, and M. Bibes. Electric-field control of magnetic order above room temperature. *Nature Materials*, 13(4):345–351, apr 2014.

- [31] Alexandr Chernyshov, Mason Overby, Xinyu Liu, Jacek K. Furdyna, Yuli Lyanda-Geller, and Leonid P. Rokhinson. Evidence for reversible control of magnetization in a ferromagnetic material by means of spin-orbit magnetic field. *Nature Physics*, 5(9):656–659, aug 2009.
- [32] Daichi Chiba, Maciej Sawicki, Y Nishitani, Y Nakatani, Fumihiko Matsukura, and Hideo Ohno. Magnetization vector manipulation by electric fields. *Nature*, 455(7212):515–518, 2008.
- [33] M Cormier, V. Jeudy, T. Niazi, D Lucot, M Granada, J Cibert, and A. Lemaître. Electric-field-induced magnetization reorientation in a (Ga,Mn)As/(Ga,Mn)(As,P) bilayer with out-of-plane anisotropy. *Physical Review B*, 90(17):174418, nov 2014.
- [34] M. Cubukcu, H. J. von Bardeleben, J.L. Cantin, and A. Lemaître. Temperature induced in-plane/out-of-plane magnetization transition in ferromagnetic Ga<sub>0.93</sub>Mn<sub>0.07</sub>As<sub>0.94</sub>P<sub>0.06</sub>/(100)GaAs thin films. *Applied Physics Letters*, 96(10):102502, mar 2010.
- [35] M. Cubukcu, H.J. von Bardeleben, J.L. Cantin, I. Vickridge, and A. Lemaître. Ferromagnetism in Ga<sub>0.90</sub>Mn<sub>0.10</sub>As<sub>1-x</sub>Py: From the metallic to the impurity band conduction regime. *Thin Solid Films*, 519(23):8212–8214, sep 2011.
- [36] J. Curiale, A. Lemaître, C. Ulysse, G. Faini, and V. Jeudy. Spin Drift Velocity, Polarization, and Current-Driven Domain-Wall Motion in (Ga,Mn)(As,P). *Physical Review Letters*, 108(7):076604, feb 2012.
- [37] E. De Ranieri, P E Roy, D. Fang, E K Vehstedt, a C Irvine, D Heiss, a. Casiraghi, Richard P. Campion, Bryan L. Gallagher, Tomáš Jungwirth, and J. Wunderlich. Piezoelectric control of the mobility of a domain wall driven by adiabatic and non-adiabatic torques. *Nature materials*, 12(9):808–14, sep 2013.
- [38] Marwan Deb, Elena Popova, Michel Hehn, Niels Keller, Stéphane Mangin, and Gregory Malinowski. Picosecond acoustic-excitation-driven ultrafast magnetization dynamics in dielectric Bi-substituted yttrium iron garnet. *Physical Review B*, 98(17):1–7, 2018.
- [39] Marwan Deb, Elena Popova, Steffen Peer Zeuschner, Michel Hehn, Niels Keller, Stéphane Mangin, Gregory Malinowski, and Matias Bargheer. Generation of spin waves via spin-phonon interaction in a buried dielectric thin film. *Physical Review B*, 103(2):024411, jan 2021.
- [40] Per Delsing, Andrew N Cleland, Martin J A Schuetz, Johannes Knörzer, Géza Giedke, J Ignacio Cirac, Kartik Srinivasan, Marcelo Wu, Krishna Coimbatore Balram, Christopher Bäuerle, Tristan Meunier, Christopher J B Ford, Paulo V. Santos, Edgar Cerda-Méndez, Hailin Wang, Hubert J. Krenner, Emeline D S Nysten, Matthias Weiß, Geoff R Nash, Laura Thevenard, Catherine Gourdon, Pauline Rovillain, Max Marangolo, Jean-Yves Duquesne, Gerhard Fischerauer, Werner Ruile, Alexander Reiner, Ben Paschke, Dmytro Denysenko, Dirk Volkmer, Achim Wixforth, Henrik Bruus, Martin Wiklund, Julien Reboud, Jonathan M Cooper, YongQing Fu, Manuel S Brugger, Florian Rehfeldt, and Christoph Westerhausen. The 2019 surface acoustic waves roadmap. *Journal of Physics D: Applied Physics*, 52(35):353001, aug 2019.
- [41] Thibaut Devolder and Claude Chappert. Cell writing selection when using precessional switching in a magnetic random access memory. *Journal of Applied Physics*, 95:1933–1941, 2004.
- [42] Tomasz Dietl and Hideo Ohno. Dilute ferromagnetic semiconductors: Physics and spintronic structures. *Reviews of Modern Physics*, 86(1):187–251, mar 2014.
- [43] Tomasz Dietl, Hideo Ohno, and Fumihiko Matsukura. Hole-mediated ferromagnetism in tetrahedrally coordinated semiconductors. *Phys. Rev. B*, 63(19):195205, 2001.
- [44] A. Dourlat, V. Jeudy, A. Lemaître, and Catherine Gourdon. Field-driven domain-wall dynamics in (Ga,Mn)As films with perpendicular anisotropy. *Physical Review B (Condensed Matter and Materials Physics)*, 78(16):161303, 2008.
- [45] L. Dreher, Mathias Weiler, M. Pernpeintner, H. Huebl, R. Gross, M. S. Brandt, and Sebastian T.B. Goennenwein. Surface acoustic wave driven ferromagnetic resonance in nickel thin films: Theory and experiment. *Physical Review B*, 86(13):134415, oct 2012.
- [46] J.-Y. Duquesne, Pauline Rovillain, C. Hepburn, M. Eddrief, P. Atkinson, A. Anane, R. Ranchal, and M. Marangolo. Surface-Acoustic-Wave Induced Ferromagnetic Resonance in Fe Thin Films and Magnetic Field Sensing. *Physical Review Applied*, 12(2):024042, 2019.

- [47] Westin Edrington, Uday Singh, Maya Abo Dominguez, James Rehwaldt Alexander, Rabindra Nepal, and S. Adenwalla. SAW assisted domain wall motion in Co/Pt multilayers. *Applied Physics Letters*, 112(5):052402, jan 2018.
- [48] Marc Elsen. *Magnétorésistances et transfert de spin dans des hétérostructures tunnel à base de (Ga,Mn)As*. PhD thesis, UNIVERSITE PARIS VI, 2007.
- [49] D. Fang, Hidekazu Kurebayashi, J. Wunderlich, K. Výborný, L P Zârbo, Richard P. Campion, a. Casiraghi, Bryan L. Gallagher, Tomáš Jungwirth, and Andrew Ferguson. Spin-orbit-driven ferromagnetic resonance. *Nature nanotechnology*, 6(7):413–7, jan 2011.
- [50] Jacek K. Furdyna. Diluted magnetic semiconductors. *Journal of Applied Physics*, 64(4):R29–R64, aug 1988.
- [51] A. K. Ganguly, Davis K.L., D.C. Webb, and C. Vittoria. Magnetoelastic surface waves in a magnetic filmâpiezoelectric substrate configuration. *Journal of Applied Physics*, 47(6):2696, 1976.
- [52] Ion Garate, K. Gilmore, M. D. Stiles, and A. MacDonald. Nonadiabatic spin-transfer torque in real materials. *Physical Review B*, 79(10):104416, mar 2009.
- [53] Georgeta Ciuta. *Une étude expérimentale de la coercivité des aimants NdFeB*. PhD thesis, 2014.
- [54] D. Givord, Q. Lu, M.F. Rossignol, P. Tenaud, and T. Viadieu. Experimental approach to coercivity analysis in hard magnetic materials. *Journal of Magnetism and Magnetic Materials*, 83(1-3):183–188, jan 1990.
- [55] O. Gladii, M Haidar, Y. Henry, M Kostylev, and Matthieu Bailleul. Frequency nonreciprocity of surface spin wave in permalloy thin films. *Physical Review B*, 93(5):054430, feb 2016.
- [56] F. Godejohann, A. V. Scherbakov, S. M. Kukhtaruk, A. N. Poddubny, D. D. Yaremkevich, M. Wang, A. Nadzeyka, D. R. Yakovlev, A. W. Rushforth, A. V. Akimov, and M. Bayer. Magnon polaron formed by selectively coupled coherent magnon and phonon modes of a surface patterned ferromagnet. *Physical Review B*, 102(14):144438, oct 2020.
- [57] Sebastian T.B. Goennenwein, T. Graf, T Wassner, M. S. Brandt, M Stutzmann, J B Philipp, R Gross, M Krieger, K Zürn, P Ziemann, A Koeder, S Frank, W Schoch, and A Waag. Spin wave resonance in GaMnAs. *Applied Physics Letters*, 82(5):730–732, 2003.
- [58] Olena Gomonay, V. Baltz, Arne Brataas, and Yaroslav Tserkovnyak. Antiferromagnetic spin textures and dynamics. *Nature Physics*, 14(3):213–216, mar 2018.
- [59] Olena Gomonay and Vadim M Loktev. Magnetostriction and magnetoelastic domains in antiferromagnets. *Journal of Physics: Condensed Matter*, 14(15):3959–3971, apr 2002.
- [60] Catherine Gourdon, V. Jeudy, A C\=ebers, A. Doulat, Kh. Khazen, and A Lema\^itre. Unusual domain-wall motion in ferromagnetic semiconductor films with tetragonal anisotropy. *Physical Review B (Condensed Matter and Materials Physics)*, 80(16):161202, 2009.
- [61] Catherine Gourdon, Laura Thevenard, S. Haghgoo, and A. CÄbers. Domain-wall flexing instability and propagation in thin ferromagnetic films. *Physical Review B*, 88(1):014428, jul 2013.
- [62] P. G. Gowtham, T. Moriyama, Dan Ralph, and R. A. Buhrman. Traveling surface spin-wave resonance spectroscopy using surface acoustic waves. *Journal of Applied Physics*, 118(23):233910, dec 2015.
- [63] Marta Gryglas-Borysiewicz, Adam Kwiatkowski, Piotr Juszyński, Zuzanna Ogorzałek, Konrad Puźniak, Mateusz Tokarczyk, Grzegorz Kowalski, Michał Baj, Dariusz Wasik, Nevill Gonzalez Szwacki, Jacek Przybytek, Janusz Sadowski, Maciej Sawicki, Piotr Dziawa, and Jaroslaw Z. Domagala. Hydrostatic pressure influence on Tc in (Ga,Mn)As. *Physical Review B*, 101(5):054413, feb 2020.
- [64] Thai Ha Pham, J. Vogel, Joao Sampaio, M. VaĀatka, J.-C. Rojas-Sánchez, M. Bonfim, D. S. Chaves, F. Choueikani, P. Ohresser, E. Otero, André Thiaville, and Stefania Pizzini. Very large domain wall velocities in Pt/Co/GdOx and Pt/Co/Gd trilayers with Dzyaloshinskii-Moriya interaction. *EPL (Europhysics Letters)*, 113(6):67001, mar 2016.



- [65] S. Haghgoo, M. Cubukcu, H. J. von Bardeleben, Laura Thevenard, A. Lemaître, and Catherine Gourdon. Exchange constant and domain wall width in (Ga,Mn)(As,P) films with self-organization of magnetic domains. *Physical Review B*, 82(4):041301(R), jul 2010.
- [66] Kjetil M.D. Hals, Anh Nguyen, and Arne Brataas. Intrinsic Coupling between Current and Domain Wall Motion in (Ga,Mn)As. *Physical Review Letters*, 102(25):256601, jun 2009.
- [67] Eloi Haltz, Joao Sampaio, R. Weil, Y. Dumont, and Alexandra Mougin. Strong current actions on ferrimagnetic domain walls in the creep regime. *Physical Review B*, 99(10):1–7, 2019.
- [68] A. Hamadeh, P. Pirro, J.-P. Adam, Y. Lu, M. Hehn, S. Petit Watelot, and S. Mangin. Inversion of the domain wall propagation in synthetic ferrimagnets. *Applied Physics Letters*, 111(2):022407, jul 2017.
- [69] Yusuke Hashimoto, Davide Bossini, Tom H. Johansen, Eiji Saitoh, Andrei Kirilyuk, and Theo Rasing. Frequency and wavenumber selective excitation of spin waves through coherent energy transfer from elastic waves. *Physical Review B*, 97(14):140404, apr 2018.
- [70] Yusuke Hashimoto, Y. Iye, and S. Katsumoto. Control of magnetic anisotropy in (Ga,Mn)As with etching depth of specimen boundaries. *Journal of Crystal Growth*, 378:381–384, sep 2013.
- [71] Yusuke Hashimoto, Tom H. Johansen, and Eiji Saitoh.  $180^\circ$ -phase shift of magnetoelastic waves observed by phase-resolved spin-wave tomography. *Applied Physics Letters*, 112(23):232403, jun 2018.
- [72] Yusuke Hashimoto and Hiro Munekata. Coherent manipulation of magnetization precession in ferromagnetic semiconductor (Ga,Mn)As with successive optical pumping. *Applied Physics Letters*, 93(20):202506, 2008.
- [73] Masamitsu Hayashi, Luc Thomas, Charles Rettner, Rai Moriya, and Stuart S.P. Parkin. Direct observation of the coherent precession of magnetic domain walls propagating along permalloy nanowires. *Nature Physics*, 3(1):21–25, dec 2006.
- [74] A. Hernández-Mínguez, F. Macià, J. M. Hernández, J. Herfort, and P. V. Santos. Large non-reciprocal propagation of surface acoustic waves in epitaxial ferromagnetic/semiconductor hybrid structures. pages 1–20, 2019.
- [75] Liza Herrera Diez, Jan Honolka, K. Kern, Ernesto Placidi, Fabrizio Arciprete, Andrew W. Rushforth, Richard P. Campion, and Bryan L. Gallagher. Magnetic aftereffect in compressively strained GaMnAs studied using Kerr microscopy. *Physical Review B*, 81(9):094412, mar 2010.
- [76] J. Holanda, D. S. Maior, A. Azevedo, and S. M. Rezende. Detecting the phonon spin in magnon-phonon conversion experiments. *Nature Physics*, 14(5):500–506, 2018.
- [77] A. Hubert and Rudolf Schäfer. *Magnetic domains*. Berlin, springer edition, 2000.
- [78] A. Hubert and G. Traeger. Magneto-optical sensitivity functions of thin-film systems. *Journal of Magnetism and Magnetic Materials*, 124(1-2):185–202, jun 1993.
- [79] Sho Inoue, Nguyen N. Phuoc, Jiangwei Cao, Nguyen T. Nam, Hnin Yu Yu Ko, and Takao Suzuki. Structural and magneto-optical properties of FeRh thin films. *Journal of Applied Physics*, 103(7):1–4, 2008.
- [80] Y. Ishii, R. Sasaki, Y. Nii, T. Ito, and Y. Onose. Magnetically Controlled Surface Acoustic Waves on Multiferroic BiFeO<sub>3</sub>. *Physical Review Applied*, 9(3):34034, 2018.
- [81] J. V. Jařger, A.V. Scherbakov, T.L. Linnik, D.R. Yakovlev, M. Wang, Peter Wadley, V. Holy, Stuart Cavill, Tatsushi Akazaki, Andrew W. Rushforth, and Manfred Bayer. Picosecond inverse magnetostriction in gallenol thin films. *Applied Physics Letters*, 103(3):032409, 2013.
- [82] J. Januřonis, C. L. Chang, T. Jansma, A. Gatilova, V. S. Vlasov, A. M. Lomonosov, Vasily V. Temnov, and R. I. Tobey. Ultrafast magnetoelastic probing of surface acoustic transients. *Physical Review B*, 94(2):024415, jul 2016.
- [83] J. Januřonis, C. L. Chang, P. H. M. van Loosdrecht, and R. I. Tobey. Frequency tunable surface magneto elastic waves. *Applied Physics Letters*, 106(18):181601, may 2015.

- [84] Soong-Geun Je, Juan-Carlos Rojas-Sánchez, Thai Ha Pham, Pierre Vallobra, Gregory Malinowski, Daniel Lacour, Thibaud Fache, Marie-Claire Cyrille, Dae-Yun Kim, Sug-Bong Choe, Mohamed Belmeguenai, Michel Hehn, Stéphane Mangin, Gilles Gaudin, and Olivier Boulle. Spin-orbit torque-induced switching in ferrimagnetic alloys: Experiments and modeling. *Applied Physics Letters*, 112(6):062401, feb 2018.
- [85] V. Jeudy, J. Curiale, Jean-Paul Adam, André Thiaville, A. Lemaître, and G. Faini. Current induced domain wall motion in GaMnAs close to the Curie temperature. *Journal of physics. Condensed matter : an Institute of Physics journal*, 23(44):446004, nov 2011.
- [86] V. Jeudy, Alexandra Mougin, S. Bustingorry, W. Savero Torres, J. Gorchon, A. B. Kolton, A. Lemaître, and J.-P. Jamet. Universal Pinning Energy Barrier for Driven Domain Walls in Thin Ferromagnetic Films. *Physical Review Letters*, 117(5):057201, jul 2016.
- [87] Kaushalya Jhuria, Julius Hohlfeld, Akshay Pattabi, Elodie Martin, Aldo Ygnacio Arriola Córdoba, Xinpeng Shi, Roberto Lo Conte, Sebastien Petit-Watelot, Juan Carlos Rojas-Sanchez, Gregory Malinowski, Stéphane Mangin, Aristide Lemaître, Michel Hehn, Jeffrey Bokor, Richard B. Wilson, and Jon Gorchon. Spin-orbit torque switching of a ferromagnet with picosecond electrical pulses. *Nature Electronics*, 3(11):680–686, nov 2020.
- [88] D.C. Jiles. Theory of the magnetomechanical effect. *Journal of Physics D*, 28:1537, 1995.
- [89] Tomáš Jungwirth, X Marti, P. Wadley, and J. Wunderlich. Antiferromagnetic spintronics. *Nature Nanotechnology*, 11(3):231–241, 2016.
- [90] Tomáš Jungwirth, Qian Niu, and A H Macdonald. Anomalous Hall Effect in Ferromagnetic Semiconductors. *Physics*, pages 1–4, 2002.
- [91] Tomáš Jungwirth, Jairo Sinova, A. Manchon, X Marti, J. Wunderlich, and C. Felser. The multiple directions of antiferromagnetic spintronics. *Nature Physics*, 14(3):200–203, mar 2018.
- [92] Tomáš Jungwirth, K. Wang, J. Mašek, Kevin Edmonds, Jürgen König, Jairo Sinova, M. Polini, N. Goncharuk, a. MacDonald, Maciej Sawicki, Andrew W. Rushforth, Richard P. Campion, L. Zhao, C.T. Foxon, and Bryan L. Gallagher. Prospects for high temperature ferromagnetism in (Ga,Mn)As semiconductors. *Physical Review B*, 72(16):165204, oct 2005.
- [93] Akashdeep Kamra and Hans G. Bauer. Actuation, propagation, and detection of transverse magnetoelastic waves in ferromagnets. *Solid State Communications*, 198:35–39, nov 2014.
- [94] V. N. Kats, T.L. Linnik, A. S. Salasyuk, Andrew W. Rushforth, M. Wang, Peter Wadley, A. V. Akimov, S. A. Cavill, V. Holy, A. M. Kalashnikova, and A.V. Scherbakov. Ultrafast changes of magnetic anisotropy driven by laser-generated coherent and noncoherent phonons in metallic films. *Physical Review B*, 93(21):214422, 2016.
- [95] Kh. Khazen, H. J. von Bardeleben, J.L. Cantin, A. Mauger, Lianlian Chen, and J. H. Zhao. Intrinsically limited critical temperatures of highly doped  $\text{Ga}_{1-x}\text{Mn}_x\text{As}$ . *Physical Review B*, 81(23):235201, jun 2010.
- [96] Ji-Wan Kim, Mircea Vomir, and Jean-Yves Bigot. Ultrafast Magnetoacoustics in Nickel Films. *Physical Review Letters*, 109(16), oct 2012.
- [97] Kab-Jin Kim, Se Kwon Kim, Yuushou Hirata, Se-Hyeok Oh, Takayuki Tono, Duck-Ho Kim, Takaya Okuno, Woo Seung Ham, Sanghoon Kim, Gyoungchoon Go, Yaroslav Tserkovnyak, Arata Tsukamoto, Takahiro Moriyama, Kyung-Jin Lee, and Teruo Ono. Fast domain wall motion in the vicinity of the angular momentum compensation temperature of ferrimagnets. *Nature Materials*, 16(12):1187–1192, dec 2017.
- [98] Alexey Kimel, G. V. Astakhov, G M Schott, A. Kirilyuk, D.R. Yakovlev, Grzegorz Karczewski, W. Ossau, G Schmidt, L W Molenkamp, and Theo Rasing. Picosecond Dynamics of the Photoinduced Spin Polarization in Epitaxial (Ga,Mn)As Films. *Phys. Rev. Lett.*, 92(23):237203, 2004.

- [99] A. Kirilyuk, Alexey Kimel, and Theo Rasing. Ultrafast optical manipulation of magnetic order. *Reviews of Modern Physics*, 82(3):2731–2784, sep 2010.
- [100] Charles Kittel. Interaction of Spin Waves and Ultrasonic Waves in Ferromagnetic Crystals. *Physical Review*, 110(4):836–841, may 1958.
- [101] E. Kojima, J. Héroux, R. Shimano, Yusuke Hashimoto, S. Katsumoto, Y. Iye, and M. Kuwata-Gonokami. Experimental investigation of polaron effects in Ga<sub>1-x</sub>Mn<sub>x</sub>As by time-resolved and continuous-wave midinfrared spectroscopy. *Physical Review B*, 76(19), nov 2007.
- [102] P Kossacki, W Pacuski, W Maślana, J.A Gaj, M Bertolini, D Ferrand, S Tatarenko, and J Cibert. Spin engineering of carrier-induced magnetic ordering in (Cd,Mn)Te quantum wells. *Physica E: Low-dimensional Systems and Nanostructures*, 21(2-4):943–946, mar 2004.
- [103] Oleksandr Kovalenko, Thomas Pezeril, and Vasily V. Temnov. New Concept for Magnetization Switching by Ultrafast Acoustic Pulses. *Physical Review Letters*, 110(26):266602, jun 2013.
- [104] M Kraimia. *Magnéto-élasticité et magnéto-acoustique dans le semiconducteur ferromagnétique (Ga,Mn)As*. PhD thesis, 2020.
- [105] M Kraimia, P Kuszewski, J.-Y. Duquesne, A. Lemaître, F Margaiilan, Catherine Gourdon, and L Thevenard. Time- and space-resolved nonlinear magnetoacoustic dynamics. *Physical Review B*, 101(14):144425, apr 2020.
- [106] M Kraimia, L Largeau, K Boujdaria, B Croset, C Mocuta, A. Lemaître, Catherine Gourdon, and L. Thevenard. Exploring the shear strain contribution to the uniaxial magnetic anisotropy of (Ga,Mn)As. *Journal of Applied Physics*, 127(9):093901, mar 2020.
- [107] Hidekazu Kurebayashi, Jairo Sinova, D. Fang, a. C. Irvine, T. D. Skinner, J. Wunderlich, V. Novák, Richard P. Campion, Bryan L. Gallagher, E. K. Vehstedt, L. P. Zárbo, K. Vybórný, Andrew Ferguson, and Tomáš Jungwirth. An antidamping spin-orbit torque originating from the Berry curvature. *Nature Nanotechnology*, 9(March):211, mar 2014.
- [108] P. Kuszewski, Ibrahima Sock Camara, N. Biarrotte, L. Becerra, J. Von Bardeleben, W. Saverio Torres, A. Lemaître, Catherine Gourdon, J.-Y. Duquesne, and L. Thevenard. Resonant magneto-Acoustic switching: Influence of Rayleigh wave frequency and wavevector. *Journal of Physics Condensed Matter*, 30(24), 2018.
- [109] P Kuszewski, J.-Y. Duquesne, L Becerra, A. Lemaître, S Vincent, S Majrab, F Margaiilan, Catherine Gourdon, and Laura Thevenard. Optical Probing of Rayleigh Wave Driven Magnetoacoustic Resonance. *Physical Review Applied*, 10(3):034036, sep 2018.
- [110] Piotr Kuszewski. *Optical detection of magneto-acoustic dynamics*. PhD thesis, Sorbonne Université, 2018.
- [111] Piotr Kuszewski, Ibrahima Sock Camara, Nicolas Biarrotte, Loic Becerra, Jürgen von Bardeleben, W Saverio Torres, A. Lemaître, Catherine Gourdon, Jean-Yves Duquesne, and Laura Thevenard. Resonant magneto-acoustic switching: influence of Rayleigh wave frequency and wavevector. *Journal of Physics: Condensed Matter*, 30(24):244003, jun 2018.
- [112] B. Lacoste, M. Marins de Castro, Thibaut Devolder, R. C. Sousa, L. D. Buda-Prejbeanu, S. Auffret, U. Ebels, C. Ducruet, I. L. Prejbeanu, L. Vila, B. Rodmacq, and B. Dieny. Modulating spin transfer torque switching dynamics with two orthogonal spin-polarizers by varying the cell aspect ratio. *Physical Review B*, 90(22):224404, dec 2014.
- [113] Ludovic Largeau, Ibrahima Camara, J.-Y. Duquesne, Catherine Gourdon, Pauline Rovillain, Laura Thevenard, and Bernard Croset. Laboratory X-ray characterization of a surface acoustic wave on GaAs: the critical role of instrumental convolution. *Journal of Applied Crystallography*, 49(6):2073–2081, dec 2016.
- [114] Jae-Chul Lee, Kab-Jin Kim, Jisu Ryu, Kyoung-Woong Moon, Sang-Jun Yun, Gi-Hong Gim, Kang-Soo Lee, Kyung-Ho Shin, Hyun-Woo Lee, and Sug-Bong Choe. Universality Classes of Magnetic Domain Wall Motion. *Physical Review Letters*, 107(6):067201, aug 2011.
- [115] A. Lemaître, A. Miard, L Travers, O. Mauguin, Ludovic Largeau, Catherine Gourdon, V. Jeudy, M Tran, and J.-M. George. Strain control of the magnetic anisotropy in Ga<sub>1-x</sub>Mn<sub>x</sub>As<sub>1-y</sub>P<sub>y</sub> ferromagnetic semiconductor layers. *Appl. Phys. Lett.*, 93(2):21123, 2008.

- [116] Steven Lequeux, Joao Sampaio, Vincent Cros, Kay Yakushiji, Akio Fukushima, Rie Matsumoto, Hitoshi Kubota, Shinji Yuasa, and Julie Grollier. A magnetic synapse: multilevel spin-torque memristor with perpendicular anisotropy. *Scientific Reports*, 6(1):31510, nov 2016.
- [117] E. Lewis, D Petit, L. O'Brien, A. Fernández-Pacheco, Joao Sampaio, Ana-Vanessa Jaušovec, Huang T. Zeng, Dan Read, and Russell P. Cowburn. Fast domain wall motion in magnetic comb structures. *Nature materials*, 9(12):980–3, dec 2010.
- [118] Weiyang Li, Benjamin Buford, Albrecht Jander, and Pallavi Dhagat. Acoustically Assisted Magnetic Recording: A New Paradigm in Magnetic Data Storage. *IEEE Transactions on Magnetics*, 50(3):3100704, mar 2014.
- [119] Lukas Liensberger, Akashdeep Kamra, Hannes Maier-Flaig, Stephan Geprägs, Andreas Erb, Sebastian T.B. Goennenwein, Rudolf Gross, Wolfgang Belzig, Hans Huebl, and Mathias Weiler. Exchange-enhanced ultra-strong magnon-magnon coupling in a compensated ferrimagnet. *Physical Review Letters*, 123(11):117204, 2019.
- [120] T.L. Linnik, V. N. Kats, J. Jager, A. S. Salasyuk, D. R. Yakovlev, Andrew W. Rushforth, A. V. Akimov, A. M. Kalashnikova, M. Bayer, and A.V. Scherbakov. The effect of dynamical compressive and shear strain on magnetic anisotropy in a low symmetry ferromagnetic film. *Physica Scripta*, 92(5):54006, 2017.
- [121] T.L. Linnik, A.V. Scherbakov, D.R. Yakovlev, X. Liu, Jacek K. Furdyna, and Manfred Bayer. Theory of magnetization precession induced by a picosecond strain pulse in ferromagnetic semiconductor (Ga,Mn)As. *Physical Review B*, 84(21):214432, dec 2011.
- [122] Marco Madami, Gianluca Gubbiotti, Silvia Tacchi, and Giovanni Carlotti. Magnetization dynamics of single-domain nanodots and minimum energy dissipation during either irreversible or reversible switching. *Journal of Physics D: Applied Physics*, 50(45):453002, nov 2017.
- [123] A P Malozemoff and J. C. Slonczewski. *Magnetic domain walls in bubble materials*. Academic press, New York, 1979.
- [124] Haoran Man, Zhong Shi, Guangyong Xu, Yadong Xu, Xi Chen, Sean Sullivan, Jianshi Zhou, Ke Xia, Jing Shi, and Pengcheng Dai. Direct observation of magnon-phonon coupling in yttrium iron garnet. *Physical Review B*, 96(10):3–7, 2017.
- [125] Aurélien Manchon and S. Zhang. Theory of nonequilibrium intrinsic spin torque in a single nanomagnet. *Physical Review B*, 78(21):212405, dec 2008.
- [126] Aurélien Manchon and S Zhang. Theory of spin torque due to spin-orbit coupling. *Physical Review B*, 79(9):094422, 2009.
- [127] Stéphane Mangin, Matthias Gottwald, C.-H. Lambert, D Steil, V Uhlíř, L Pang, Michel Hehn, Sabine Brand, Mirko Cinchetti, G Malinowski, Y. Fainman, Martin Aeschlimann, and Eric E. Fullerton. Engineered materials for all-optical helicity-dependent magnetic switching. *Nature Materials*, 13(3):286–292, feb 2014.
- [128] Massimiliano Marangolo, W. Karboul-Trojet, J.-Y. Prieur, V. H. Etgens, M. Eddrief, Loïc Becerra, and J.-Y. Duquesne. Surface acoustic wave triggering of giant magnetocaloric effect in MnAs/GaAs devices. *Applied Physics Letters*, 105(16):162403, oct 2014.
- [129] S. Mark, P. Dürrenfeld, Katrin Pappert, L. Ebel, Karl Brunner, C. Gould, and L. W. Molenkamp. Fully Electrical Read-Write Device Out of a Ferromagnetic Semiconductor. *Physical Review Letters*, 106(5):057204, jan 2011.
- [130] X. Marti, I. Fina, C. Frontera, Jian Liu, P. Wadley, Q. He, R. J. Paull, J. D. Clarkson, J. Kudrnovský, I. Turek, J. Kuneš, D. Yi, J-H. Chu, C. T. Nelson, L. You, E. Arenholz, S. Salahuddin, J. Fontcuberta, T. Jungwirth, and R. Ramesh. Room-temperature antiferromagnetic memory resistor. *Nature Materials*, 13(4):367–374, apr 2014.
- [131] Eduardo Martinez, Satoru Emori, and Geoffrey S.D. Beach. Current-driven domain wall motion along high perpendicular anisotropy multilayers: The role of the Rashba field, the spin Hall effect, and the Dzyaloshinskii-Moriya interaction. *Applied Physics Letters*, 103(7):072406, 2013.

- [132] J. Mašek, J. Kudrnovský, Frantisek Máca, Jairo Sinova, A H Macdonald, Richard P. Champion, Bryan L. Gallagher, and Tomáš Jungwirth. Mn-doped Ga ( As , P ) and ( Al , Ga ) As ferromagnetic semiconductors : Electronic structure calculations. *Phys. Rev. B*, 75(4):45202, 2007.
- [133] S C Masmanidis, H. X. Tang, E. B. Myers, Mo Li, K De Greve, G Vermeulen, W Van Roy, and M. Roukes. Nanomechanical Measurement of Magnetostriction and Magnetic Anisotropy in (Ga,Mn)As. *Physical Review Letters*, 95(18):187206, 2005.
- [134] C. Maunoury, Thibaut Devolder, C. K. Lim, P. Crozat, Claude Chappert, J. Wecker, and L. Baër. Precessional direct-write switching in micrometer-sized magnetic tunnel junctions. *Journal of Applied Physics*, 97(7):074503, 2005.
- [135] Aurelien Mazzamurro, Abdelkrim Talbi, Yannick Dusch, Philippe Pernod, Olivier Bou Matar, and Nicolas Tiercelin. Giant magnetoelastic coupling in Love acoustic waveguide based on uniaxial multilayered TbCo<sub>2</sub>/FeCo nanostructured thin film on Quartz ST-cut. pages 1–16, 2019.
- [136] Peter John Metaxas, Jean-Pierre Jamet, Alexandra Mougín, M Cormier, Jacques Ferré, V Baltz, B Rodmacq, B. Dieny, and R L Stamps. Creep and Flow Regimes of Magnetic Domain-Wall Motion in Ultrathin Pt/Co/Pt Films with Perpendicular Anisotropy. *Physical Review Letters*, 99(21):217208, 2007.
- [137] Ioan Mihai Miron, Gilles Gaudin, Stéphane Auffret, Bernard Rodmacq, Alain Schuhl, Stefania Pizzini, Jan Vogel, and Pietro Gambardella. Current-driven spin torque induced by the Rashba effect in a ferromagnetic metal layer. *Nature materials*, 9(3):230–4, mar 2010.
- [138] Ioan Mihai Miron, Thomas Moore, Helga Szambolics, Liliana Daniela Buda-Prejbeanu, Stéphane Auffret, Bernard Rodmacq, Stefania Pizzini, Jan Vogel, Marlio Bonfim, Alain Schuhl, and Gilles Gaudin. Fast current-induced domain-wall motion controlled by the Rashba effect. *Nature materials*, 10(6):419–23, jun 2011.
- [139] J Moritz, B. Dieny, J. Nozières, Y Pennec, J Camarero, and Stefania Pizzini. Experimental evidence of a 1âH activation law in nanostructures with perpendicular magnetic anisotropy. *Physical Review B*, 71(10):2–5, 2005.
- [140] Rai Moriya, Masamitsu Hayashi, Luc Thomas, Charles Rettner, and Stuart S.P. Parkin. Dependence of field driven domain wall velocity on cross-sectional area in Ni<sub>65</sub>Fe<sub>20</sub>Co<sub>15</sub> nanowires. *Applied Physics Letters*, 97(14):142506, 2010.
- [141] Takahiro Moriyama, Noriko Matsuzaki, Kab-Jin Kim, Ipppei Suzuki, Tomoyasu Taniyama, and Teruo Ono. Sequential write-read operations in FeRh antiferromagnetic memory. *Applied Physics Letters*, 107(12):122403, sep 2015.
- [142] Hiro MuneKata, H. Ohno, S. von Molnar, Armin Segmüller, L. L. Chang, and L. Esaki. Diluted magnetic III-V semiconductors. *Physical Review Letters*, 63(17):1849–1852, oct 1989.
- [143] Ahsan M Nazmul, S Kobayashi, S Sugahara, and M Tanaka. Control of ferromagnetism in Mn delta-doped GaAs-based semiconductor heterostructures. *Physica E: Low-dimensional Systems and Nanostructures*, 21(2-4):937–942, mar 2004.
- [144] P. Němec, V. Novák, N. Tesařová, E. Rozkotová, H Reichlová, D. Butkovičová, F Trojánek, K. Olejník, P. Malý, R.P. Champion, Bryan L. Gallagher, Jairo Sinova, and Tomáš Jungwirth. The essential role of carefully optimized synthesis for elucidating intrinsic material properties of (Ga,Mn)As. *Nature Communications*, 4(1):1422, dec 2013.
- [145] P. Němec, E. Rozkotová, N. Tesařová, F. Trojánek, E. De Ranieri, K. Olejník, J. Zemen, V. Novák, M. Cukr, P. Malý, and Tomáš Jungwirth. Experimental observation of the optical spin transfer torque. *Nature Physics*, 8(5):411–415, apr 2012.
- [146] Lukas Novotny. Strong coupling, energy splitting, and level crossings: A classical perspective. *American Journal of Physics*, 78(11):1199–1202, nov 2010.
- [147] Katsunori Obata and Gen Tatara. Current-induced domain wall motion in Rashba spin-orbit system. *Physical Review B*, 77(21):1–12, jun 2008.

- [148] Naoki Ogawa, Wataru Koshibae, Aron Jonathan Beekman, Naoto Nagaosa, Masashi Kubota, Masashi Kawasaki, and Yoshinori Tokura. Photodrive of magnetic bubbles via magnetoelastic waves. *Proceedings of the National Academy of Sciences*, 112(29):201504064, 2015.
- [149] H. Ohno, A. Shen, F. Matsukura, A. Oiwa, A. Endo, S. Katsumoto, and Y. Iye. (Ga,Mn)As: A new diluted magnetic semiconductor based on GaAs. *Applied Physics Letters*, 69(3):363–365, jul 1996.
- [150] a. Oiwa, Y. Mitsumori, R. Moriya, T. Shupinski, and Hiro Munekata. Effect of Optical Spin Injection on Ferromagnetically Coupled Mn Spins in the III-V Magnetic Alloy Semiconductor (Ga,Mn)As. *Physical Review Letters*, 88(13):137202, mar 2002.
- [151] Mason Overby, Alexandr Chernyshov, L P Rokhinson, X. Liu, and Jacek K. Furdyna. GaMnAs-based hybrid multiferroic memory device. *Applied Physics Letters*, 92(19):192501, 2008.
- [152] C. Papusoi, B. Delaët, B. Rodmacq, D. Houssameddine, J.-P. Michel, U. Ebels, R. C. Sousa, Liliana Daniela Buda-Prejbeanu, and B. Dieny. 100 ps precessional spin-transfer switching of a planar magnetic random access memory cell with perpendicular spin polarizer. *Applied Physics Letters*, 95(7):072506, 2009.
- [153] Stuart S.P. Parkin, Masamitsu Hayashi, and Luc Thomas. Magnetic domain-wall racetrack memory. *Science (New York, N.Y.)*, 320(5873):190–4, apr 2008.
- [154] Emmanuel Péronne, Nicolas Chuecos, Laura Thevenard, and Bernard Perrin. Acoustic solitons: A robust tool to investigate the generation and detection of ultrafast acoustic waves. *Physical Review B*, 95(6):064306, 2017.
- [155] Natalia Polzikova, Sergey Alekseev, Iosif Kotelyanskii, Alexander Raevskiy, and Yuri Fetisov. Magnetic field tunable acoustic resonator with ferromagnetic-ferroelectric layered structure. *Journal of Applied Physics*, 113(17):17C704, may 2013.
- [156] M Pomerantz. Excitation of Spin-Wave Resonance by Microwave Phonons. *Physical Review Letters*, 7(8):312–313, 1961.
- [157] I. A. Privorotskii, R. A. B. Devine, and G. C. Alexandrakis. Generation and attenuation of phonons at ferromagnetic resonance in thick Ni films. *Journal of Applied Physics*, 50(B11):7732, 1979.
- [158] J Qi, Y Xu, A Steigerwald, X. Liu, Jacek K. Furdyna, Ilias E. Perakis, and N H Tolk. Ultrafast laser-induced coherent spin dynamics in ferromagnetic GaMnAs/GaAs structures. *Physical Review B (Condensed Matter and Materials Physics)*, 79(8):85304, 2009.
- [159] A. J. Ramsay, P. E. Roy, J. A. Haigh, Ruben M. Otxoa, A. C. Irvine, T Janda, Richard P. Champion, Bryan L. Gallagher, and J. Wunderlich. Optical Spin-Transfer-Torque-Driven Domain-Wall Motion in a Ferromagnetic Semiconductor. *Physical Review Letters*, 114(6):067202, feb 2015.
- [160] V. V. Randoshkin. Unusual characteristics of the spin-wave mechanism of domain-wall motion in iron-garnet films with orthorhombic magnetic anisotropy. *Physics of the Solid State*, 39(8):1260–1266, aug 1997.
- [161] A H. M. Reid, G. V. Astakhov, Alexey Kimel, G. M. Schott, W. Ossau, Karl Brunner, Andrei Kirilyuk, L. W. Molenkamp, and Theo Rasing. Single picojoule pulse switching of magnetization in ferromagnetic (Ga,Mn)As. *Applied Physics Letters*, 97(23):232503, 2010.
- [162] Hassen Riahi, W. Ouerghui, Laura Thevenard, Catherine Gourdon, M.A. Maaref, A. Lemaître, O. Mauguin, and C. Testelin. Annealing effect on the magnetization reversal and Curie temperature in a GaMnAs layer. *Journal of Magnetism and Magnetic Materials*, 342:149–151, sep 2013.
- [163] Hassen Riahi, Laura Thevenard, M.A. Maaref, B. Gallas, A. Lemaître, and Catherine Gourdon. Optimizing magneto-optical effects in the ferromagnetic semiconductor GaMnAs. *Journal of Magnetism and Magnetic Materials*, 395:340–344, dec 2015.
- [164] Pauline Rovillain, Ronei Cardoso De Oliveira, Massimiliano Marangolo, and Jean Yves Duquesne. Nonsymmetric spin pumping in a multiferroic heterostructure. *Physical Review B*, 102(18):184409, 2020.

- [165] E. Rozkotová, P. Němec, N. Tesařová, P. Malý, V. Novák, K. Olejník, M. Cukr, and Tomáš Jungwirth. Coherent control of magnetization precession in ferromagnetic semiconductor (Ga,Mn)As. *Applied Physics Letters*, 93(23):232505, dec 2008.
- [166] Andrew W. Rushforth, E. De Ranieri, J. Zemen, J. Wunderlich, Kevin Edmonds, C. S. King, E. Ahmad, Richard P. Campion, C.T. Foxon, Bryan L. Gallagher, K. Výborný, J. Kučera, and Tomáš Jungwirth. Voltage control of magnetocrystalline anisotropy in ferromagnetic-semiconductor-piezoelectric hybrid structures. *Physical Review B*, 78(8):085314, aug 2008.
- [167] A. S. Salasyuk, A. V. Rudkovskaya, A. P. Danilov, B. A. Glavin, S. M. Kukhtaruk, M. Wang, Andrew W. Rushforth, P. A. Nekludova, S. V. Sokolov, A. A. Elistratov, D. R. Yakovlev, M. Bayer, A. V. Akimov, and A.V. Scherbakov. Generation of a localized microwave magnetic field by coherent phonons in a ferromagnetic nanograting. *Physical Review B*, 97(6):060404, feb 2018.
- [168] R. Sasaki, Y. Nii, and Y. Onose. Surface acoustic wave coupled to magnetic resonance on multiferroic CuB<sub>2</sub>O<sub>4</sub>. *Physical Review B*, 99(1):014418, jan 2019.
- [169] Maciej Sawicki, Fumihiko Matsukura, A Idziaszek, Tomasz Dietl, G M Schott, C Ruester, C. Gould, Grzegorz Karczewski, G Schmidt, and L W Molenkamp. Temperature dependent magnetic anisotropy in (Ga,Mn)As layers. *Physical Review B (Condensed Matter and Materials Physics)*, 70(24):245325, 2004.
- [170] A.V. Scherbakov, A.P. Danilov, F. Godejohann, T.L. Linnik, B.A. Glavin, L.A. Shelukhin, D.P. Pattnaik, M. Wang, A.W. Rushforth, D.R. Yakovlev, A.V. Akimov, and M. Bayer. Optical Excitation of Single- and Multimode Magnetization Precession in FeGa Nanolayers. *Physical Review Applied*, 11(3):031003, mar 2019.
- [171] A.V. Scherbakov, a. S. Salasyuk, Tatsushi Akazaki, X. Liu, M. Bombeck, C. Brüggenmann, D.R. Yakovlev, V. F. Sapega, Jacek K. Furdyna, and Manfred Bayer. Coherent Magnetization Precession in Ferromagnetic (Ga,Mn)As Induced by Picosecond Acoustic Pulses. *Physical Review Letters*, 105(11):117204, sep 2010.
- [172] Ernst Schloïmann. Wave propagation along domain walls in magnetic films. *IEEE Transactions on Magnetics*, 10(1):11–17, mar 1974.
- [173] N L Schryer and L R Walker. The motion of 180[degree] domain walls in uniform dc magnetic fields. *Journal of Applied Physics*, 45(12):5406–5421, 1974.
- [174] Florian J. R. Schülein, Eugenio Zallo, Paola Atkinson, Oliver G. Schmidt, Rinaldo Trotta, Armando Rastelli, Achim Wixforth, and Hubert J. Krenner. Fourier synthesis of radiofrequency nanomechanical pulses with different shapes. *Nature Nanotechnology*, 10(6):512–516, apr 2015.
- [175] Piyush J. Shah, Derek A. Bas, Ivan Lisenkov, Alexei Matyushov, Nianxiang Sun, and Michael R. Page. Giant Nonreciprocity of Surface Acoustic Waves enabled by the Magnetoelastic Interaction. apr 2020.
- [176] S. Shihab, Hassen Riahi, Laura Thevenard, H. J. von Bardeleben, A. Lemaître, and Catherine Gourdon. Systematic study of the spin stiffness dependence on phosphorus alloying in the ferromagnetic semiconductor (Ga,Mn)As. *Applied Physics Letters*, 106:142408, 2015.
- [177] S. Shihab, Laura Thevenard, A. Lemaître, Jean-Yves Duquesne, and Catherine Gourdon. Steady-state thermal gradient induced by pulsed laser excitation in a ferromagnetic layer. *Journal of Applied Physics*, 119(15):153904, apr 2016.
- [178] S. Shihab, Laura Thevenard, A. Lemaître, and Catherine Gourdon. Counter-rotating standing spin waves: A magneto-optical illusion. *Physical Review B*, 95(14):144411, 2017.
- [179] Sylvain Shihab. *Excitation et détection optiques de la dynamique de l'aimantation dans le semi-conducteur ferromagnétique (Ga, Mn)(As, P)*. PhD thesis, 2015.
- [180] Yoichi Shiota, Takayuki Nozaki, Frédéric Bonell, Shinichi Murakami, Teruya Shinjo, and Yoshishige Suzuki. Induction of coherent magnetization switching in a few atomic layers of FeCo using voltage pulses. *Nature Materials*, 11(1):39–43, jan 2012.
- [181] T Shono, T Hasegawa, T Fukumura, Fumihiko Matsukura, and Hideo Ohno. Observation of magnetic domain structure in a ferromagnetic semiconductor (Ga, Mn)As with a scanning Hall probe microscope. *Applied Physics Letters*, 77(9):1363–1365, 2000.

- [182] J. C. Slonczewski. Theory of domain-wall motion in magnetic films and platelets. *Journal of Applied Physics*, 44(4):1759–1770, 1973.
- [183] E. G. Spencer and R. C. LeCraw. Magnetoacoustic Resonance in Yttrium Iron Garnet. *Physical Review Letters*, 1(7):241–243, oct 1958.
- [184] C. D. Stanciu, F. Hansteen, Alexey Kimel, Andrei Kirilyuk, A. Tsukamoto, A. Itoh, and Theo Rasing. All-Optical Magnetic Recording with Circularly Polarized Light. *Physical Review Letters*, 99(4), jul 2007.
- [185] Peter R Stone, Jeffrey W Beeman, Kin M Yu, and Oscar D Dubon. Tuning of ferromagnetism through anion substitution in Ga  $\delta$  Mn  $\delta$  pnictide ferromagnetic semiconductors. *Physica B*, 402:454–457, 2007.
- [186] H. X. Tang, R. K. Kawakami, D. D. Awschalom, and M. L. Roukes. Propagation dynamics of individual domain walls in  $\langle \text{mrow} \langle \text{msub} \langle \text{mi mathvariant="normal"} \rangle \text{Ga} \langle \text{mi} \langle \text{mrow} \langle \text{mn} \rangle 1 \langle \text{mn} \rangle \langle \text{mo} \rangle \hat{\langle \text{mi} \rangle x \langle \text{mi} \rangle \langle \text{mrow} \langle \text{msub} \langle \text{mi mathvariant="normal"} \rangle \text{Mn} \langle \text{mi} \rangle x \langle \text{mi} \rangle \langle \text{msub} \langle \text{mi mathvariant="n"} \rangle$ . *Physical Review B*, 74(4):041310, jul 2006.
- [187] Gen Tatara and Hiroshi Kohno. Theory of Current-Driven Domain Wall Motion: Spin Transfer versus Momentum Transfer. *Physical Review Letters*, 92(8):1–4, feb 2004.
- [188] Shoma Tateno, Yukio Nozaki, and Yukio Nozaki. Highly nonreciprocal spin waves excited by magnetoelastic coupling in a ni / si bilayer. *Physical Review Applied*, 13(1):1, 2020.
- [189] N. Tesařová, P. Němec, and E. Rozkotořová. Experimental observation of the optical spin-orbit torque. *Nature Photonics*, 7(June):1–7, 2013.
- [190] Laura Thevenard. *Étude des propriétés ferromagnétiques de ( Ga , Mn ) As au moyen de l ' hydrogénation*. PhD thesis, 2007.
- [191] Laura Thevenard, B Boutigny, Nicholas A Güsken, Loïc Becerra, C. Ulysse, S. Shihab, A. Lemaître, J.-V. Kim, V. Jeudy, and Catherine Gourdon. Spin transfer and spin-orbit torques in in-plane magnetized (Ga,Mn)As tracks. *Physical Review B*, 95(5):054422, feb 2017.
- [192] Laura Thevenard, Ibrahima Sock Camara, S Majrab, M. Bernard, Pauline Rovillain, A. Lemaître, Catherine Gourdon, and Jean-Yves Duquesne. Precessional magnetization switching by a surface acoustic wave. *Physical Review B*, 93(13):134430, apr 2016.
- [193] Laura Thevenard, Ibrahima Sock Camara, J.-Y. Prieur, Pauline Rovillain, A. Lemaître, Catherine Gourdon, and Jean-yves Duquesne. Strong reduction of the coercivity by a surface acoustic wave in an out-of-plane magnetized epilayer. *Physical Review B*, 93(14):140405, apr 2016.
- [194] Laura Thevenard, J.-Y. Duquesne, E. Peronne, H. J. von Bardeleben, H. Jaffres, S. Ruttala, J.-M. George, A. Lemaître, and Catherine Gourdon. Irreversible magnetization switching using surface acoustic waves. *Physical Review B*, 87(14):144402, apr 2013.
- [195] Laura Thevenard, Catherine Gourdon, S. Haghoo, J-P. Adam, H. J. von Bardeleben, A. Lemaître, W Schoch, and André Thiaville. Domain wall propagation in ferromagnetic semiconductors: Beyond the one-dimensional model. *Physical Review B*, 83(24):245211, jun 2011.
- [196] Laura Thevenard, Catherine Gourdon, J.-Y. Prieur, H. J. von Bardeleben, S. Vincent, Loïc Becerra, Ludovic Largeau, and Jean-Yves Duquesne. Surface-acoustic-wave-driven ferromagnetic resonance in (Ga,Mn)(As,P) epilayers. *Physical Review B*, 90(9):094401, sep 2014.
- [197] Laura Thevenard, S. Hussain, H. J. von Bardeleben, M. Bernard, A. Lemaître, and Catherine Gourdon. High domain wall velocities in in-plane magnetized (Ga,Mn)(As,P) layers. *Physical Review B*, 85(6):064419, feb 2012.
- [198] Laura Thevenard, Ludovic Largeau, O. Mauguin, A. Lemaître, Kh. Khazen, and H. J. von Bardeleben. Evolution of the magnetic anisotropy with carrier density in hydrogenated Ga $\delta$ Mn $\delta$ As. *Physical Review B*, 75(19):195218, may 2007.



- [199] Laura Thevenard, Ludovic Largeau, O. Mauguin, A. Lemaître, and B. Theys. Tuning the ferromagnetic properties of hydrogenated GaMnAs. *Applied Physics Letters*, 87(18):182506, oct 2005.
- [200] Laura Thevenard, Ludovic Largeau, O. Mauguin, G Patriarche, A. Lemaître, N. Vernier, and Jacques Ferré. Magnetic properties and domain structure of (Ga,Mn)As films with perpendicular anisotropy. *Physical Review B*, 73(19):195331, 2006.
- [201] Laura Thevenard, A Miard, L Vila, G. Faini, A. Lemaître, N. Vernier, Jacques Ferré, and S. Fusil. Magnetic patterning of (Ga,Mn)As by hydrogen passivation. *Applied Physics Letters*, 91(14):142511, 2007.
- [202] Laura Thevenard, E. Peronne, Catherine Gourdon, C. Testelin, M. Cubukcu, E. Charron, S. Vincent, A. Lemaître, and Bernard Perrin. Effect of picosecond strain pulses on thin layers of the ferromagnetic semiconductor (Ga,Mn)(As,P). *Physical Review B*, 82(10):104422, sep 2010.
- [203] André Thiaville, Y Nakatani, A N D JACQUES MILTAT, and Yoshishige Suzuki. Micromagnetic understanding of current-driven domain wall motion in patterned nanowires. *Europhysics Letters (EPL)*, 69(6):990–996, mar 2005.
- [204] A. A. Thiele. Theory of the stability of cylindrical domains in uniaxial platelets. *Journal of Applied Physics*, 41:1139, 1970.
- [205] Olivier Thomas, Q Shen, P Schieffer, N Tournerie, and B Lépine. Interplay between Anisotropic Strain Relaxation and Uniaxial Interface Magnetic Anisotropy in Epitaxial Fe Films on (001) GaAs. *Physical Review Letters*, 90(1):017205, jan 2003.
- [206] M. Tortarolo, Laura Thevenard, H. J. von Bardeleben, M. Cubukcu, V. H. Etgens, M. Eddrief, and Catherine Gourdon. Fast domain wall dynamics in MnAs/GaAs films. *Applied Physics Letters*, 101(7):072408, aug 2012.
- [207] Rémi Tucoulou, François de Bergevin, Olivier Mathon, and Dmitry Roshchupkin. X-ray Bragg diffraction of LiNbO<sub>3</sub> crystals excited by surface acoustic waves. *Physical Review B*, 64(13):134108, sep 2001.
- [208] Ken-ichi Uchida, Toshu An, Yosuke Kajiwara, Masaya Toda, and Eiji Saitoh. Surface-acoustic-wave-driven spin pumping in Y 3 Fe 5 O 12 /Pt hybrid structure. *Applied Physics Letters*, 99(21):212501, nov 2011.
- [209] P. Van Dorpe, Z. Liu, W. Van Roy, V. F. Motsnyi, Maciej Sawicki, G. Borghs, and J. De Boeck. Very high spin polarization in GaAs by injection from a (Ga,Mn)As Zener diode. *Applied Physics Letters*, 84(18):3495–3497, may 2004.
- [210] G. P. Vella-Coleiro. Domain wall velocity during magnetic bubble collapse. *AIP Conference Proceedings*, 24:595, 1975.
- [211] Roman Verba, Ivan Lisenkov, Ilya Krivorotov, Vasil Tiberkevich, and Andrei N. Slavin. Nonreciprocal Surface Acoustic Waves in Multilayers with Magnetoelastic and Interfacial Dzyaloshinskii-Moriya Interactions. *Physical Review Applied*, 9(6):064014, jun 2018.
- [212] Roman Verba, Vasil Tiberkevich, and Andrei Slavin. Wide-Band Nonreciprocity of Surface Acoustic Waves Induced by Magnetoelastic Coupling with a Synthetic Antiferromagnet. *Physical Review Applied*, 12(5):054061, nov 2019.
- [213] M. Viret, D. Vignoles, D. Cole, J. Coey, W. Allen, D. Daniel, and J. Gregg. Spin scattering in ferromagnetic thin films. *Physical Review B*, 53(13):8464–8468, apr 1996.
- [214] D M Wang, Y H Ren, X. Liu, Jacek K. Furdyna, M Grimsditch, and R Merlin. Light-induced magnetic precession in (Ga,Mn)As slabs: Hybrid standing-wave Damon-Eshbach modes. *Physical Review B (Condensed Matter and Materials Physics)*, 75(23):233308, 2007.
- [215] Jigang Wang, Chanjuan Sun, Yusuke Hashimoto, Junichiro Kono, G. A. Khodaparast, Łukasz Cywiński, L J Sham, Gary D Sanders, Christopher J Stanton, and Hiro Munekata. Ultrafast magneto-optics in ferromagnetic IIIâV semiconductors. *Journal of Physics: Condensed Matter*, 18(31):R501–R530, 2006.
- [216] M. Wang, Kevin Edmonds, Bryan L. Gallagher, Andrew W. Rushforth, O. Makarovskiy, A. Patanè, Richard P. Champion, C.T. Foxon, V. Novák, and Tomáš Jungwirth. High Curie temperatures at low compensation in the ferromagnetic semiconductor (Ga,Mn)As. *Physical Review B*, 87(12):121301, mar 2013.

- [217] Qi Wang, Philipp Pirro, Roman Verba, Andrei N. Slavin, Burkard Hillebrands, and Andrii V. Chumak. Reconfigurable nanoscale spin-wave directional coupler. *Science Advances*, 4(1):e1701517, jan 2018.
- [218] Xuhui Wang and Aurélien Manchon. Diffusive Spin Dynamics in Ferromagnetic Thin Films with a Rashba Interaction. *Physical Review Letters*, 108(11):117201, mar 2012.
- [219] Mathias Weiler, L. Dreher, C. Heeg, H. Huebl, R Gross, M. S. Brandt, and Sebastian T.B. Goennenwein. Elastically Driven Ferromagnetic Resonance in Nickel Thin Films. *Physical Review Letters*, 106(11):117601, mar 2011.
- [220] Mathias Weiler, H. Huebl, F. S. Goerg, F. D. Czeschka, R. Gross, and Sebastian T.B. Goennenwein. Spin Pumping with Coherent Elastic Waves. *Physical Review Letters*, 108(17):176601, apr 2012.
- [221] Yali Xie, Qingfeng Zhan, Tian Shang, Huali Yang, Yiwei Liu, Baomin Wang, and Run-Wei Li. Electric field control of magnetic properties in FeRh/PMN-PT heterostructures. *AIP Advances*, 8(5):055816, may 2018.
- [222] Mingran Xu, Jorge Puebla, Florent Auvray, Bivas Rana, Kouta Kondou, and Yoshichika Otani. Inverse Edelstein effect induced by magnon-phonon coupling. *Physical Review B*, 97(18):180301, may 2018.
- [223] Mingran Xu, Kei Yamamoto, Jorge Puebla, Korbinian Baumgaertl, Bivas Rana, Katsuya Miura, Hiromasa Takahashi, Dirk Grundler, Sadamichi Maekawa, and Yoshichika Otani. Nonreciprocal surface acoustic wave propagation via magneto-rotation coupling. jan 2020.
- [224] Mingran Xu, Kei Yamamoto, Jorge Puebla, Korbinian Baumgaertl, Bivas Rana, Katsuya Miura, Hiromasa Takahashi, Dirk Grundler, Sadamichi Maekawa, and Yoshichika Otani. Nonreciprocal surface acoustic wave propagation via magneto-rotation coupling. *Science Advances*, 6(32):2–6, 2020.
- [225] Y. Yahagi, B. Harteneck, S. Cabrini, and Holger Schmidt. Controlling nanomagnet magnetization dynamics via magnetoelastic coupling. *Physical Review B*, 90(14):140405, oct 2014.
- [226] M. Yahyaoui, Hassen Riahi, M A Maaref, K. Boujdaria, A. Lemaitre, Laura Thevenard, and Catherine Gourdon. Magneto-optical Kerr spectroscopy of (Ga,Mn)(As,P) ferromagnetic layers: Experiments and k.p theory. *Journal of Applied Physics*, 121(12):125702, mar 2017.
- [227] Keisuke Yamada, Jean-Pierre Jamet, Yoshinobu Nakatani, Alexandra Mougin, André Thiaville, Teruo Ono, and Jacques Ferré. Influence of Instabilities on High-Field Magnetic Domain Wall Velocity in (Co/Ni) Nanostrips. *Applied Physics Express*, 4(11):113001, oct 2011.
- [228] M. Yamanouchi, J. Ieda, F. Matsukura, S. E. Barnes, S. Maekawa, and Hideo Ohno. Universality Classes for Domain Wall Motion in the Ferromagnetic Semiconductor (Ga,Mn)As. *Science*, 317(5845):1726–1729, sep 2007.
- [229] Michihiko Yamanouchi, Daichi Chiba, Fumihiko Matsukura, Tomasz Dietl, and Hideo Ohno. Velocity of Domain-Wall Motion Induced by Electrical Current in the Ferromagnetic Semiconductor (Ga,Mn)As. *Physical Review Letters*, 96(9):096601, mar 2006.
- [230] Michihiko Yamanouchi, Daichi Chiba, Fumihiko Matsukura, and Hideo Ohno. Current-induced domain-wall switching in a ferromagnetic semiconductor structure. *Nature*, 428:539–542, 2004.
- [231] H F Yang, F. Garcia-Sanchez, X K Hu, S Sievers, T Böhnert, J D Costa, M. Tarequzzaman, R. Ferreira, M. Bieler, and H. W. Schumacher. Excitation and coherent control of magnetization dynamics in magnetic tunnel junctions using acoustic pulses. pages 1–17, apr 2018.
- [232] J P Zahn, A Gamouras, S March, X. Liu, Jacek K. Furdyna, and K C Hall. Ultrafast studies of carrier and magnetization dynamics in GaMnAs. *Journal of Applied Physics*, 107(3):033908, feb 2010.
- [233] J. Zemen, J. Kučera, K. Olejník, and Tomáš Jungwirth. Magnetocrystalline anisotropies in (Ga,Mn)As: Systematic theoretical study and comparison with experiment. *Physical Review B*, 80(15):155203, oct 2009.
- [234] Huang T. Zeng, Dan Read, Liam O’Brien, Joao Sampaio, E. R. Lewis, D. Petit, and Russell P. Cowburn. Asymmetric magnetic <sc>NOT</sc> gate and shift registers for high density data storage. *Applied Physics Letters*, 96(26):262510, jun 2010.

- [235] Boyu Zhang, Yong Xu, Weisheng Zhao, Daoqian Zhu, Huaiwen Yang, Xiaoyang Lin, Michel Hehn, Gregory Malinowski, Nicolas Vernier, Dafiné Ravelosona, and Stéphane Mangin. Domain-wall motion induced by spin transfer torque delivered by helicity-dependent femtosecond laser. *Physical Review B*, 99(14):144402, apr 2019.
- [236] S. Zhang and Z. Li. Roles of Nonequilibrium Conduction Electrons on the Magnetization Dynamics of Ferromagnets. *Physical Review Letters*, 93(12):127204, sep 2004.
- [237] V. L. Zhang, F. S. Ma, H. H. Pan, C. S. Lin, H. S. Lim, S. C. Ng, M. H. Kuok, S. Jain, and A. O. Adeyeye. Observation of dual magnonic and phononic bandgaps in bi-component nanostructured crystals. *Applied Physics Letters*, 100(16):163118, apr 2012.
- [238] H. Zhou, A. Talbi, Nicolas Tiercelin, and Olivier Boumatar. Multilayer magnetostrictive structure based surface acoustic wave devices. *Applied Physics Letters*, 104(11):114101, mar 2014.
- [239] A.K Zvezdin and V.A Kotov. *Modern Magneto-optics and Magneto-optical Materials*. Crc edition, 1997.